

**INVESTIGATION OF
DOUBLE DIFFUSIVE MAGNETOHYDRODYNAMIC MIXED CONVECTIVE
FLOW ALONG AN INCLINED FLAT PLATE IN A POROUS MEDIUM**

MD. NASIR UDDIN

**A THESIS
SUBMITTED IN PARTIAL FULFILLMENT OF THE REQUIREMENT FOR THE DEGREE OF
MASTER OF PHILOSOPHY IN MATHEMATICS**



**DEPARTMENT OF MATHEMATICS
BANGLADESH UNIVERSITY OF ENGINEERING AND TECHNOLOGY
DHAKA-1000, BANGLADESH**

OCTOBER, 2013

**INVESTIGATION OF
DOUBLE DIFFUSIVE MAGNETOHYDRODYNAMIC MIXED CONVECTIVE
FLOW ALONG AN INCLINED FLAT PLATE IN A POROUS MEDIUM**

by

MD. NASIR UDDIN

ROLL NO. : 0411093003F, REGISTRATION NO. : 0411093003

SESSION: APRIL- 2011, STATUS: FULL -TIME

A THESIS

**SUBMITTED IN PARTIAL FULFILLMENT OF THE REQUIREMENT FOR THE DEGREE OF
MASTER OF PHILOSOPHY IN MATHEMATICS**



**DEPARTMENT OF MATHEMATICS
BANGLADESH UNIVERSITY OF ENGINEERING AND TECHNOLOGY
DHAKA-1000, BANGLADESH**

OCTOBER, 2013

The thesis titled
**Investigation of
Double Diffusive Magnetohydrodynamic Mixed Convective Flow
along an Inclined Flat Plate in a Porous Medium**

Submitted by

Md. Nasir Uddin


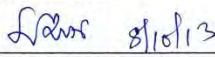
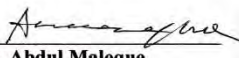
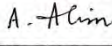
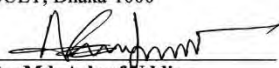
Roll No. : 0411093003F, Registration No. : 0411093003

Session : April- 2011, Status : Full -Time

has been accepted as satisfactory in partial fulfillment of the requirement for the
degree of

Master of Philosophy in Mathematics
on October 08, 2013

BOARD OF EXAMINERS

- (i) 
Dr. Md. Mustafa Kamal Chowdhury
Professor
Department of Mathematics
BUET, Dhaka-1000
Chairman
(Supervisor)
- (ii) 
Dr. Md. Manirul Alam Sarker
Professor & Head
Dept. of Mathematics
BUET, Dhaka-1000
Member
(Ex-Officio)
- (iii) 
Dr. Md. Abdul Maleque
Professor
Department of Mathematics
BUET, Dhaka-1000
Member
- (iv) 
Dr. Md. Abdul Alim
Professor
Department of Mathematics
BUET, Dhaka-1000
Member
- (v) 
Dr. Md. Ashraf Uddin
Professor
Department of Mathematics
Shahjalal University of Science and Technology, Sylhet - 3114
Member
(External)

Declaration

I do hereby declaring that the present investigation in this thesis has been carried out in accordance with the regulations of the Bangladesh University of Engineering and Technology, Dhaka, Bangladesh. This investigation is original except where indicated by special reference in the text. To the best of my knowledge, no part of this thesis has been accepted for any degree or diploma to submit any other University either in the home or abroad.

No part of this thesis may be reproduced in any form or any other means except the written permission of the author.

Date: October 08, 2013

Md. Nasir Uddin
(Md. Nasir Uddin)

Contents

| | |
|--|----------------|
| Title Page----- | i |
| Board of Examiners----- | ii |
| Declaration----- | iii |
| Contents ----- | iv |
| List of Figures----- | v |
| Nomenclature----- | xii |
| Acknowledgements----- | xiv |
| Abstract----- | xv |
| Chapter 1 ----- | 1 - 24 |
| General Introduction | |
| 1.1 Uniform Flow and Steady Flow | 1 |
| 1.2 Compressible and Incompressible Flow | 2 |
| 1.3 Viscosity | 2 |
| 1.4 Modes of Heat Transfer | 3 |
| 1.5 Concept of Boundary Layers | 10 |
| 1.6 Dimensional Analysis | 16 |
| 1.7 Porous Medium | 23 |
| Chapter 2 ----- | 25 - 59 |
| Investigation of Double Diffusive Magnetohydrodynamic Mixed Convective Flow along an Inclined Flat Plate in a Porous Medium | |
| 2.1 Introduction | 25 |
| 2.2 Mathematical Analysis | 27 |
| 2.3 Numerical Solutions | 31 |
| 2.4 Comparison | 31 |
| 2.5 Results and Discussion | 32 |
| 2.6 Conclusions | 58 |
| Chapter 3 ----- | 60 - 91 |
| Investigation of Double Diffusive Magnetohydrodynamic Mixed Convective Flow with Thermodiffusion along an Inclined Flat Plate in a Porous Medium | |
| 3.1 Introduction | 60 |
| 3.2 Mathematical Analysis | 61 |
| 3.3 Numerical Solutions | 62 |
| 3.4 Comparison | 62 |
| 3.5 Results and Discussion | 63 |
| 3.6 Conclusions | 91 |
| Chapter 5 ----- | 92 - 93 |
| Concluding Remarks | 92 |
| References ----- | 94 - 95 |

List of Figures

| | | |
|-------------|--|----|
| Fig. 1.1 | Natural convection heat transfer from a hot body | 07 |
| Fig. 1.2 | Velocity boundary layer development on a flat plate | 11 |
| Fig. 1.3 | Thermal boundary layer developments on an isothermal flat plate. | 12 |
| Fig. 1.4 | Species concentration boundary layer development on a flat plate. | 14 |
| Fig. 1.5 | Schematic drawing of a porous medium filled with one or two fluids | 23 |
| Fig. 2.1 | Schematic view of flow configuration and coordinates system | 28 |
| Fig. 2.2 | Comparison of velocity distribution for $Gr_t = 2.0$, $Gr_m = 2.0$, $M = 0.5$, $Q = 0.5$, $K = 0.5$, $\alpha = 30^\circ$, $Pr = 0.71$, $f_w = 0.0$ and $Sc = 0.6$ | 31 |
| Fig. 2.3(a) | Representative velocity distribution for different values of fluid suction parameter f_w | 40 |
| Fig. 2.3(b) | Representative temperature distribution for different values of fluid suction parameter f_w | 40 |
| Fig. 2.3(c) | Representative concentration distribution for different values of fluid suction parameter f_w | 40 |
| Fig. 2.3(d) | Effect of fluid suction parameter f_w on local skin friction coefficient C_f against the streamwise distance x | 41 |
| Fig. 2.3(e) | Effect of fluid suction parameter f_w on local Nusselt number N_u against the streamwise distance x | 41 |
| Fig. 2.3(f) | Effect of fluid suction parameter f_w on local Sherwood number S_h against the streamwise distance x | 41 |
| Fig. 2.4(a) | Representative velocity distribution for different values of local thermal Grashof number Gr_t | 42 |
| Fig. 2.4(b) | Representative temperature distribution for different values of local thermal Grashof number Gr_t | 42 |
| Fig. 2.4(c) | Representative concentration distribution for different values of local thermal Grashof number Gr_t | 42 |
| Fig. 2.4(d) | Effect of local thermal Grashof number Gr_t on local skin friction coefficient C_f against the streamwise distance x | 43 |
| Fig. 2.4(e) | Effect of local thermal Grashof number Gr_t on local Nusselt number N_u against the streamwise distance x | 43 |
| Fig. 2.4(f) | Effect of local thermal Grashof number Gr_t on local Sherwood number S_h against the streamwise distance x | 43 |
| Fig. 2.5(a) | Representative velocity distribution for different values of local mass Grashof number Gr_m | 44 |

List of Figures

| | | |
|-------------|---|----|
| Fig. 2.5(b) | Representative temperature distribution for different values of local mass Grashof number Gr_m | 44 |
| Fig. 2.5(c) | Representative concentration distribution for different values of local mass Grashof number Gr_m | 44 |
| Fig. 2.5(d) | Effect of local mass Grashof number Gr_m on local skin friction coefficient C_f against the streamwise distance x | 45 |
| Fig. 2.5(e) | Effect of local mass Grashof number Gr_m on local Nusselt number N_u against the streamwise distance x | 45 |
| Fig. 2.5(f) | Effect of local mass Grashof number Gr_m on local Sherwood number S_h against the streamwise distance x | 45 |
| Fig. 2.6(a) | Representative velocity distribution for different values of magnetic field parameter M | 46 |
| Fig. 2.6(b) | Representative temperature distribution for different values of magnetic field parameter M | 46 |
| Fig. 2.6(c) | Representative concentration distribution for different values of magnetic field parameter M | 46 |
| Fig. 2.6(d) | Effect of magnetic field parameter M on local skin friction coefficient C_f against the streamwise distance x | 47 |
| Fig. 2.6(e) | Effect of magnetic field parameter M on local Nusselt number N_u against the streamwise distance x | 47 |
| Fig. 2.6(f) | Effect of magnetic field parameter M on local Sherwood number S_h against the streamwise distance x | 47 |
| Fig. 2.7(a) | Representative velocity distribution for different values of heat generation parameter Q | 48 |
| Fig. 2.7(b) | Representative temperature distribution for different values of heat generation parameter Q | 48 |
| Fig. 2.7(c) | Representative concentration distribution for different values of heat generation parameter Q | 48 |
| Fig. 2.7(d) | Effect of heat generation parameter Q on local skin friction coefficient C_f against the streamwise distance x | 49 |
| Fig. 2.7(e) | Effect of heat generation parameter Q on local Nusselt number N_u against the streamwise distance x | 49 |
| Fig. 2.7(f) | Effect of heat generation parameter Q on local Sherwood number S_h against the streamwise distance x | 49 |
| Fig. 2.8(a) | Representative velocity distribution for different values of permeability parameter K | 50 |
| Fig. 2.8(b) | Representative temperature distribution for different values of permeability parameter K | 50 |

List of Figures

| | | |
|--------------|--|----|
| Fig. 2.8(c) | Representative concentration distribution for different values of permeability parameter K | 50 |
| Fig. 2.8(d) | Effect of permeability parameter K on local skin friction coefficient C_f against the streamwise distance x | 51 |
| Fig. 2.8(e) | Effect of permeability parameter K on local Nusselt number N_u against the streamwise distance x | 51 |
| Fig. 2.8(f) | Effect of permeability parameter K on local Sherwood number S_h against the streamwise distance x | 51 |
| Fig. 2.9(a) | Representative velocity distribution for different values of angle of inclination α | 52 |
| Fig. 2.9(b) | Representative temperature distribution for different values of angle of inclination α | 52 |
| Fig. 2.9(c) | Representative concentration distribution for different values of angle of inclination α | 52 |
| Fig. 2.9(d) | Effect of angle of inclination α on local skin friction coefficient C_f against the streamwise distance x | 53 |
| Fig. 2.9(e) | Effect of angle of inclination α on local Nusselt number N_u against the streamwise distance x | 53 |
| Fig. 2.9(f) | Effect of angle of inclination α on local Sherwood number S_h against the streamwise distance x | 53 |
| Fig. 2.10(a) | Representative velocity distribution for different values of Prandtl number Pr | 54 |
| Fig. 2.10(b) | Representative temperature distribution for different values of Prandtl number Pr | 54 |
| Fig. 2.10(c) | Representative concentration distribution for different values of Prandtl number Pr | 54 |
| Fig. 2.10(d) | Effect of Prandtl number Pr on local skin friction coefficient C_f against the streamwise distance x | 55 |
| Fig. 2.10(e) | Effect of Prandtl number Pr on local Nusselt number N_u against the streamwise distance x | 55 |
| Fig. 2.10(f) | Effect of Prandtl number Pr on local Sherwood number S_h against the streamwise distance x | 55 |
| Fig. 2.11(a) | Representative velocity distribution for different values of Schmidt number Sc | 56 |
| Fig. 2.11(b) | Representative temperature distribution for different values of Schmidt number Sc | 56 |
| Fig. 2.11(c) | Representative concentration distribution for different values of Schmidt number Sc | 56 |

List of Figures

| | | |
|--------------|--|----|
| Fig. 2.11(d) | Effect of Schmidt number Sc on local skin friction coefficient C_f against the streamwise distance x | 57 |
| Fig. 2.11(e) | Effect of Schmidt number Sc on local Nusselt number N_u against the streamwise distance x | 57 |
| Fig. 2.11(f) | Effect of Schmidt number Sc on local Sherwood number S_h against the streamwise distance x | 57 |
| Fig. 3.1(a) | Representative velocity distribution for different values of fluid suction parameter f_w while $\tau = 0.10$ | 71 |
| Fig. 3.1(b) | Representative temperature distribution for different values of fluid suction parameter f_w while $\tau = 0.10$ | 71 |
| Fig. 3.1(c) | Representative concentration distribution for different values of fluid suction parameter f_w while $\tau = 0.10$ | 71 |
| Fig. 3.1(d) | Effect of fluid suction parameter f_w on local skin friction coefficient C_f against the streamwise distance x while $\tau = 0.10$ | 72 |
| Fig. 3.1(e) | Effect of fluid suction parameter f_w on local Nusselt number N_u against the streamwise distance x while $\tau = 0.10$ | 72 |
| Fig. 3.1(f) | Effect of fluid suction parameter f_w on local Sherwood number S_h against the streamwise distance x while $\tau = 0.10$ | 72 |
| Fig. 3.2(a) | Representative velocity distribution for different values of local thermal Grashof number Gr_t while $\tau = 0.10$ | 73 |
| Fig. 3.2(b) | Representative temperature distribution for different values of local thermal Grashof number Gr_t while $\tau = 0.10$ | 73 |
| Fig. 3.2(c) | Representative concentration distribution for different values of local thermal Grashof number Gr_t while $\tau = 0.10$ | 73 |
| Fig. 3.2(d) | Effect of local thermal Grashof number Gr_t on local skin friction coefficient C_f against the streamwise distance x while $\tau = 0.10$ | 74 |
| Fig. 3.2(e) | Effect of local thermal Grashof number Gr_t on local Nusselt number N_u against the streamwise distance x while $\tau = 0.10$ | 74 |
| Fig. 3.2(f) | Effect of local thermal Grashof number Gr_t on local Sherwood number S_h against the streamwise distance x while $\tau = 0.10$ | 74 |
| Fig. 3.3(a) | Representative velocity distribution for different values of local mass Grashof number Gr_m while $\tau = 0.10$ | 75 |
| Fig. 3.3(b) | Representative temperature distribution for different values of local mass Grashof number Gr_m while $\tau = 0.10$ | 75 |
| Fig. 3.3(c) | Representative concentration distribution for different values of local mass Grashof number Gr_m while $\tau = 0.10$ | 75 |

List of Figures

| | | |
|-------------|---|----|
| Fig. 3.3(d) | Effect of local mass Grashof number Gr_m on local skin friction coefficient C_f against the streamwise distance x while $\tau = 0.10$ | 76 |
| Fig. 3.3(e) | Effect of local mass Grashof number Gr_m on local Nusselt number N_u against the streamwise distance x while $\tau = 0.10$ | 76 |
| Fig. 3.3(f) | Effect of local mass Grashof number Gr_m on local Sherwood number S_h against the streamwise distance x while $\tau = 0.10$ | 76 |
| Fig. 3.4(a) | Representative velocity distribution for different values of magnetic field parameter M while $\tau = 0.10$ | 77 |
| Fig. 3.4(b) | Representative temperature distribution for different values of magnetic field parameter M while $\tau = 0.10$ | 77 |
| Fig. 3.4(c) | Representative concentration distribution for different values of magnetic field parameter M while $\tau = 0.10$ | 77 |
| Fig. 3.4(d) | Effect of magnetic field parameter M on local skin friction coefficient C_f against the streamwise distance x while $\tau = 0.10$ | 78 |
| Fig. 3.4(e) | Effect of magnetic field parameter M on local Nusselt number N_u against the streamwise distance x while $\tau = 0.10$ | 78 |
| Fig. 3.4(f) | Effect of magnetic field parameter M on local Sherwood number S_h against the streamwise distance x while $\tau = 0.10$ | 78 |
| Fig. 3.5(a) | Representative velocity distribution for different values of heat generation parameter Q while $\tau = 0.10$ | 79 |
| Fig. 3.5(b) | Representative temperature distribution for different values of heat generation parameter Q while $\tau = 0.10$ | 79 |
| Fig. 3.5(c) | Representative concentration distribution for different values of heat generation parameter Q while $\tau = 0.10$ | 79 |
| Fig. 3.5(d) | Effect of heat generation parameter Q on local skin friction coefficient C_f against the streamwise distance x while $\tau = 0.10$ | 80 |
| Fig. 3.5(e) | Effect of heat generation parameter Q on local Nusselt number N_u against the streamwise distance x while $\tau = 0.10$ | 80 |
| Fig. 3.5(f) | Effect of heat generation parameter Q on local Sherwood number S_h against the streamwise distance x while $\tau = 0.10$ | 80 |
| Fig. 3.6(a) | Representative velocity distribution for different values of permeability parameter K while $\tau = 0.10$ | 81 |
| Fig. 3.6(b) | Representative temperature distribution for different values of permeability parameter K while $\tau = 0.10$ | 81 |
| Fig. 3.6(c) | Representative concentration distribution for different values of permeability parameter K while $\tau = 0.10$ | 81 |
| Fig. 3.6(d) | Effect of permeability parameter K on local skin friction coefficient C_f against the streamwise distance x while $\tau = 0.10$ | 82 |

List of Figures

| | | |
|-------------|--|----|
| Fig. 3.6(e) | Effect of permeability parameter K on local Nusselt number N_u against the streamwise distance x while $\tau = 0.10$ | 82 |
| Fig. 3.6(f) | Effect of permeability parameter K on local Sherwood number S_h against the streamwise distance x while $\tau = 0.10$ | 82 |
| Fig. 3.7(a) | Representative velocity distribution for different values of angle of inclination α while $\tau = 0.10$ | 83 |
| Fig. 3.7(b) | Representative temperature distribution for different values of angle of inclination α while $\tau = 0.10$ | 83 |
| Fig. 3.7(c) | Representative concentration distribution for different values of angle of inclination α while $\tau = 0.10$ | 83 |
| Fig. 3.7(d) | Effect of angle of inclination α on local skin friction coefficient C_f against the streamwise distance x while $\tau = 0.10$ | 84 |
| Fig. 3.7(e) | Effect of angle of inclination α on local Nusselt number N_u against the streamwise distance x while $\tau = 0.10$ | 84 |
| Fig. 3.7(f) | Effect of angle of inclination α on local Sherwood number S_h against the streamwise distance x while $\tau = 0.10$ | 84 |
| Fig. 3.8(a) | Representative velocity distribution for different values of Prandtl number Pr while $\tau = 0.10$ | 85 |
| Fig. 3.8(b) | Representative temperature distribution for different values of Prandtl number Pr while $\tau = 0.10$ | 85 |
| Fig. 3.8(c) | Representative concentration distribution for different values of Prandtl number Pr while $\tau = 0.10$ | 85 |
| Fig. 3.8(d) | Effect of Prandtl number Pr on local skin friction coefficient C_f against the streamwise distance x while $\tau = 0.10$ | 86 |
| Fig. 3.8(e) | Effect of Prandtl number Pr on local Nusselt number N_u against the streamwise distance x while $\tau = 0.10$ | 86 |
| Fig. 3.8(f) | Effect of Prandtl number Pr on local Sherwood number S_h against the streamwise distance x while $\tau = 0.10$ | 86 |
| Fig. 3.9(a) | Representative velocity distribution for different values of Schmidt number Sc while $\tau = 0.10$ | 87 |
| Fig. 3.9(b) | Representative temperature distribution for different values of Schmidt number Sc while $\tau = 0.10$ | 87 |
| Fig. 3.9(c) | Representative concentration distribution for different values of Schmidt number Sc while $\tau = 0.10$ | 87 |
| Fig. 3.9(d) | Effect of Schmidt number Sc on local skin friction coefficient C_f against the streamwise distance x while $\tau = 0.10$ | 88 |
| Fig. 3.9(e) | Effect of Schmidt number Sc on local Nusselt number N_u against the streamwise distance x while $\tau = 0.10$ | 88 |

List of Figures

| | | |
|--------------|--|----|
| Fig. 3.9(f) | Effect of Schmidt number Sc on local Sherwood number S_h against the streamwise distance x while $\tau = 0.10$ | 88 |
| Fig. 3.10(a) | Representative velocity distribution for different values of thermophoretic parameter τ | 89 |
| Fig. 3.10(b) | Representative temperature distribution for different values of thermophoretic parameter τ | 89 |
| Fig. 3.10(c) | Representative concentration distribution for different values of thermophoretic parameter τ | 89 |
| Fig. 3.10(d) | Effect of thermophoretic parameter τ on local skin friction coefficient C_f against the streamwise distance x | 90 |
| Fig. 3.10(e) | Effect of thermophoretic parameter τ on local Nusselt number N_u against the streamwise distance x | 90 |
| Fig. 3.10(f) | Effect of thermophoretic parameter τ on local Sherwood number S_h against the streamwise distance x | 90 |

Nomenclature

| | |
|------------|--|
| B_0 | Applied magnetic field |
| C | Species, mass fraction or concentration |
| C_f | Local skin friction coefficient |
| C_p | Specific heat at constant pressure |
| D | Mass diffusivity |
| f | Reduced stream function or dimensionless stream function |
| f_w | Fluid suction or injection parameter |
| g | Acceleration due to gravity |
| Gr_t | Local thermal Grashof number |
| Gr_m | Local mass Grashof number |
| K | Permeability parameter |
| K^* | Permeability of the porous medium |
| k | Thermal conductivity |
| k_n | Knudsen number |
| M | Magnetic parameter |
| N_u | Local Nusselt number |
| Pr | Prandtl number |
| Q_0 | Heat generation constant |
| Q | Heat generation parameter |
| Re_x | Local Reynolds number |
| Sc | Schmidt number |
| S_h | Local Sherwood number |
| T | Temperature of the fluid in the boundary layer |
| T_{ref} | Reference temperature |
| U_∞ | Free stream velocity |
| u, v | Streamwise and normal velocity components, respectively |
| V_T | Thermophoretic velocity |
| $v_w(x)$ | Permeability of the porous plate |
| x, y | Coordinates along and normal to the inclined plate, respectively |

Greek Symbols

| | |
|-----------|--|
| α | Angle of inclination |
| β | Volumetric coefficient of thermal expansion |
| β^* | Volumetric coefficient of expansion with mass fraction |
| σ | Electrical conductivity |
| η | Similarity variable |
| ρ | Density of the fluid |
| ν | Kinematic viscosity of the fluid |
| θ | Dimensionless temperature |
| v | Dimensionless concentration |
| τ | Thermophoretic parameter |
| κ | Thermophoretic coefficient |
| μ | Dynamic viscosity of the fluid |
| ψ | Stream function |

Subscripts

| | |
|----------|------------------------------|
| w | Condition at the wall |
| ∞ | Condition at the free stream |

Superscript

| | |
|-------|--|
| “ ’ ” | Differentiation with respect to η |
|-------|--|

Acknowledgements

First of all, I would like to say *shukria* to Almighty ALLAH, *alhamdulillah* for giving me the ability to complete research work of such volume.

The success of any like as thesis depends largely on the encouragement and guidelines of many others. I take this opportunity to express my gratitude to the people who have been instrumental in the successful completion of this thesis.

I would like to express my gratitude and the deepest appreciation to my supervisor Professor Dr. M. M. Kamal Chowdhury for his useful comments, remarks and continuous encouragement through the learning process of this thesis. Without his encouragement and guidance, this thesis would not have been possible to complete. My special thanks to Professor Dr. M. A. Alim for the necessary support on the way.

I am extremely grateful to Professor Dr. Nooruddin Ahmed, Ex. Vice-Chancellor, Bangladesh University of Engineering and Technology, Dhaka, Mr. Md. Mydul Islam, Associate Professor, Govt. Azizul Haque College, Bogra and Mr. M. S. Alam, Deputy Director, University Grants Commission, Dhaka for their constant encouragement with valuable suggestions.

I take this opportunity to record my sincere thanks to all the faculty members of the Department of Mathematics for their encouragement with insightful comments. Furthermore I would also like to thanks to all the staff of the Department of Mathematics for all necessary help from the Department during my thesis.

My heartfelt appreciation goes to my respectful parents, elder and youngest sister with youngest brother for their unceasing encouragement, endless love and support during not only my thesis but also all the time of my life.

I also place on record, my sense of gratitude to one my friends Syed Asifur Rahman, all the references and all who, directly or indirectly, have lent their helping hand in this venture.

Abstract

An analysis is performed to study the momentum, heat and mass transfer characteristics of Magnetohydrodynamic mixed convective flow along an inclined flat plate in a porous medium on the basis of boundary layer approximations, neglecting and including the effect of thermodiffusion respectively. The fluid is assumed to be steady, incompressible and dense, and a uniform magnetic field is applied normal to the direction of the flow. A Similarity transformation is used to transform the momentum, energy and concentration equations under consideration into coupled nonlinear boundary layer equations which are then solved numerically using the Runge-Kutta sixth-order integration scheme together with Nachtsheim-Swigert shooting iteration technique. The behavior of the velocity, temperature, concentration, local skin-friction coefficient, local Nusselt number and local Sherwood number for different values of relevant parameters have been computed and the results are presented graphically, and analyzed thereafter. The validity of the numerical methodology is checked by comparing the results obtained for some specific cases with those available in the literature, and a comparatively good agreement is reached.

Chapter 1

General Introduction

Fluid mechanics is the branch of science which studies fluids such as liquids, gases and plasmas, and forces on them. The study of fluids at rest is the fluid statics and the study of fluids in motion is the fluid kinematics. The study of the effect of forces on fluid motion is the fluid dynamics. It has several sub disciplines of itself, including aerodynamics which is the study of air and other gases in motion and hydrodynamics which is the study of liquids in motion.

A number of fundamental properties of fluids and important modes which are related to the present investigations will be described in this chapter with references.

1.1 Uniform Flow and Steady Flow

Conditions in a body of fluid can vary from point to point and, at any given point, can vary from one moment of time to the next. Flow is described as uniform if the velocity at a given instant is the same in magnitude and direction at every point in the fluid. If, at the given instant, the velocity changes from point to point, the flow is described as non-uniform. In practice, when a fluid flows past a solid boundary there will be variations of velocity in the region close to the boundary. However, if the size and shape of the cross-section of the stream of fluid are constant, the flow is considered to be uniform.

A steady flow is one in which the velocity, pressure and cross-section of the stream may vary from point to point but do not change with time. If, at a given point, conditions do change with time, the flow is described as unsteady. In practice, there will always be slight variations of velocity and pressure, but, if the average values are constant, the flow is considered to be steady. There are four possible types of flow:

- 1) **Steady uniform flow:** Conditions do not change with position or time. The velocity and cross-sectional area of the stream of fluid are the same at each cross-section: for example, flow of a liquid through a pipe of uniform bore running completely full at constant velocity.

- 2) Steady non-uniform flow: Conditions change from point to point but not with time. The velocity and cross-sectional area of the stream may vary from cross-section to cross-section, but, for each cross-section, they will not vary with time: for example, flow of a liquid at a constant rate through a tapering pipe running completely full.
- 3) Unsteady uniform flow: At a given instant of time the velocity at every point is the same, but this velocity will change with time: for example, accelerating flow of a liquid through a pipe of uniform bore running full, such as would occur when a pump is started up.
- 4) Unsteady non-uniform flow: The cross-sectional area and velocity vary from point to point and also change with time: for example, a wave travelling along a channel.

1.2 Compressible and Incompressible Flow

All fluids are compressible, so that their density will change with pressure, but, under steady flow conditions and provided that the changes of density are small, it is often possible to simplify the analysis of a problem by assuming that the fluid is incompressible and of constant density. Since liquids are relatively difficult to compress, it is usual to treat them as if they were incompressible for all cases of steady flow. However, in unsteady flow conditions, high pressure differences can develop and the compressibility of liquids must be taken into account. Gases are easily compressed and, except when changes of pressure and, therefore, density are very small, the effects of compressibility and changes of internal energy must be taken into account.

1.3 Viscosity

A fluid at rest cannot resist shearing forces, and if such forces act on a fluid which is in contact with a solid boundary, the fluid will flow over the boundary in such a way that the particles immediately in contact with the boundary have the same velocity as the boundary, while successive layers of fluid parallel to the boundary move with increasing velocities. Shear stresses opposing the relative motion of these layers are set up, their magnitude depending on the velocity gradient from layer to layer. For

fluids obeying Newton's law of viscosity, taking the direction of motion as the x direction and v as the velocity of the fluid in the x direction at a distance y from the boundary, the shear stress in the x direction is given by

$$\tau = \mu \frac{dv}{dy}$$

1.3.1 Coefficient of Dynamic Viscosity

The coefficient of dynamic viscosity μ can be defined as the shear force per unit area (or shear stress τ) required dragging one layer of fluid with unit velocity past another layer a unit distance away from it in the fluid. Rearranging above equation

$$\mu = \frac{\tau}{\frac{dv}{dy}}$$

Units: Newton seconds per square meter (N s m^{-2}) or kilograms per meter per second ($\text{kg m}^{-1} \text{s}^{-1}$). (But note that the coefficient of viscosity is often measured in poise (P); $10 \text{ P} = 1 \text{ kg m}^{-1} \text{s}^{-1}$.)

Dimensions: $\text{ML}^{-1}\text{T}^{-1}$.

Typical values: water, $1.14 \times 10^{-3} \text{ kg m}^{-1} \text{s}^{-1}$; air, $1.78 \times 10^{-5} \text{ kg m}^{-1} \text{s}^{-1}$.

1.3.2 Kinematic Viscosity

The kinematic viscosity ν is defined as the ratio of dynamic viscosity to mass density:

$$\nu = \frac{\mu}{\rho}$$

Units: square meters per second ($\text{m}^2 \text{s}^{-1}$). (But note that kinematic viscosity is often measured in stokes (St); $10^4 \text{ St} = 1 \text{ m}^2 \text{s}^{-1}$.)

Dimensions: L^2T^{-1} .

Typical values: water, $1.14 \times 10^{-6} \text{ m}^2 \text{s}^{-1}$; air, $1.46 \times 10^{-5} \text{ m}^2 \text{s}^{-1}$.

1.4 Modes of Heat Transfer

The study of heat transfer is directed to (i) the estimation of rate of flow of energy as heat through the boundary of a system both under steady and transient conditions, and (ii) the determination of temperature field under steady and transient conditions, which also will provide the information about the gradient and time rate of change of

temperature at various locations and time, i.e. $T(x, y, z, \tau)$ and dT/dx , dT/dy , dT/dz , $dT/d\tau$ etc. These two are interrelated, one being dependent on the other. However explicit solutions may be generally required for one or the other.

The basic laws governing heat transfer and their application are as below:

- 1) First law of thermodynamics postulating the energy conservation principle:
This law provides the relation between the heat flow, energy stored and energy generated in a given system. The relationship for a closed system is: The net heat flow across the system boundary + heat generated inside the system = change in the internal energy, of the system. This will also apply for an open system with slight modifications. The change in internal energy in a given volume is equal to the product of volume density and specific heat ρcV and dT where the group ρcV is called the heat capacity of the system. The basic analysis in heat transfer always has to start with one of these relations.
- 2) The first law of thermodynamics is also known as the conservation of energy principal, which states that energy can neither be created nor destroyed during a process, it can only change forms.
- 3) The second law of thermodynamics establishing the direction of energy transport as heat. The law postulates that the flow of energy as heat through a system boundary will always be in the direction of lower temperature or along the negative temperature gradient.
- 4) Newton's laws of motion used in the determination of fluid flow parameters.
- 5) Law of conservation of mass, used in the determination of flow parameters.
- 6) The rate equations as applicable to the particular mode of heat transfer.

1.4.1 Conduction

Conduction is the mode of energy transfer as heat due to temperature difference within a body or between bodies in thermal contact without the involvement of mass flow and mixing.

A cup of hot coffee is an example of heat transfer by conduction. The exposed end of a metal spoon suddenly immersed in a cup of hot coffee is eventually warmed due to the conduction of energy through the spoon. On a winter day, there is significant energy loss from a heated room to the outside air. This loss is principally due to

conduction heat transfer through the wall that separates the room air from the outside air.

Heat transfer processes can be quantified in terms of appropriate rate equations. These equations may be used to compute the amount of energy being transferred per unit time. For heat conduction, the rate equation is known as Fourier's law.

Fourier's law of heat conduction states that the rate of heat flow by conduction is proportional to the temperature difference across the layer and the heat transfer area but inversely proportional to the thickness of the boundary. The proportionality constant obtained in the relation is known as thermal conductivity, k , of the material. The mathematical formulation is given in equation:

$$\text{Heat flow, } Q = -kA \, dT/dx$$

where Q is the heat-transfer rate in the x direction, in Watts (W); A is the area normal to the direction of heat flow, in m^2 ; dT/dx is the temperature gradient in the x direction, in K/m ; and k is the thermal conductivity, in $\text{W}/(\text{mK})$ and the minus sign is a consequence of the fact that heat is transferred in the direction of decreasing temperature. The above equation can be written as

$$Q/A = -k \, dT/dx$$

Where the ratio Q/A , having the dimensions of W/m^2 , is referred to as the heat flux in the x direction that is, the rate of heat transfer per *unit area*.

1.4.2 Thermal Conductivity

Thermal Conductivity of a material is a measure of the ability of the material to conduct heat. It is the constant of proportionality in Fourier's equation and plays an important role in heat transfer. The unit in SI system for conductivity is W/mK .

Thermal conductivity varies with temperature. In good conductors, thermal conductivity decreases with temperature due to impedance to electron flow of higher electron densities. In insulators, as temperature increases, thermal atomic activity also increases and hence thermal conductivity increases with temperature. In the case of gases, thermal conductivity increases with temperature due to increased random activity of atoms and molecules.

1.4.3 Convection

In conduction, energy is transferred as heat either due to free electron flux or lattice vibration. There is no movement of mass in the direction of energy flow. Convection is the transfer of heat between a solid surface and a fluid flowing in contact with it and it involves the combined effects of conduction and fluid motion. The process of heat transfer between a surface and a fluid flowing in contact with it is called convection.

In convection, energy flow occurs at the surface purely by conduction. But in the next layers both conduction and diffusion-mass movement in the molecular level or macroscopic level occurs. Due to the mass movement, the rate of energy transfer is higher. Higher the rate of mass movement, higher will be the heat flow rate.

The rate equation for convective heat transfer was first expressed by Newton in 1701, and is referred to as the Newton's „law“ of cooling. This equation is

$$Q = hA(T_w - T_\infty)$$

where Q is the rate of convective heat transfer, in W; A is the area normal to direction of heat flow, in m^2 ; T_w is the surface temperature and T_∞ is the fluid temperature of the free stream, $(T_w - T_\infty)$ is the temperature difference between surface and fluid, in K; and h is the convective heat transfer coefficient, in W/m^2K .

The heat flux by convection is, $Q/A = h (T_w - T_\infty)$

Considering that the heat transfer from the solid surface to the fluid layer adjacent to the surface is by pure conduction, since the fluid layer is motionless, and it can be expressed as

$$Q/A = -k (dT/dy)_{y=0}$$

where T represents the temperature distribution in the fluid and $(dT/dy)_{y=0}$ is the temperature gradient at the surface. Heat is then convected away from a surface as a result of fluid motion.

Combining above equations, we obtain an equation for convection coefficient as

$$h = -k (dT/dy)_{y=0} / (T_w - T_\infty)$$

1.4.4 Natural Convection

Natural convection is a mechanism, or type of heat transport, in which the fluid motion is not generated by any external source (like a pump, fan, suction device, etc.) but only by density differences in the fluid occurring due to temperature gradients. In natural convection, fluid surrounding a heat source receives heat, becomes less dense and rises. The surrounding, cooler fluid then moves to replace it. This cooler fluid is then heated and the process continues, forming convection current; this process transfers heat energy from the bottom of the convection cell to top. The driving force for natural convection is buoyancy, a result of differences in fluid density. Because of this, the presence of a proper acceleration such as arises from resistance to gravity, or an equivalent force (arising from acceleration, centrifugal force or Coriolis effect), is essential for natural convection. For example, natural convection essentially does not operate in free-fall (inertial) environments, such as that of the orbiting International Space Station, where other heat transfer mechanisms are required to prevent electronic components from overheating. For example, the cooling of a boiled egg in a cooler environment is by natural convection.

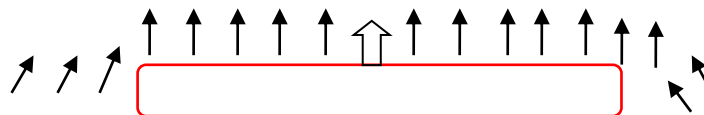


Fig. 1.1: Natural convection heat transfer from a hot body

The temperature of the air adjacent to the hot object is higher, thus its density is lower. As a result, the heated air rises. This movement is called the natural convection current. Note that in the absence of this movement, heat transfer would be by conduction only and its rate would be much lower.

In a gravitational field, there is a net force that pushes a light fluid placed in a heavier fluid upwards. This force is called the buoyancy force.

1.4.5 Forced Convection

Forced convection is a mechanism, or type of transport in which fluid motion is generated by an external source (like a pump, fan, suction device, etc.). It should be considered as one of the main methods of useful heat transfer as significant amounts of heat energy can be transported very efficiently and this mechanism is found very

commonly in everyday life, including central heating, air conditioning, steam turbines and in many other machines. Forced convection is often encountered in engineering problems for designing or analyzing heat exchangers, pipe flow, and flow over a plate at a different temperature than the stream (the case of a shuttle wing during re-entry, for example). However, in any forced convection situation, some amount of natural convection is always present whenever there are g-forces present (i.e., unless the system is in free fall). When the natural convection is not negligible, such flows are typically referred to as mixed convection.

1.4.6 Mixed Convection

Combined forced convection and natural convection, or mixed convection, occurs when natural convection and forced convection mechanisms act together to transfer heat. This is also defined as situations where both pressure forces and buoyant forces interact. How much each form of convection contributes to the heat transfer is largely determined by the flow, temperature, geometry, and orientation. The nature of the fluid is also influential, since the Grashof constant increases in a fluid as temperature increases, but is maximized at some point for a gas.

Because of the wide range of variables, hundreds of papers have been published for experiments involving various types of fluids and geometries. This variety makes a comprehensive correlation difficult to obtain, and when it is, it is usually for very limited cases. Combined forced and natural convection, however, can be generally described in one of three ways.

The first case is when natural convection aids forced convection. This is seen when the buoyant motion is in the same direction as the forced motion, thus enhancing the heat transfer. An example of this would be a fan blowing upward on a hot plate. Since heat naturally rises, the air being forced upward over the plate adds to the heat transfer.

The second case is when natural convection acts in the opposite way of the forced convection. Consider a fan forcing air upward over a cold plate. In this case, the buoyancy force of the cold air naturally causes it to fall, but the air being forced upward opposes this natural motion, keeping the cool air hovering around the cold plate. This, in turn, diminishes the amount of heat transfer.

The third case is referred to as transverse flow. This occurs when the buoyant motion acts perpendicular to the forced motion. This enhances fluid mixing, and enhances the heat transfer. An example of this is air flowing horizontally over a hot or cold pipe. This can encourage phase changes, which often creates a very high heat transfer coefficient. For example, steam leaving a boiler can pass through a pipe that has a fan blowing over it, cooling the steam back to a saturated liquid.

While it may seem like it is possible to simply add or subtract the heat transfer values to or from each other, this will yield inaccurate results. In order to determine the total heat transfer, experimental data has suggested that

$$Nu_{\text{combined}} = (Nu_{\text{forced}}^n \pm Nu_{\text{natural}}^n)^{1/n}$$

where the plus sign is for cases where heat transfer is assisted (i.e. case one and three) and the minus sign is for when it is hindered (i.e. case two). The value of n ranges between 3 and 4 as the geometry aligns from vertically to horizontally respectively.

Combined forced and natural convection is often seen in very-high-power-output devices where the forced convection is not enough to dissipate all of the heat necessary. At this point, combining natural convection with forced convection will often deliver the desired results. Examples of these processes are nuclear reactor technology and some aspects of electronic cooling.

When analyzing potentially mixed convection, a parameter called the Archimedes number (Ar) parameterizes the relative strength of free and forced convection. The Archimedes number is the ratio of Grashof number (Gr) and the square of Reynolds number (Re), which represents the ratio of buoyancy force and inertia force, and which stands in for the contribution of natural convection.

$$Ar = \frac{Gr}{Re^2}$$

When $Ar \gg 1$, natural convection dominates and when $Ar \ll 1$, forced convection dominates.

1.4.7 Radiation

Radiation is the transfer of heat from one object to another by means of electromagnetic waves. Radiative heat transfer does not require that objects be in contact or that a fluid flow between those objects. Radiative heat transfer occurs in the void of space (that's how the sun warms us).

The rate equation is due to Stefan-Boltzmann law which states that heat radiated is proportional to the fourth power of the absolute temperature of the surface and heat transfer rate between surfaces is given as

$$Q = F \sigma A (T_1^4 - T_2^4)$$

where, F is a factor depending on geometry and surface properties, σ is Stefan Boltzmann constant $5.67 \times 10^{-8} \text{ W/m}^2\text{K}^4$ (SI units) A is m^2 , and $T_1, T_2 \rightarrow \text{K}$ (only absolute unit of temperature to be used).

People in a room at 72°F air temperature may feel uncomfortably cold if the walls and ceiling are at 50°F . Conversely, they may feel uncomfortably warm if the walls are 85°F . Even though the air temperature is the same in both cases, the radiative cooling or warming of their bodies relative to the walls and ceiling will affect their comfort level (people sense heat loss or gain, not temperature).

1.5 Concept of Boundary Layers

The concept of boundary layers is central to the understanding of convection heat and mass transfer between a surface and a fluid flowing past it. In this section, velocity, thermal, and concentration boundary layers are described, and their relationships to the friction coefficient, convection heat transfer coefficient, and convection mass transfer coefficient are introduced.

1.5.1 The Velocity Boundary Layer

To introduce the concept of a boundary layer, consider flow over the flat plate of Fig. 1.2. When fluid particles make contact with the surface, their velocity is reduced significantly relative to the fluid velocity upstream of the plate, and for most situations it is valid to assume that the particle velocity is zero at the wall.

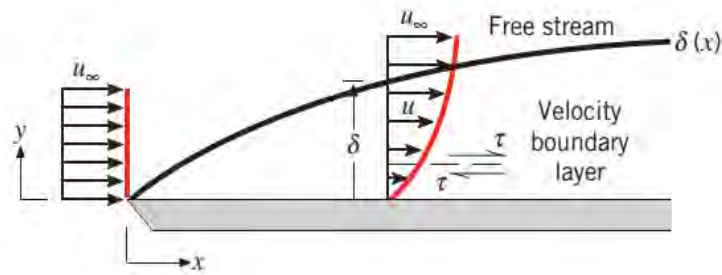


Fig. 1.2: Velocity boundary layer development on a flat plate

These particles then act to retard the motion of particles in the adjoining fluid layer, which act to retard the motion of particles in the next layer, and so on until, at a distance $y=\delta$ from the surface, the effect becomes negligible. This retardation of fluid motion is associated with shear stresses τ acting in planes that are parallel to the fluid velocity (Fig.1.2). With increasing distance y from the surface, the x velocity component of the fluid, u , must then increase until it approaches the free stream value u_∞ . The subscript ∞ is used to designate conditions in the free stream outside the boundary layer.

The quantity is termed the boundary layer thickness, and it is typically defined as the value of y for which $u = 0.99u_\infty$. The boundary layer velocity profile refers to the manner in which u varies with y through the boundary layer. Accordingly, the fluid flow is characterized by two distinct regions, a thin fluid layer (the boundary layer) in which velocity gradients and shear stresses are large and a region outside the boundary layer in which velocity gradients and shear stresses are negligible. With increasing distance from the leading edge, the effects of viscosity penetrate farther into the free stream and the boundary layer grows (δ increases with x). Because it pertains to the fluid velocity, the foregoing boundary layer may be referred to more specifically as the velocity boundary layer. It develops whenever there is fluid flow over a surface, and it is of fundamental importance to problems involving convection transport. In fluid mechanics its significance to the engineer stems from its relation to the surface shear stress τ_s , and hence to surface frictional effects. For external flows it provides the basis for determining the local friction coefficient

$$C_f = \frac{\tau_s}{\rho u_\infty^2 / 2}$$

a key dimensionless parameter from which the surface frictional drag may be determined. Assuming a Newtonian fluid, the surface shear stress may be evaluated from knowledge of the velocity gradient at the surface

$$\tau_s = \mu \left(\frac{\partial u}{\partial y} \right)_{y=0}$$

Where μ is a fluid property known as the dynamic viscosity. In a velocity boundary layer, the velocity gradient at the surface depends on the distance x from the leading edge of the plate. Therefore, the surface shear stress and friction coefficient also depend on x .

1.5.2 The Thermal Boundary Layer

Just as a velocity boundary layer develops when there is fluid flow over a surface, a thermal boundary layer must develop if the fluid free stream and surface temperatures differ. Consider flow over an isothermal flat plate. At the leading edge the temperature profile is uniform, with $T(y) = T_\infty$.

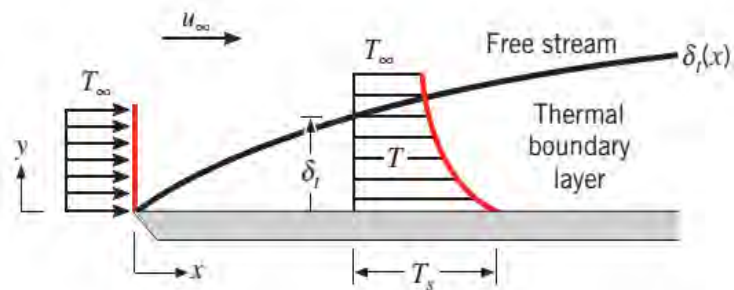


Fig. 1.3: Thermal boundary layer developments on an isothermal flat plate

However, fluid particles that come into contact with the plate achieve thermal equilibrium at the plate's surface temperature. In turn, these particles exchange energy with those in the adjoining fluid layer, and temperature gradients develop in the fluid. The region of the fluid in which these temperature gradients exist is the thermal boundary layer, and its thickness δ_t is typically defined as the value of y for which the ratio $[(T_s - T)/(T_s - T_\infty)] = 0.99$. With increasing distance from the leading edge, the effects of heat transfer penetrate farther into the free stream and the thermal boundary layer grows.

The relation between conditions in this boundary layer and the convection heat transfer coefficient may readily be demonstrated. At any distance x from the leading edge, the local surface heat flux may be obtained by applying Fourier's law to the fluid at $y = 0$. That is,

$$q_s'' = -K_f \left(\frac{\partial T}{\partial y} \right)_{y=0}$$

The subscript s has been used to emphasize that this is the surface heat flux, but it will be dropped in later sections. This expression is appropriate because, at the surface, there is no fluid motion and energy transfer occurs only by conduction. Recalling Newton's law of cooling, we see that

$$q_s'' = h(T_s - T_\infty)$$

and combining above two equations, we obtain

$$h = \frac{-K_f \left(\frac{\partial T}{\partial y} \right)_{y=0}}{(T_s - T_\infty)}$$

Hence, conditions in the thermal boundary layer, which strongly influence the wall temperature gradient $\left(\frac{\partial T}{\partial y} \right)_{y=0}$, determine the rate of heat transfer across the boundary layer. Since $(T_s - T_\infty)$ is a constant, independent of x , while δ_t increases with increasing x , temperature gradients in the boundary layer must decrease with increasing x . Accordingly, the magnitude of $\left(\frac{\partial T}{\partial y} \right)_{y=0}$, decreases with increasing x , and it follows that q_s and h decrease with increasing x .

1.5.3 The Concentration Boundary Layer

When air moves past the surface of a pool of water, the liquid water will evaporate, and water vapor will be transferred into the airstream. This is an example of convection mass transfer. More generally, consider a binary mixture of chemical species A and B that flows over a surface.

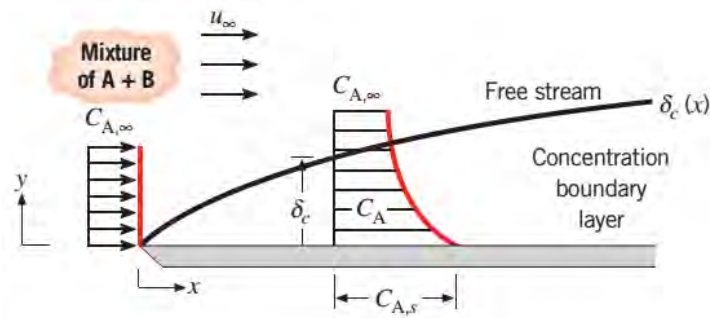


Fig. 1.4: Species concentration boundary layer development on a flat plate

The molar concentration (kmol/m^3) of species A at the surface is $C_{A,s}$, and in the free stream it is $C_{A,\infty}$. If $C_{A,s}$ differs from $C_{A,\infty}$, transfer of species A by convection will occur. For example, species A could be a vapor that is transferred into a gas stream (species B) due to evaporation at a liquid surface (as in the water example) or due to sublimation at a solid surface. In this situation, a concentration boundary layer will develop that is similar to the velocity and thermal boundary layers. The concentration boundary layer is the region of the fluid in which concentration gradients exist, and its thickness δ_c is typically defined as the value of y for which $[(C_{A,s} - C_A)/(C_{A,s} - C_{A,\infty})] = 0.99$. With increasing distance from the leading edge, the effects of species transfer penetrate farther into the free stream and the concentration boundary layer grows.

Species transfer by convection between the surface and the free stream fluid is determined by conditions in the boundary layer, and we are interested in determining the rate at which this transfer occurs. In particular, we are interested in the molar flux of species A , N_A'' (kmol/s.m^2). It is helpful to recognize that the molar flux associated with species transfer by diffusion is determined by an expression that is analogous to Fourier's law. For the conditions of interest in this chapter, the expression, which is termed Fick's law, has the form

$$N_A'' = -D_{AB} \frac{\partial C_A}{\partial y}$$

where, D_{AB} is a property of the binary mixture known as the binary diffusion coefficient. At any point corresponding to $y > 0$ in the concentration boundary layer of Figure 6.3, species transfer is due to both bulk fluid motion (advection) and diffusion. However, absent nanoormicroscale effects and the influence of species

diffusion on the velocity normal to the surface, fluid motion at the surface can be neglected. Accordingly, species transfer at the surface is only by diffusion and applying Fick's law at $y = 0$, the molar flux is

$$N''_{A,s} = -D_{AB} \left(\frac{\partial C_A}{\partial y} \right)_{y=0}$$

The subscript s has been used to emphasize that this is the molar flux at the surface, but it will be dropped in later sections. Analogous to Newton's law of cooling, an equation can be written that relates the molar flux to the concentration difference across the boundary layer, as

$$N''_{A,s} = h_m (C_{A,s} - C_{A,\infty})$$

Where h_m (m/s) is the convection mass transfer coefficient, analogous to the convection heat transfer coefficient. Combining above equations, we obtain

$$h_m = \frac{-D_{AB} \left(\frac{\partial C_A}{\partial y} \right)_{y=0}}{(C_{A,s} - C_{A,\infty})}$$

Therefore, conditions in the concentration boundary layer, which strongly influence the surface concentration gradient $\left(\frac{\partial C_A}{\partial y} \right)_{y=0}$, also influence the convection mass transfer coefficient and hence the rate of species transfer in the boundary layer.

1.5.4 Significance of the Boundary Layers:

For flow over any surface, there will always exist a velocity boundary layer and hence surface friction. Likewise, a thermal boundary layer, and hence convection heat transfer, will always exist if the surface and free stream temperatures differ. Similarly, a concentration boundary layer and convection mass transfer will exist if the fluid's species concentration at the surface differs from its species concentration in the free stream. The velocity boundary layer is of extent $\delta(x)$ and is characterized by the presence of velocity gradients and shear stresses. The thermal boundary layer is of extent $\delta_t(x)$ and is characterized by temperature gradients and heat transfer. Finally, the concentration boundary layer is of extent $\delta_c(x)$ and is characterized by concentration gradients and species transfer. Situations can arise in which all three

boundary layers are present. In such cases, the boundary layers rarely grow at the same rate, and the values of δ , δ_b , and δ_c at a given location are not the same.

For the engineer, the principal manifestations of the three boundary layers are, respectively, surface friction, convection heat transfer, and convection mass transfer. The key boundary layer parameters are then the friction coefficient C_f and the heat and mass transfer convection coefficients h and h_m , respectively.

1.5.5 Boundary Layer Thicknesses

So far the boundary layer thickness has been referred to only in physical terms; namely, boundary layer thickness is defined as that distance from the surface where the local velocity equals 99 percent of the free stream velocity

$$\delta = y_{(u=.99u_\infty)}$$

where, u_∞ is the free stream velocity. It is possible, however, to define boundary layer thickness in terms of the effect on the flow.

1.6 Dimensional Analysis

The roots of fluid mechanics lie in the experimental investigation of the mechanisms of fluid flow. In order to determine the form of the dependence of one variable upon a range of other controlling parameters in the absence of an analytical solution it is necessary to undertake an experimental investigation; however, simply recording the effect of one variable on another with all others held constant and repeating until all the possible combinations are exhausted is not an option, in terms neither of time nor the utility of the outcome. Dimensional analysis offers a route out of this dilemma by allowing the identification of groups of variables whose interrelationships may be determined experimentally. Dimensional analysis therefore offers a qualitative route to the understanding of fluid flow mechanisms; the quantitative understanding is provided experimentally.

1.6.1 Dimensions and Units

Any physical situation involving an object or a system may be described in terms of its fundamental properties, which must include its possible mass, length (which

obviously also describes its area and volume), velocity or acceleration (combinations of length and time), or density (based on mass and length) or the forces or stresses acting on the system (defined in terms of mass, length and time). Similarly, thermodynamic and electrical properties may also be included. These properties of the system are fundamental and universal and are known as its dimensions.

While dimensions are universal, units are chosen as convenient and therefore have a long history, from the ancient cubit (allegedly based on the length of the forearm), or rural distances measured by the number of cigarettes smoked on the journey between villages, to the modern standard kilometre or light year. Modern units therefore provide a convenient and standardized measure of the dimension under consideration so that conversions between different measures of the same dimension are possible.

A physical property, such as density or mass per unit volume, may thus be defined in terms of its dimensions as $[ML^{-3}]$, where the $[]$ brackets indicate that we are only interested in the qualitative dimensions of the property and not its quantitative value. The units for density would be expressed in the system of units currently in place, which in SI terms are kg/m^3 .

1.6.2 Reynolds Number

In fluid mechanics, the Reynolds number (Re) is a dimensionless number that gives a measure of the ratio of inertial forces to viscous forces and consequently quantifies the relative importance of these two types of forces for given flow conditions.

The Reynolds number is defined as

$$Re = \frac{\text{inertial forces}}{\text{viscous forces}}$$

$$= \frac{vL}{\nu}$$

where,

v is the mean velocity of the object relative to the fluid (SI units: m/s)

L is a characteristic linear dimension, (travelled length of the fluid; hydraulic diameter when dealing with river systems) (m)

ν is the kinematic viscosity (m^2/s)

The concept was introduced by George Gabriel Stokes in 1851, but the Reynolds number is named after Osborne Reynolds (1842–1912), who popularized its use in 1883.

Reynolds numbers frequently arise when performing dimensional analysis of fluid dynamics problems, and as such can be used to determine dynamic similitude between different experimental cases.

They are also used to characterize different flow regimes, such as laminar or turbulent flow: laminar flow occurs at low Reynolds numbers, where viscous forces are dominant, and is characterized by smooth, constant fluid motion; turbulent flow occurs at high Reynolds numbers and is dominated by inertial forces, which tend to produce chaotic eddies, vortices and other flow instabilities.

The Reynolds number can be used to determine if flow is laminar, transient or turbulent. The flow is (for flat plate)

- laminar when $Re < 2300$
- transient when $2300 < Re < 4000$
- turbulent when $Re > 4000$

1.6.3 Grashof Number

The Grashof number (Gr) is a dimensionless number in fluid dynamics and heat transfer which approximates the ratio of the buoyancy to viscous force acting on a fluid. It is named after the German engineer Franz Grashof.

For vertical flat plates,

$$Gr_L = \frac{g\beta(T_s - T_\infty)L^3}{\nu^2}$$

For pipes,

$$Gr_D = \frac{g\beta(T_s - T_\infty)D^3}{\nu^2}$$

For bluff bodies,

$$Gr_D = \frac{g\beta(T_s - T_\infty)D^3}{\nu^2}$$

where, the L and D subscripts indicates the length scale basis for the Grashof number

g = acceleration due to Earth's gravity

β = volumetric thermal expansion coefficient (equal to approximately $1/T$, for ideal fluids, where T is absolute temperature)

T_s = surface temperature

T_∞ = bulk temperature

L = length

D = diameter

ν = kinematic viscosity

At higher Grashof numbers, the boundary layer is turbulent; at lower Grashof numbers, the boundary layer is laminar.

The product of the Grashof number and the Prandtl number gives the Rayleigh number, a dimensionless number that characterizes convection problems in heat transfer.

1.6.4 Knudsen Number

The Knudsen number (k_n) is a dimensionless number defined as the ratio of the molecular mean free path length to a representative physical length scale.

$$k_n = \lambda / L$$

where,

λ = mean free path [L^1]

L = representative physical length scale [L^1].

This length scale could be, for example, the radius of the body in a fluid. The number is named after Danish physicist Martin Knudsen (1871–1949).

For particle dynamics in the atmosphere, and assuming standard temperature and pressure, i.e. 25 °C and 1 atm, we have $\lambda \approx 8 \times 10^{-8}$ m.

1.6.5 Prandtl Number

The Prandtl number Pr is a dimensionless number; the ratio of momentum diffusivity (kinematic viscosity) to thermal diffusivity. It is named after the German physicist Ludwig Prandtl.

It is defined as:

$$\text{Pr} = \frac{\nu}{\alpha} = \frac{\text{viscous diffusion rate}}{\text{thermal diffusion rate}} = \frac{c_p \mu}{k}$$

where,

$$\nu(\text{kinematic viscosity}) = \mu/\rho \quad (\text{SI units : m}^2/\text{s})$$

$$\alpha(\text{thermal diffusivity}) = k/(\rho c_p) \quad (\text{SI units : m}^2/\text{s})$$

$$\mu(\text{dynamic viscosity}), \quad (\text{SI units : Pa s} = \text{N s/m}^2)$$

$$k(\text{thermal conductivity}), \quad (\text{SI units : W/(mK)})$$

$$c_p(\text{specific heat}), \quad (\text{SI units : J/(kg K)})$$

$$\rho(\text{density}), \quad (\text{SI units : kg/m}^3)$$

Note that whereas the Reynolds number and Grashof number are subscripted with a length scale variable, the Prandtl number contains no such length scale in its definition and is dependent only on the fluid and the fluid state. As such, the Prandtl number is often found in property tables alongside other properties such as viscosity and thermal conductivity.

Typical values for Pr are:

- around 0.015 for mercury
- around 0.16-0.7 for mixtures of noble gases or noble gases with hydrogen
- around 0.7-0.8 for air and many other gases,
- between 4 and 5 for R-12 refrigerant
- around 7 for water (At 20 degrees Celsius)
- 13.4 and 7.2 for seawater (At 0 degrees Celsius and 20 degrees Celsius respectively)
- between 100 and 40,000 for engine oil
- around 1×10^{25} for Earth's mantle.

For mercury, heat conduction is very effective compared to convection: thermal diffusivity is dominant. For engine oil, convection is very effective in transferring energy from an area, compared to pure conduction: momentum diffusivity is dominant.

In heat transfer problems, the Prandtl number controls the relative thickness of the momentum and thermal boundary layers. When Pr is small, it means that the heat diffuses very quickly compared to the velocity (momentum). This means that for liquid metals the thickness of the thermal boundary layer is much bigger than the velocity boundary layer. The mass transfer analog of the Prandtl number is the Schmidt number.

1.6.6 Schmidt Number

The Schmidt number is a dimensionless number defined as the ratio of momentum diffusivity (viscosity) and mass diffusivity, and is used to characterize fluid flows in which there are simultaneous momentum and mass diffusion convection processes. It was named after the German engineer Ernst Heinrich Wilhelm Schmidt (1892-1975).

Schmidt number is the ratio of the shear component for diffusivity viscosity/density to the diffusivity for mass transfer D . It physically relates the relative thickness of the hydrodynamic layer and mass-transfer boundary layer.

It is defined as:

$$Sc = \frac{\nu}{D} = \frac{\mu}{\rho D} = \frac{\text{viscous diffusion rate}}{\text{molecular (mass) diffusion rate}}$$

where,

$$\nu(\text{kinematic viscosity}) = \mu/\rho \quad (\text{SI units : m}^2/\text{s})$$

$$D(\text{mass diffusivity}), \quad (\text{SI units : m}^2/\text{s})$$

$$\mu(\text{dynamic viscosity}), \quad (\text{SI units : N s/m}^2)$$

$$\rho(\text{density}), \quad (\text{SI units : kg/m}^3)$$

The heat transfer analog of the Schmidt number is the Prandtl number.

1.6.7 Nusselt Number

In heat transfer at a boundary (surface) within a fluid, the Nusselt number is the ratio of convective to conductive heat transfer across (normal to) the boundary. In this context, convection includes both advection and conduction. Named after Wilhelm

Nusselt, it is a dimensionless number. The conductive component is measured under the same conditions as the heat convection but with a (hypothetically) stagnant (or motionless) fluid.

A Nusselt number close to one, namely convection and conduction of similar magnitude, is characteristic of "slug flow" or laminar flow. A larger Nusselt number corresponds to more active convection, with turbulent flow typically in the 100–1000 range.

The convection and conduction heat flows are parallel to each other and to the surface normal of the boundary surface, and are all perpendicular to the mean fluid flow in the simple case.

$$\text{Nu}_L = \frac{\text{Convective heat transfer}}{\text{Conductive heat transfer}} = \frac{hL}{k_f}$$

where,

L = characteristic length

k_f = thermal conductivity of the fluid

h = convective heat transfer coefficient

The mass transfer analog of the Nusselt number is the Sherwood number.

1.6.8 Sherwood Number

The Sherwood number, **Sh** (also called the mass transfer Nusselt number) is a dimensionless number used in mass-transfer operation. It represents the ratio of convective to diffusive mass transport, and is named in honor of Thomas Kilgore Sherwood.

It is defined as follows

$$\text{Sh} = \frac{K \cdot L}{D} = \frac{\text{Convective mass transfer coefficient}}{\text{Diffusive mass transfer coefficient}}$$

where,

L is a characteristic length (m)

D is mass diffusivity ($\text{m}^2 \cdot \text{s}^{-1}$)

K is the mass transfer coefficient ($\text{m} \cdot \text{s}^{-1}$)

1.7 Porous Medium

A porous medium is a body composed of a persistent solid part, called solid matrix, and the remaining void space (or pore space) that can be filled with one or more fluids (e. g. water, oil and gas).

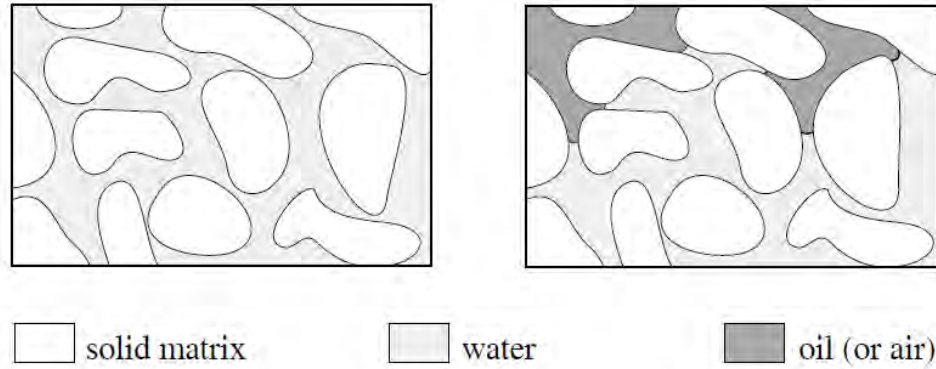


Fig.1.5: Schematic drawing of a porous medium filled with one or two fluids

The concept of porous media is used in many areas of applied science and engineering: filtration, mechanics (acoustics, geomechanics, soil mechanics, rock mechanics), engineering (petroleum engineering, bio-remediation, construction engineering), geosciences (hydrogeology, petroleum geology, geophysics), biology and biophysics, material science, etc. Fluid flow through porous media is a subject of most common interest and has emerged a separate field of study. Typical examples of a porous medium are soil, sand, cemented sandstone, foam rubber, bread, lungs or kidneys.

1.7.1 Permeability

Permeability is the single-phase fluid conductivity of a porous material. The equation that defines permeability in terms of measurable quantities is Darcy's law. Consider an incompressible fluid, with viscosity μ , which is forced to flow, at flow rate q , through a porous medium, of length L and with cross section A , such that the pressure difference across the length of the porous medium is ΔP . Then the permeability K of the material is defined as:

$$K = \frac{q\mu L}{A\Delta P}$$

The value of the permeability is determined by the structure of the porous rock. A tight rock, with small pore diameter will have in general a smaller permeability than a coarse rock with larger pores. From above equation, it is seen that K has dimensions of length squared. The unit most widely employed for the permeability is the Darcy (D); $1 \text{ D} \approx (1 \mu\text{m})^2 = 10^{-12} \text{ m}^2$.

All of the above definitions in this chapter are defined by different author. The fluid flow such as uniform flow, steady flow, incompressible and compressible flow, and viscosity, coefficient of dynamic viscosity, kinematic viscosity, boundary layer thickness, dimensional analysis and dimensions are defined by Douglas et al. [9]. Modes of heat transfer such as conduction, thermal conductivity, convection and radiation are defined by Kothandaraman [10] whereas natural convection, forced convection and mixed convection are defined in references [18, 15, and 14]. The concepts of boundary layers like as velocity, thermal and concentration boundary layers with significance are described by the author Bergman et al. [6]. The dimensionless numbers such as Reynolds number, Grashof number, Knudsen number, Prandtl number, Schmidt number, Nusselt number and Sherwood number are reported by references [21, 16, 17, 20, 22, 19 and 23]. The definition of permeability is defined by reference [24].

Chapter 2

Investigation of Double Diffusive Magnetohydrodynamic Mixed Convective Flow along an Inclined Flat Plate in a Porous Medium

2.1 Introduction

Magnetohydrodynamics (MHD) is a branch of the science that concerns the dynamics of magnetic fields in electrically conducting fluids, e.g. in ionised gases (sometimes called plasmas) such as the solar atmosphere and liquid metals (such as mercury, gallium, sodium or molten iron). The word magnetohydrodynamics is derived from magneto- meaning magnetic field, hydro- meaning water (or liquid) and -dynamics referring to the movement of an object by forces. Synonyms of MHD that are less frequently used are the terms magnetofluidynamics and hydromagnetics. One of the most famous scholars associated with MHD was the Swedish physicist Hannes Alfvén (1908-1995), who received the Nobel Prize in Physics, 1970 for fundamental work and discoveries in magnetohydrodynamics with fruitful applications in different parts of plasma physics.

Magnetohydrodynamics occurs when a conducting fluid flows in the presence of a magnetic field. The presence of magnetic fields leads to forces that in turn act on the fluid (typically a plasma), thereby potentially altering the geometry (or topology) and strength of the magnetic fields themselves. A key issue for a particular conducting fluid is the relative strength of the advecting motions in the fluid, compared to the diffusive effects caused by the electrical resistivity. Other topics belonging to the fundamental framework of magnetohydrodynamics include, e.g. MHD turbulence, MHD waves (Alfvén waves), magneto-convection, MHD reconnection, and hydromagnetic dynamo theory.

In many engineering fields, MHD is employed to study, e.g., the magnetic behavior of plasmas in fusion reactors, liquid-metal cooling of nuclear reactors, electromagnetic casting, petroleum industries, boundary layer control in aerodynamics, MHD generators, crystal growth, Ship propulsion, Jet printers and so on. Moreover the study of MHD is largely concerned with the flow, heat and mass transfer characteristics in various physical situations.

An analysis of heat and mass transfer in MHD flow by natural convection from a permeable, inclined surface with variable wall temperature and concentration, taking into consideration the effects of ohmic heating and viscous dissipation is investigated by Chen et al. [8]. In this paper, the results are presented for the major governing parameters including the magnetic parameter, and in presence of magnetic field, the velocity is found to decrease whereas the temperature and concentration increase. Alam et al. [2] studied the problem of combined free-forced convection and mass transfer flow over a vertical porous flat plate, in presence of heat generation and thermal diffusion. In this paper, the author showed the effects of suction parameter, heat generation parameter and Soret number on the flow field of a hydrogen-air mixture as a non-chemical reacting fluid pair, and observed that the flow field is significantly influenced by these parameters. The effects of thermophoresis and chemical reaction on unsteady hydromagnetic free convection and mass transfer flow past an impulsively started infinite inclined porous plate in the presence of heat generation/absorption has been examined by Alam et al. [3], and then dimensionless velocity, temperature and concentration profiles are displayed graphically for different parameters entering into the flow field. The author Alam et al. [3] reported that all the hydrodynamics, thermal as well as concentration boundary layers decrease with the increasing values of suction parameter. Alam et al. [4] also investigated the effects of thermophoresis and the homogeneous chemical reactions of first order on magnetohydrodynamics mixed convective flow past a heated inclined permeable flat plate in the presence of heat generation or absorption considering the viscous dissipation and Joule heating. The author, Alam et al. [4] considered the chemical reaction but the chemical reaction effect has been neglected from the momentum equation. Also the similarity solutions were presented neglecting the effects of Grashof number or Richardson number for mixed convection.

MHD mixed convective heat transfer about a semi-infinite inclined plate in the presence of magneto and thermal radiation effects has been examined by Aydin et al. [5]. The effects of the mixed convection parameter, the angle of inclination, the magnetic parameter and the radiation conduction parameter are discussed on the velocity and the temperature profiles as well as the local skin friction and the local

heat transfer parameters by Aydin et al. [5]. From this numerical investigation, the author reported that, an increase in the angle of inclination, decrease the local skin friction and the local heat transfer parameters. Reddy et al. [12] analyzed a steady two-dimensional MHD free convection and mass transfer flow past an inclined semi-infinite vertical surface in the presence of heat generation in a porous medium. The author considered the porous medium but an opportunity is to extend this work by including the fluid suction effects for a porous plate. In their analysis, a set of ordinary differential equations has been derived for the conservation of mass, momentum and species diffusion in the boundary layer and transformed these equations into nondimensional form using similarity transformations, and showed that the velocity as well as concentration decreases with an increase in the Schmidt number.

As mentioned above, it is more reasonable to include the chemical reaction effects on the momentum to explore the impact of the momentum, heat and mass transfer characteristics with a transverse applied magnetic field. Therefore, in the light of above literatures, the aim of the present work is to investigate the problem of double diffusive magnetohydrodynamic mixed convective flow along an inclined flat plate in a porous medium, including the effects of fluid suction. The velocity, temperature, and concentration distributions are presented for various governing parameters which are of physical interest such as magnetic parameter, heat generation parameter, fluid suction parameter, permeability parameter, local thermal Grashof number, local mass Grashof number, Prandtl number and Schmidt number. Also the effects of various entering parameters on the local skin friction, the Nusselt number, and the Sherwood number are presented against the streamwise distance.

2.2 Mathematical Analysis

A steady two-dimensional MHD laminar mixed convective flow of a viscous, incompressible electrically conducting fluid along a semi-infinite inclined porous plate with an acute angle α to the vertical is considered. The physical coordinates (x,y) are chosen such that x is measured from the leading edge in the streamwise direction and y is measured normal to the inclined plate. The velocity components in the direction of flow and normal to the flow are u and v respectively. A magnetic

field of uniform strength B_0 is applied normal to the direction of flow. The external flow with a uniform velocity U_∞ takes place in the direction parallel to the inclined plate. It is assumed that T and C are the temperature and concentration of the fluid which are the same, everywhere in the fluid. The surface is maintained at a constant temperature T_w , which is higher than the constant temperature T_∞ of the surrounding fluid and the concentration C_w , is greater than the constant concentration C_∞ .

The schematic view of flow configuration and coordinates system is shown in Fig. 2.1.

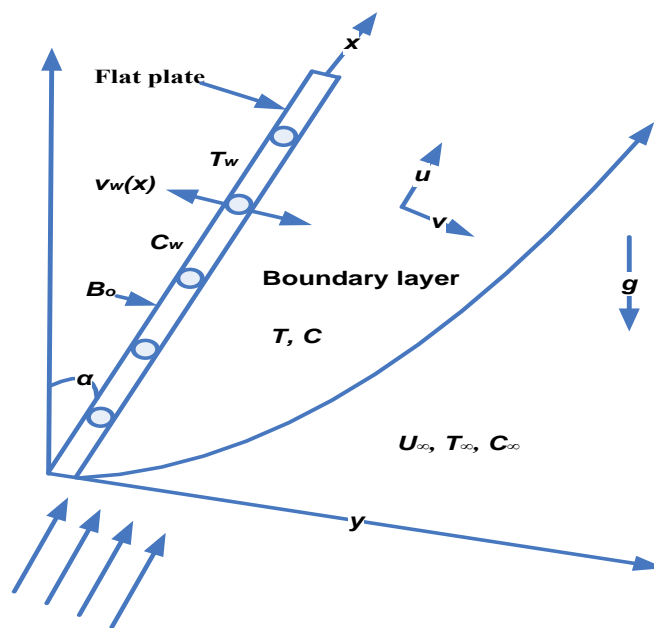


Fig. 2.1: Schematic view of flow configuration and coordinates system

Under the usual Boussinesq approximation, the governing equations for steady, two-dimensional, laminar boundary layer flow with the above assumptions are as follows:

Continuity equation:

$$\frac{\partial u}{\partial x} + \frac{\partial v}{\partial y} = 0 \quad (2.1)$$

Momentum equation:

$$u \frac{\partial u}{\partial x} + v \frac{\partial u}{\partial y} = \nu \frac{\partial^2 u}{\partial y^2} + g\beta(T - T_\infty)\cos\alpha + g\beta^*(C - C_\infty)\cos\alpha - \frac{\sigma B_0^2}{\rho}u - \frac{\nu}{K^*}u \quad (2.2)$$

Energy equation:

$$u \frac{\partial T}{\partial x} + v \frac{\partial T}{\partial y} = \frac{k}{\rho c_p} \frac{\partial^2 T}{\partial y^2} + \frac{Q_0}{\rho c_p} (T - T_\infty) \quad (2.3)$$

Concentration equation:

$$u \frac{\partial C}{\partial x} + v \frac{\partial C}{\partial y} = D \frac{\partial^2 C}{\partial y^2} \quad (2.4)$$

In the above equations, ν is the kinematic viscosity, g is the acceleration due to gravity, β is the volumetric coefficient of thermal expansion, β^* is the volumetric coefficient of expansion with mass fraction, σ is the electrical conductivity, K^* is permeability of the porous medium, ρ is the density of the fluid, k is the thermal conductivity of the fluid, c_p is the specific heat at constant pressure, Q_0 is the heat generation constant and D is the mass diffusivity. The appropriate boundary conditions for the velocity, temperature and concentration of this problem are as follows:

$$u = 0, \quad v = \pm v_w(x), \quad T = T_w, \quad C = C_w \quad \text{at } y = 0 \quad (2.5.1)$$

$$u = U_\infty, \quad T = T_\infty, \quad C = C_\infty \quad \text{as } y \rightarrow \infty \quad (2.5.2)$$

In addition, U_∞ is the free stream velocity and $v_w(x)$ represent the permeability of the porous plate where its sign indicates suction (< 0) or blowing (> 0), subscripts w and ∞ refer to the wall and boundary layer edge, respectively. To facilitate the analysis, the governing differential equations are to be made nondimensional with suitable transformations and the following dimensionless variables defined by Cebeci et al. [7] are introduced:

$$\eta = y \sqrt{\frac{U_\infty}{\nu x}}, \quad \psi = \sqrt{\nu x U_\infty} f(\eta) \quad (2.6.1)$$

$$\theta(\eta) = \frac{T - T_\infty}{T_w - T_\infty}, \quad \phi(\eta) = \frac{C - C_\infty}{C_w - C_\infty} \quad (2.6.2)$$

where, $\psi(x, y)$ is the stream function defined by $u = \partial\psi/\partial y$ and $v = -\partial\psi/\partial x$, such that the continuity equation (1) is satisfied automatically.

In terms of these new variables, the velocity components can be expressed as:

$$u = U_\infty f'(\eta) \quad (2.7)$$

$$\text{and } v = \frac{1}{2} \sqrt{\frac{\nu U_\infty}{x}} (\eta f' - f) \quad (2.8)$$

Here, the prime stands for ordinary differentiation with respect to similarity variable η .

Using dimensionless variables, the transformed momentum, energy, and concentration equations together with the boundary conditions can be written as:

$$f''' + \frac{1}{2} f f'' + Gr_t \theta \cos \alpha + Gr_m \phi \cos \alpha - (M + K) f' = 0 \quad (2.9)$$

$$\theta'' + \frac{1}{2} Pr f \theta' + Pr Q \theta = 0 \quad (2.10)$$

$$\phi'' + \frac{1}{2} Sc f \phi' = 0 \quad (2.11)$$

with the boundary conditions:

$$f = f_w, \quad f' = 0, \quad \theta = 1, \quad \phi = 1 \quad \text{at } \eta = 0 \quad (2.12.1)$$

$$f' \rightarrow 1, \quad \theta \rightarrow 0, \quad \phi \rightarrow 0 \quad \text{as } \eta \rightarrow \infty \quad (2.12.2)$$

where, $f_w = -v_w(x) \sqrt{\frac{x}{\nu U_\infty}}$ is the nondimensional wall mass transfer coefficient

such that $f_w > 0$ indicates wall suction and $f_w < 0$ indicates wall injection or blowing. The corresponding dimensionless groups that appear in the nondimensional form of governing equations are defined as:

$$Gr_t = \frac{g\beta(T_w - T_\infty)x}{U_\infty^2}, \quad Gr_m = \frac{g\beta^*(C_w - C_\infty)x}{U_\infty^2}, \quad M = \frac{\sigma B_0^2 x}{\rho U_\infty},$$

$$K = \frac{\nu x}{K^* U_\infty}, \quad Pr = \frac{\nu \rho c_p}{k}, \quad Q = \frac{Q_0 x}{\rho c_p U_\infty}, \quad Sc = \frac{\nu}{D} \quad (2.13)$$

where, Gr_t is the local thermal Grashof number, Gr_m is the local mass Grashof number, M is the magnetic field parameter, K is the permeability parameter, Pr is the Prandtl number, Q is the heat generation parameter and Sc is the Schmidt number.

By employing the definition of wall shear stress $\tau_w = \mu \left(\frac{\partial u}{\partial y}\right)_{y=0}$, along with Fourier's law $q_w = -k \left(\frac{\partial T}{\partial y}\right)_{y=0}$ and Fick's law $J_s = -D \left(\frac{\partial C}{\partial y}\right)_{y=0}$, the nondimensional forms of local skin-friction coefficient is $C_f = 2 (Re)^{-1/2} f'(0)$,

local Nusselt number is $N_u = - (Re)^{1/2} \theta'(0)$, and local Sherwood number is $S_h = - (Re)^{1/2} \phi'(0)$, where $Re_x = \frac{xU_\infty}{\nu}$ is denoting the local Reynolds number.

2.3 Numerical Solutions

The system of transformed nonlinear ordinary differential Eqns. (2.9) – (2.11), together with the boundary conditions Eqns. (2.12.1) and (2.12.2) have been solved numerically using Nachtsheim-Swigert shooting iteration technique along with sixth order Runge-Kutta initial value solver. The numerical methods have been described in details, referring to Nachtsheim and Swigert [11] and Alam et al. [2].

2.4 Comparison

For the accuracy of the numerical results, the present study is compared with the previous study Reddy et al. [12] as shown in Fig. 2.2.

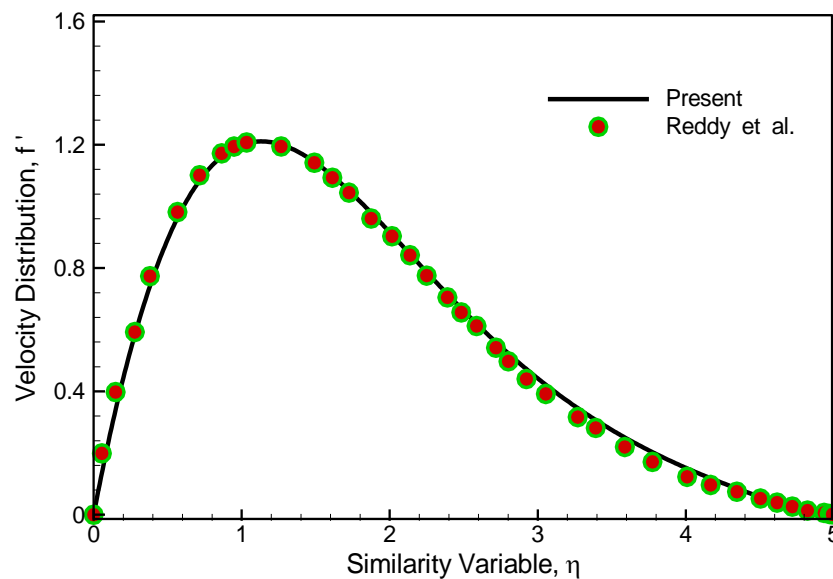


Fig. 2.2: Comparison of velocity distribution for $Gr_t = 2.0$, $Gr_m = 2.0$, $M = 0.5$, $Q = 0.5$, $K = 0.5$, $\alpha = 30^\circ$, $Pr = 0.71$, $f_w = 0.0$ and $Sc = 0.6$

It is observed that the present results are in good agreement with that of Reddy et al. [12]. This favorable comparison leads confidence in the numerical results to be reported in the next sections.

2.5 Results and Discussion

The aim of the present investigation is to investigate the flow, heat and mass transfer characteristics for the MHD mixed convective flow along an inclined flat plate in a porous medium. A spacious set of numerical results which is obtained by solving nonlinear ordinary differential equations is reported graphically. The numerical results for velocity, temperature, and concentration distributions as well as the local skin friction, the local Nusselt number, and the local Sherwood number have been carried out using different values of the various physical parameters. The set of considered values of the various physical parameters occurring into the problem for numerical investigation are $Gr_t = 0.87$, $Gr_m = 0.87$, $M = 0.005$, $Q = 0.50$, $K = 0.01$, $\alpha = 30^\circ$, $Pr = 0.71$, $f_w = 1.00$, $Sc = 0.78$ and $U_\infty / \nu = 1.0$ unless otherwise specified. The value of Prandtl number Pr is taken to be 0.71 which is corresponds physically to air and the values of Schmidt number Sc are taken 0.60, 0.78 and 0.94 for water vapor (H_2O), ammonia (NH_3) and carbon dioxide (CO_2) respectively. The effects of the above various physical parameters on the flow field are analyzed and discussed in the following subsections with the help of velocity, temperature, concentration distributions as well as the local skin friction, the local Nusselt number, and the local Sherwood number.

2.5.1 Effect of suction parameter (f_w) on flow field:

The influence of the suction parameter f_w ($f_w = 0.00, 1.00$ and 2.00) on the velocity, temperature and concentration distributions as well as the local skin friction coefficient, the local Nusselt number, and the local Sherwood number are presented in Figs. 2.3(a) - 2.3(f) keeping other parameters of the flow field constant. It is observed from Fig. 2.3(a) that the velocity of the flow field decreases with the increase of fluid suction. This is because of the fact that as the fluid suction through the plate increases, the plate is cooled down and the viscosity of the flowing fluid increases. Therefore, the velocity of the flow field decreases as the fluid suction increases. With regards to the temperature distribution in Fig. 2.3(b), it is found that in presence of the fluid suction, the temperature of the flow field decreases as the plate is cooled down due to fluid suction through the plate increases. On the basis of the concentration distribution in Fig. 2.3(c), it is seen that the concentration of the

flow field at all points decreases as the fluid suction increases, because the larger fluid suction leads to cooling of the plate. Figures 2.3(d) - 2.3(f) depict the local skin friction coefficient, the local Nusselt number, and the local Sherwood number against the streamwise distance x . The local skin friction coefficient C_f increases as the fluid suction increases causing the viscosity of the flowing fluid increases which is observed in Fig. 2.3(d). On the other hand both the local Nusselt number and the local Sherwood number increase with the increase of fluid suction parameter due to increase in temperature and concentration difference respectively, which are observed in Fig. 2.3(e) and Fig. 2.3(f).

2.5.2 Effect of local thermal Grashof number (Gr_t) on flow field:

The effect of the thermal Grashof number Gr_t ($Gr_t = 0.57, 0.87$ and 1.17) on the velocity, temperature and concentration distributions as well as the local skin friction coefficient, the local Nusselt number, and the local Sherwood number are presented in Figs. 2.4(a) - 2.4(f) keeping other parameters of the flow field constant. The local thermal Grashof number Gr_t ascertains the ratio of thermal buoyancy force to the viscous hydrodynamic force. From Fig. 2.4(a), it is observed that the fluid velocity increases due to the enhancement of the thermal buoyancy force which is expected. As the local thermal Grashof number increases, the peak values of the velocity increases rapidly near the plate and then decreases smoothly to approach the free stream velocity. According to the temperature distribution in Fig. 2.4(b), it is reported that an increase in the local thermal Grashof number, decrease the temperature of the flow field. The fact is that the positive values of local thermal Grashof number correspond to cooling of the porous plate. The concentration distribution which is presented in Fig. 2.4(c) decreases with the increasing values of local thermal Grashof number. As the local thermal Grashof number increases, the species difference increases and therefore, the concentration of the flow field decreases. The variation of the local skin friction coefficient, the local Nusselt number, and the local Sherwood number against the streamwise distance x are shown in Figs. 2.4(d) - 2.4(f). It is observed that the local skin friction coefficient, the local Nusselt number and the local Sherwood number increase due to increase in the local thermal Grashof number i.e. increase in velocity of the flow field whereas decrease in temperature and concentration of the flow field.

2.5.3 Effect of local mass Grashof number (Gr_m) on flow field:

The impact of the mass Grashof number Gr_m ($Gr_m = 0.57, 0.87$ and 1.17) on the velocity, temperature and concentration distributions as well as the local skin friction coefficient, the local Nusselt number, and the local Sherwood number are plotted in Figs. 2.4(a) - 2.4(f) while all other parameters of the flow field are kept fixed. The local mass Grashof number Gr_m ascertains the ratio of species buoyancy force to the viscous hydrodynamic force. With regards to the velocity distribution in Fig. 2.5(a), it is found that the velocity boundary layer thickness increases in the presence of growing local mass Grashof number because the presence of growing local mass Grashof number leads to increase the species buoyancy force. As the local mass Grashof number increases, the peak values of the velocity increases rapidly in the vicinity of the plate and then decreases smoothly to approach the free stream velocity. From the temperature and concentration distributions in Figs. 2.5(b) - 2.5(c), it is seen that both the temperature and concentration of the flow field decrease with the increase in local mass Grashof number. As the local mass Grashof number increases, the temperature and species difference increases and therefore, the temperature as well as concentration of the flow field decreases. Figures 2.5(d) - 2.5(f) reveal the effect of the local skin friction coefficient, the local Nusselt number, and the local Sherwood number against the streamwise distance x . From these Figs., it is observed that the local skin friction coefficient, local Nusselt number and local Sherwood number increase with increase in the local mass Grashof number i.e. increase in velocity of the flow field whereas decrease in temperature and concentration of the flow field.

2.5.4 Effect of magnetic field parameter (M) on flow field:

The behavior of the velocity, temperature and concentration as well as local skin friction, local Nusselt number and local Sherwood number on the flow field for different values of magnetic field parameter M ($M = 0.005, 0.015,$ and 0.025) are illustrated in Figs. 2.6(a) - 2.6(f) while other parameters are constant. The existence of magnetic field, normal to the flow of electrically conducting fluid generates a force called the Lorentz force, which acts against the flow. Thus the velocity of the flow field decreases with the increase of the magnetic field parameter as observed in

Fig. 2.6(a). Moreover the velocity boundary layer thickness decreases with the increase in magnetic field parameter. In Fig. 2.6(b), the temperature distribution is found to increase due to increase in the magnetic field strength. This is because of the applied magnetic field which tends to heat the fluid due to electromagnetic work, thus reduces the heat transfer from the wall. According to the concentration distribution in Fig. 2.6(c), it is reported that in presence of an increasing magnetic field parameter, the concentration of the flow field changes insignificantly. The nature of local skin friction coefficient, local Nusselt number, and local Sherwood number in presence of magnetic field parameter against the streamwise distance x are shown in Figs. 2.6(d) – 2.6(f). In Fig. 2.6(d), the local skin friction coefficient is found to decrease due to increase in the magnetic field parameter. The reason for this is that, the applied magnetic field tends to impede the flow motion and thus to reduce the surface friction force. The local Nusselt number which is plotted in Fig. 2.6(e) decreases with the increase of magnetic field parameter. As in presence of increasing magnetic field, the temperature gradient at the wall decreases which in turn leads to a reduction in the rate of heat transfer from the surface. An observation of local Sherwood number in Fig. 2.6(f), it is seen that the local Sherwood number changes insignificantly with the increase of magnetic field parameter.

2.5.5 Effect of heat generation parameter (Q) on flow field:

The variation of the velocity, temperature and concentration as well as local skin friction, local Nusselt number and local Sherwood number on the flow field with the flow parameters like as heat generation parameter Q ($Q = 0.00, 0.25, \text{ and } 0.50$) are shown in Figs. 2.7(a) - 2.7(f) while all other parameters remain unchanged. It is observed from Fig. 2.7(a) that, when heat is generated the buoyancy force increases, which induces the flow rate to increase, giving rise to the increase in the velocity of the flow field. Moreover the velocity boundary layer thickness within the boundary layer increases with the increase in heat generation parameter. With regards to the temperature distribution in Fig. 2.7(b), it is found that the temperature distribution increases with the increase of the heat generation parameter Q because the presence of a heat source on the flow field, the thermal state of the fluid increases causing the thermal boundary layer to increase. In the case that the strength of the heat source is relatively large, the maximum fluid temperature does not occur at the surface of the

plate, but rather in the fluid region close to it. From Fig. 2.7(c), the concentration distribution is observed as changes insignificantly with the increase in heat generation parameter. Figures 2.7(d) – 2.7(f) reveal the effect of heat generation parameter on the local skin friction coefficient, the local Nusselt number, and the local Sherwood number in the boundary layer against the streamwise distance x . It is noted that the local skin friction coefficient increases whereas the local Nusselt number decreases due to increase in the heat generation parameter, and however the local Sherwood number changes insignificantly.

2.5.6 Effect of permeability parameter (K) on flow field:

The effect of the permeability parameter K ($K = 0.01, 0.03$ and 0.05) on the velocity, temperature and concentration distributions as well as the local skin friction coefficient, the local Nusselt number, and the local Sherwood number are displayed in Figs. 2.8(a) - 2.8(f) keeping other parameters of the flow field fixed. On the basis of the velocity distribution in Fig. 2.8(a), it is seen that the velocity of the flow field within the velocity boundary layer decreases as the permeability of the porous medium increases. Also the velocity boundary layer thickness is found to decrease as growing in the permeability of the porous medium parameter. An observation of the temperature distribution is in Fig. 2.8(b), the temperature and the thermal boundary layer thickness of the flow field increase due to increase in the permeability of the porous medium parameter. On the other hand the concentration of the flow field increases slowly with the increase of permeability of the porous medium parameter as observed in Fig.2.8(c). Figs. 2.8(d) – 2.8(f) show the influence of permeability of the porous medium on the local skin friction coefficient, the local Nusselt number, and the local Sherwood number against the streamwise distance x . In Figs. 2.8(d) – 2.8(f), it is found that all of the local skin friction coefficient, the local Nusselt number and the local Sherwood number decrease with the increase of permeability of the porous medium parameter.

2.5.7 Effect of angle of inclination (α) on flow field:

Figures 2.9(a) - 2.9(f) reveal the behavior of the velocity, temperature and concentration as well as the local skin friction, the local Nusselt number and the local Sherwood number on the flow field for different angle of inclination α ($\alpha = 0^\circ, 30^\circ,$

and 45°) while all other parameters of the flow field are kept constant. From Fig. 2.9(a), it is seen that the velocity of the flow field inside the hydrodynamic boundary layer decreases with increasing the angle of inclination. The fact is that, as the angle of inclination increases, the effect of the buoyancy force decreases due to thermal and mass diffusion by a factor of $\cos\alpha$. Consequently, the driving force to the fluid decreases as a result the velocity of the fluid decreases. With regards to the temperature distribution in Fig. 2.9(b), increasing the angle of inclination, the temperature of the flow field and thermal boundary layer thickness increase with an accompanying decrease in the wall temperature gradient. The fact is that as the plate is inclined from the vertical to a large angular position, the reduction in the buoyancy force. From the concentration distribution in Fig. 2.9(c), the concentration gradient at the wall is seen to decrease as the buoyancy force decreases, with an associated concentration of the flow field and the concentration boundary layer thickness increase for increasing the angle of inclination. In order to examine the impact of angle of inclination on the flow field, the local skin friction coefficient, the local Nusselt number, and the local Sherwood number against the streamwise distance x are presented in Figs. 2.9(d) – 2.9(f). By inspection of this Figs. 2.9(d) – 2.9(f), it can be concluded that all of the local skin friction coefficient, the local Nusselt number, and the local Sherwood number decrease in presence of growing angle of inclination. This behavior is clear from the fact that as the plate is tilted from the vertical toward the horizontal; the buoyancy force effect diminishes by a factor of $\cos\alpha$ as the angle of inclination increases.

2.5.8 Effect of Prandtl number (Pr) on flow field:

The nature of the velocity, temperature and concentration as well as the local skin friction, the local Nusselt number and the local Sherwood number on the flow field in presence of different Prandtl number Pr ($Pr = 0.51, 0.71, \text{ and } 1.00$) are presented in Figs. 2.10(a) – 2.10(f) keeping other parameters of the flow field constant. The Prandtl number is a dimensionless number and defined by the ratio of momentum diffusivity (kinematic viscosity) to thermal diffusivity. The velocity distribution of the flow field which is presented in Fig. 2.10(a) is found to decrease as the Prandtl number increases. The reason is that when the Prandtl number increases, the momentum diffusivity of the flow field increases and as a results the velocity as well

as the hydrodynamic boundary layer thickness decrease. As observation of the temperature and concentration distributions which are presented in Fig. 2.10(b) and Fig. 2.10(c), the temperature of the flow field as well as the thermal boundary layer thickness decreases whereas the concentration of the flow field increases insignificantly due to increase in the Prandtl number. Figures 2.10(d) - 2.10(f) reveal the effect of the local skin friction coefficient, the local Nusselt number, and the local Sherwood number against the streamwise distance x . In Fig. 2.10(d) and Fig. 2.10(f), it is observed that the local skin friction coefficient as well as the local Sherwood number decrease with increase of Prandtl number. It is evident from Fig. 2.10(e) that the local Nusselt number increases while the Prandtl number increases. This is because of as the Prandtl number increases, the thermal boundary layer thickness decreases and the wall temperature gradient increases.

2.5.9 Effect of Schmidt number (Sc) on flow field:

Keeping all other parameters of the flow field constant except Schmidt number, Figs. 2.11(a) – 2.11(f) reveal the influence of Schmidt number Sc ($Sc = 0.60, 0.78,$ and 0.94) on the velocity, temperature and concentration distributions as well as the local skin friction coefficient, the local Nusselt number, and the local Sherwood number against the streamwise distance x . The Schmidt number embodies the ratio of the momentum to the mass diffusivity. The Schmidt number therefore quantifies the relative effectiveness of momentum and mass transport by diffusion in the hydrodynamic and concentration boundary layer. From Fig. 2.11(a), it can be seen that when the Schmidt number increases, the velocity of the flow field decreases because in presence of heavier diffusing species. On the other hand the temperature distribution which is presented in Figs. 2.11(b) changes insignificantly compared to the velocity of the flow field. The concentration distribution of the flow field in Fig. 2.11(c) is found to decrease as the diffusing species becomes heavier, and this leads to decrease in concentration of the flow field in the concentration boundary layer. In order to examine the impact of Schmidt number on the flow field, the local skin friction coefficient, the local Nusselt number, and the local Sherwood number against the streamwise distance x are displayed in Figs. 2.11(d) – 2.11(f). As indicated in Fig. 2.11(d), an increase in the Schmidt number produces a decrease in the local skin friction coefficient, as expected. Also it can be seen from Fig. 2.11(e) that the local

Nusselt number decreases with the increase of Schmidt number. However, with regards to the local Sherwood number in Fig. 2.11(f), it is found to increase the local Sherwood number in presence of the raising Schmidt number, as expected.

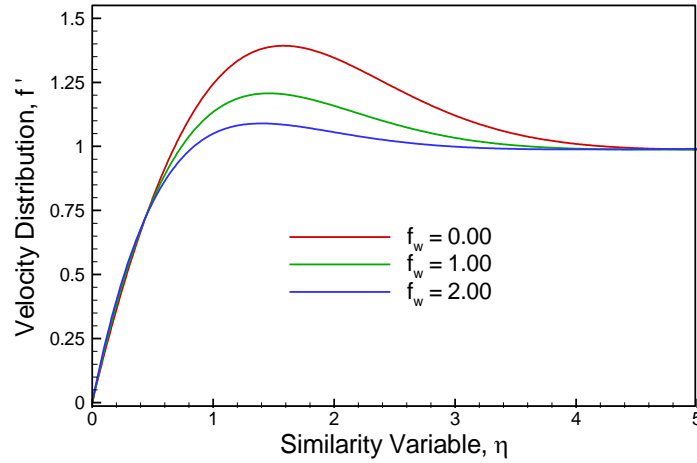


Fig. 2.3(a): Representative velocity distribution for different values of fluid suction parameter f_w

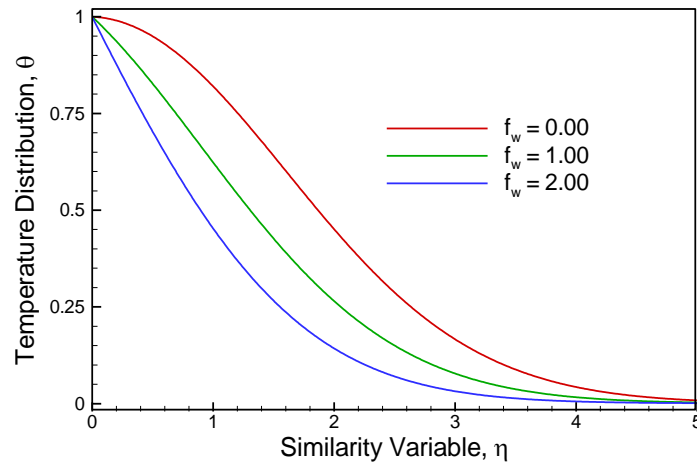


Fig. 2.3(b): Representative temperature distribution for different values of fluid suction parameter f_w

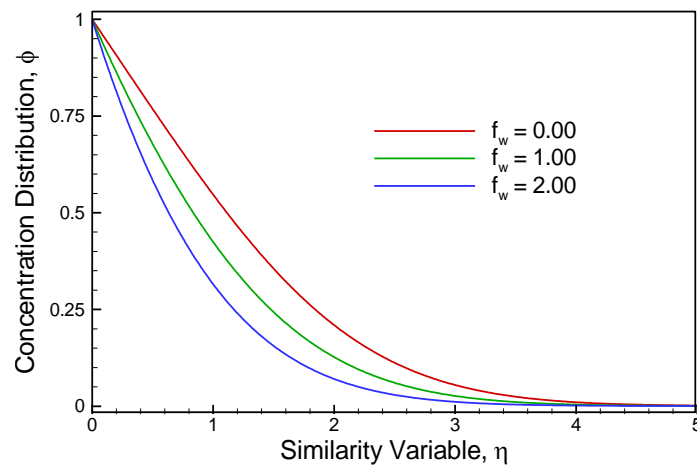


Fig. 2.3(c): Representative concentration distribution for different values of fluid suction parameter f_w

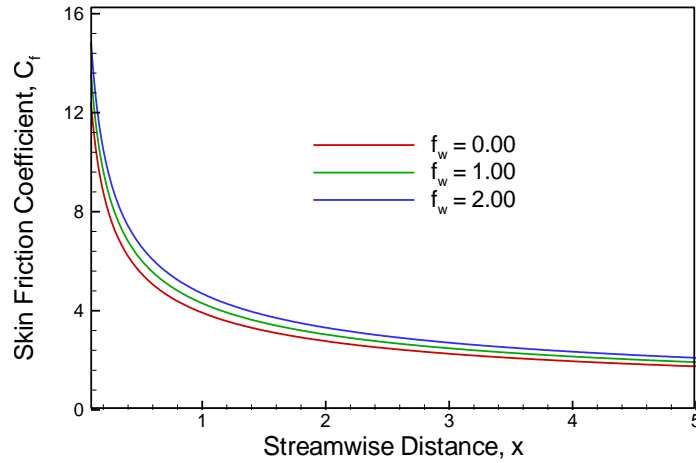


Fig. 2.3(d): Effect of fluid suction parameter f_w on local skin friction coefficient C_f against the streamwise distance x

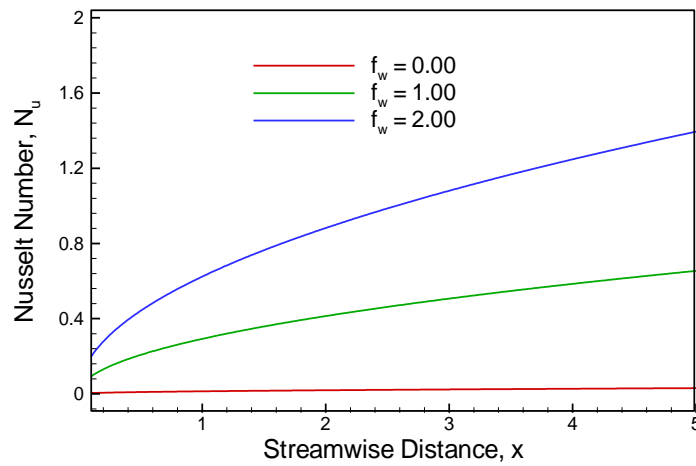


Fig. 2.3(e): Effect of fluid suction parameter f_w on local Nusselt number N_u against the streamwise distance x

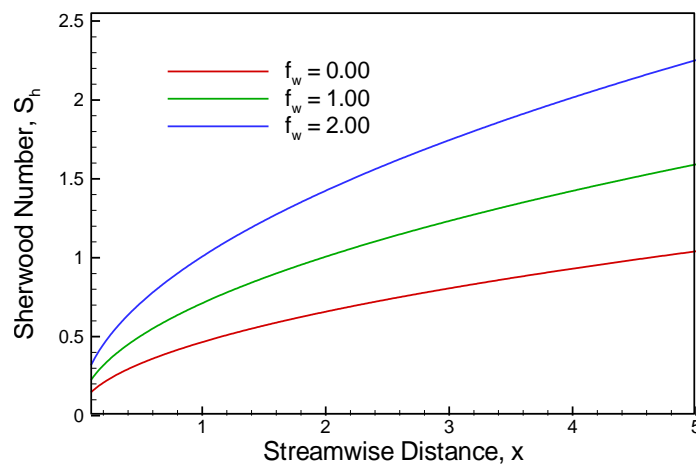


Fig. 2.3(f): Effect of fluid suction parameter f_w on local Sherwood number S_h against the streamwise distance x

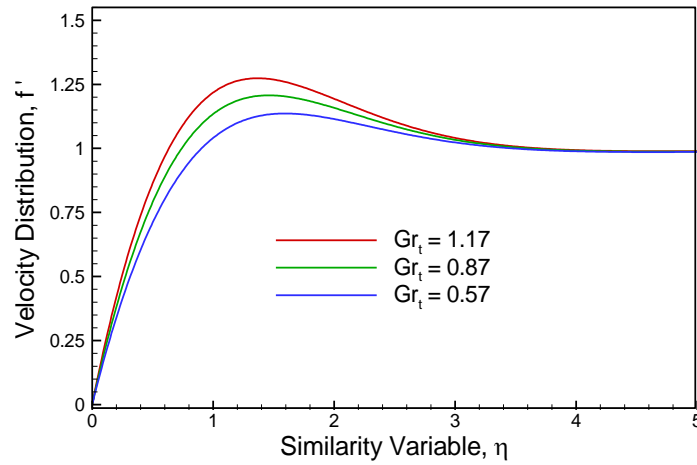


Fig. 2.4(a): Representative velocity distribution for different values of local thermal Grashof number Gr_t

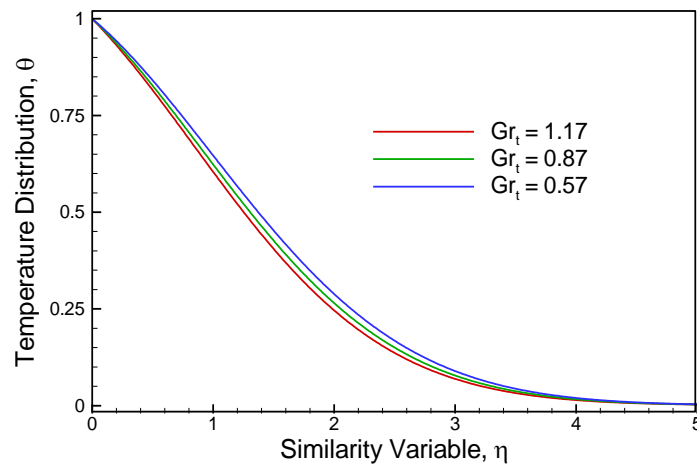


Fig. 2.4(b): Representative temperature distribution for different values of local thermal Grashof number Gr_t

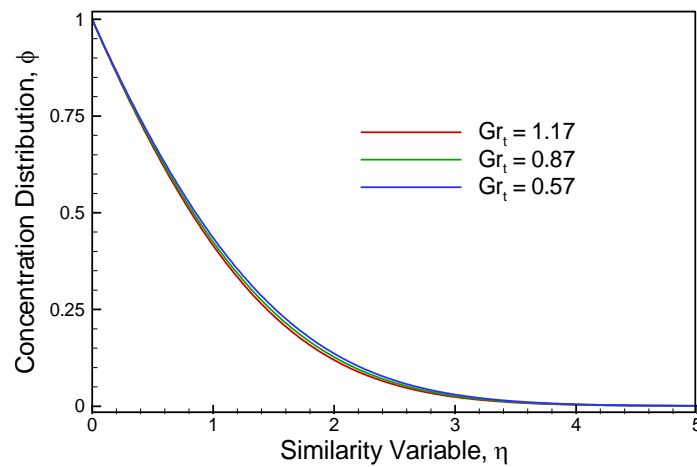


Fig. 2.4(c): Representative concentration distribution for different values of local thermal Grashof number Gr_t

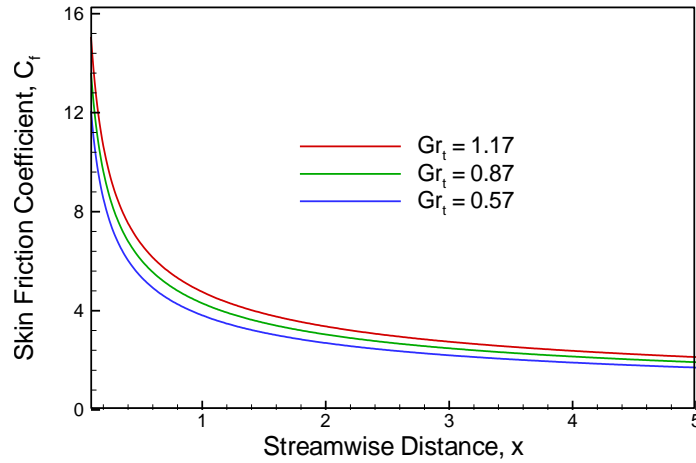


Fig. 2.4(d): Effect of local thermal Grashof number Gr_t on local skin friction coefficient C_f against the streamwise distance x

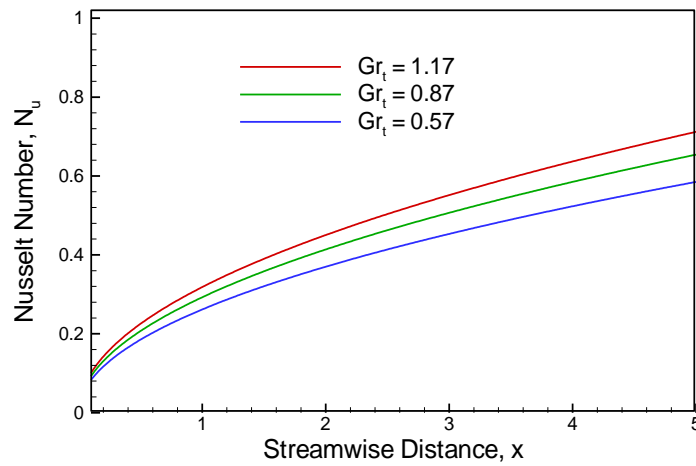


Fig. 2.4(e): Effect of local thermal Grashof number Gr_t on local Nusselt number N_u against the streamwise distance x

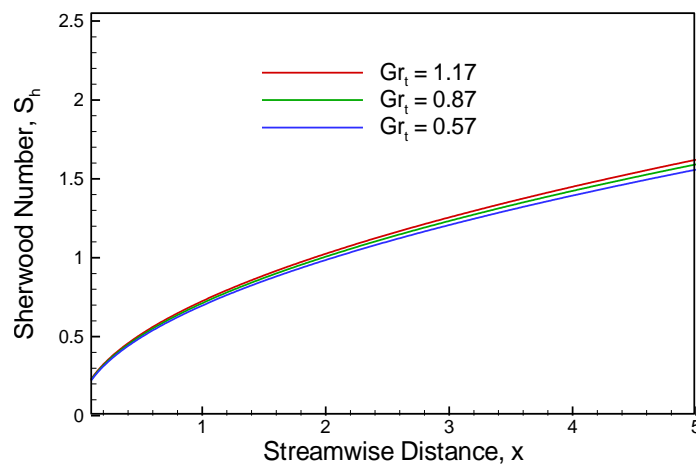


Fig. 2.4(f): Effect of local thermal Grashof number Gr_t on local Sherwood number S_h against the streamwise distance x

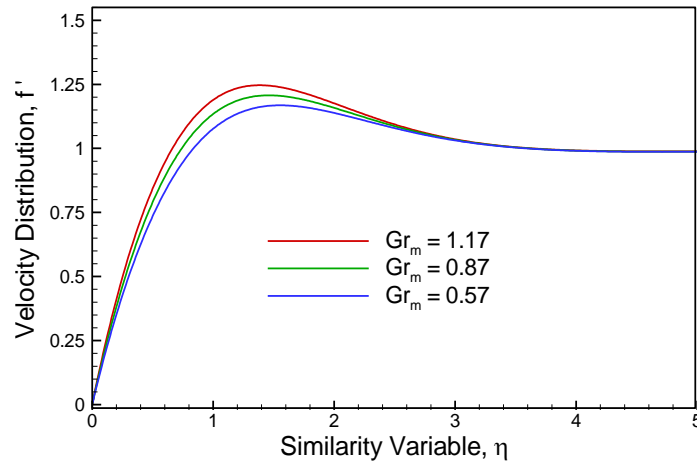


Fig. 2.5(a): Representative velocity distribution for different values of local mass Grashof number Gr_m

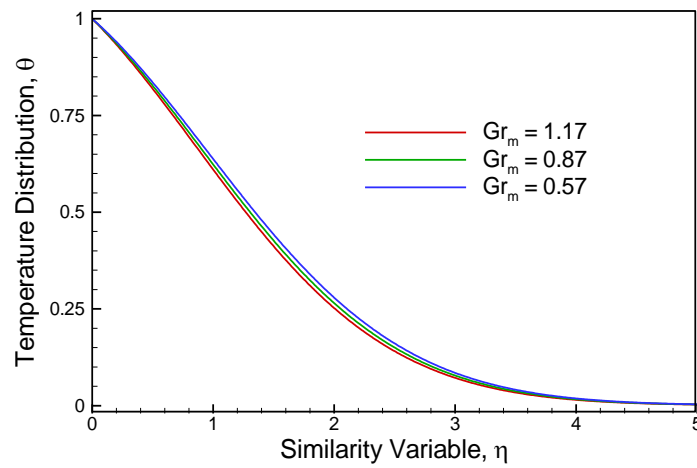


Fig. 2.5(b): Representative temperature distribution for different values of local mass Grashof number Gr_m

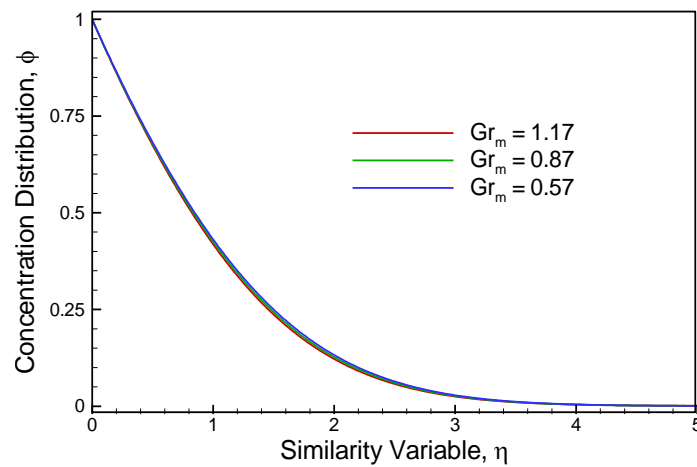


Fig. 2.5(c): Representative concentration distribution for different values of local mass Grashof number Gr_m

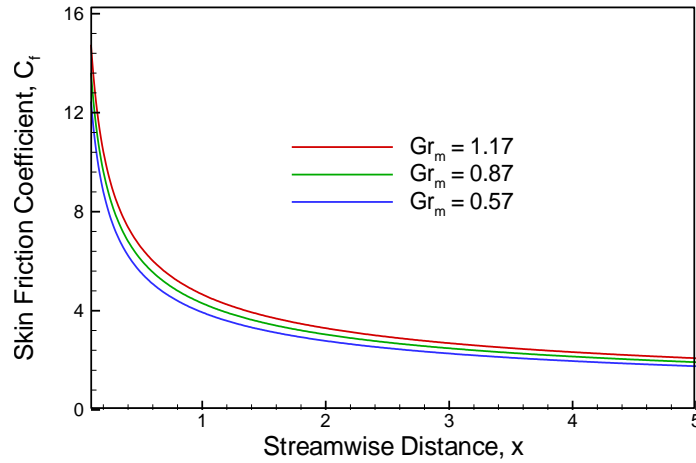


Fig. 2.5(d): Effect of local mass Grashof number Gr_m on local skin friction coefficient C_f against the streamwise distance x

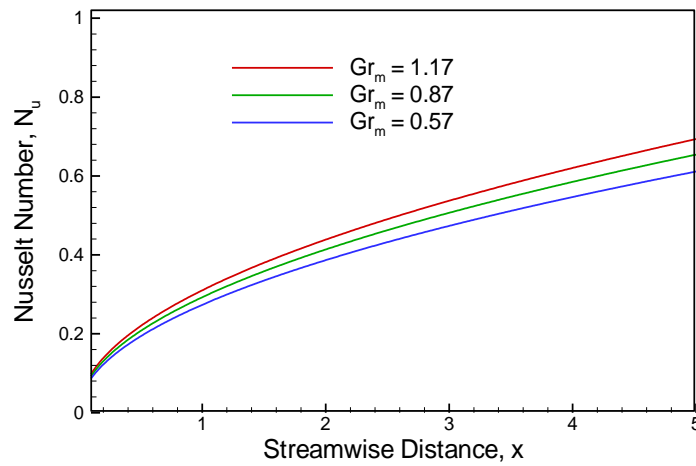


Fig. 2.5(e): Effect of local mass Grashof number Gr_m on local Nusselt number N_u against the streamwise distance x

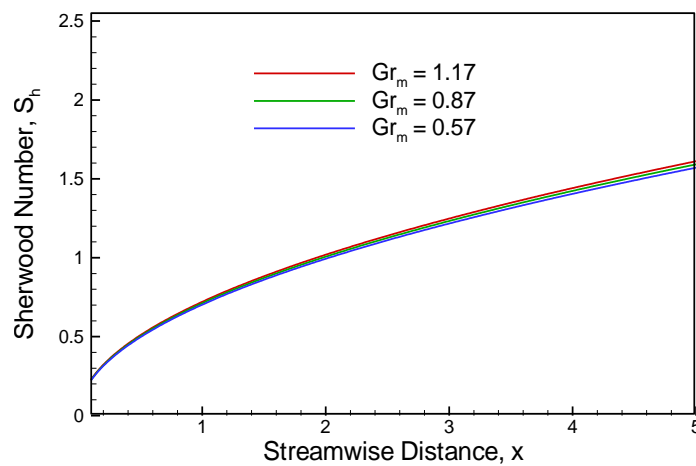


Fig. 2.5(f): Effect of local mass Grashof number Gr_m on local Sherwood number S_h against the streamwise distance x

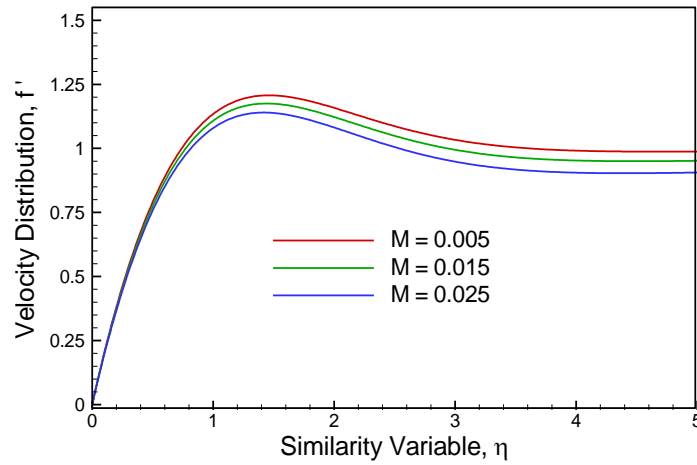


Fig. 2.6(a): Representative velocity distribution for different values of magnetic field parameter M

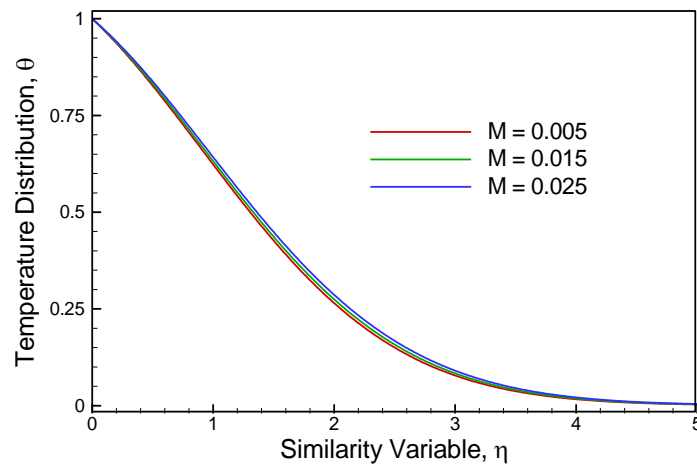


Fig. 2.6(b): Representative temperature distribution for different values of magnetic field parameter M

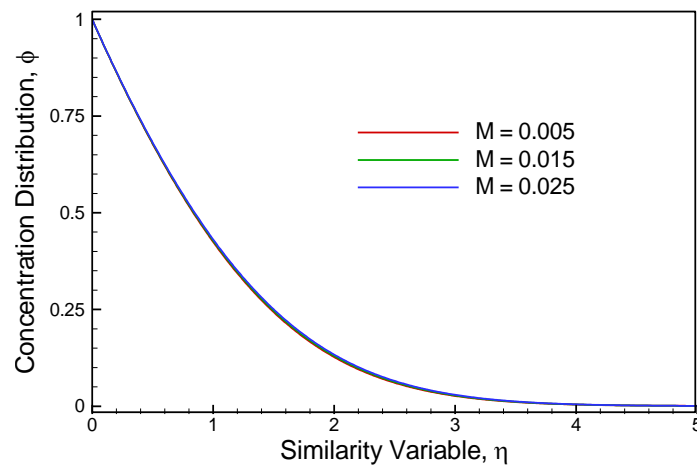


Fig. 2.6(c): Representative concentration distribution for different values of magnetic field parameter M

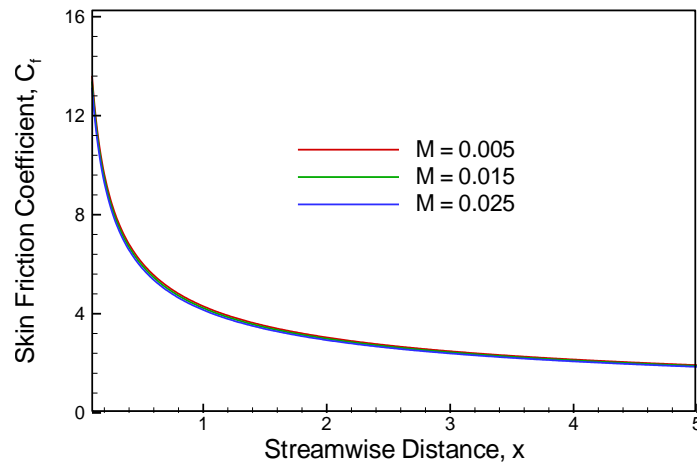


Fig. 2.6(d): Effect of magnetic field parameter M on local skin friction coefficient C_f against the streamwise distance x

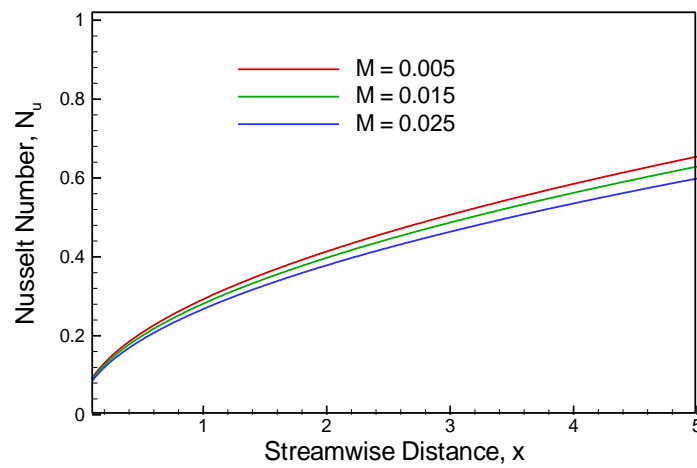


Fig. 2.6(e): Effect of magnetic field parameter M on local Nusselt number N_u against the streamwise distance x

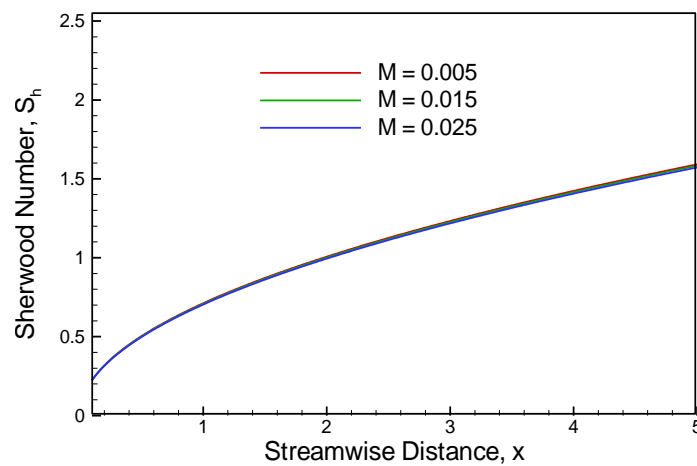


Fig. 2.6(f): Effect of magnetic field parameter M on local Sherwood number S_h against the streamwise distance x

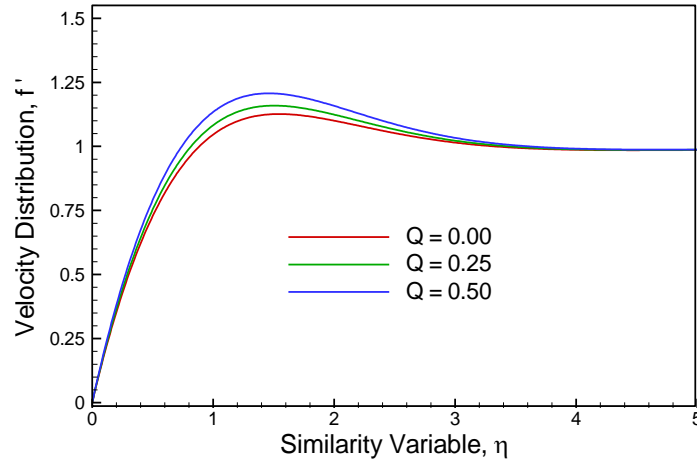


Fig. 2.7(a): Representative velocity distribution for different values of heat generation parameter Q

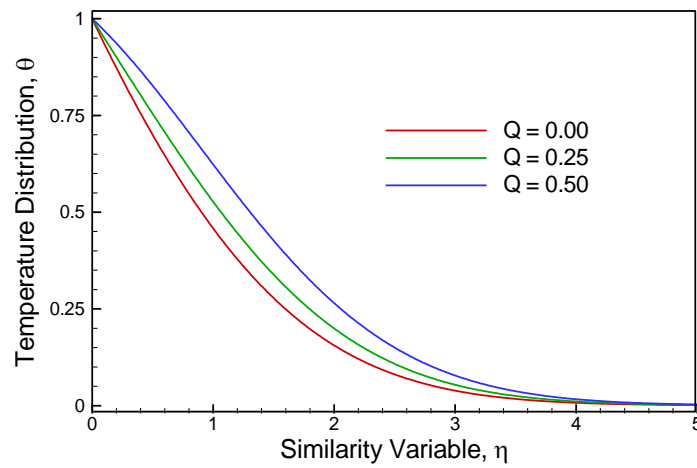


Fig. 2.7(b): Representative temperature distribution for different values of heat generation parameter Q

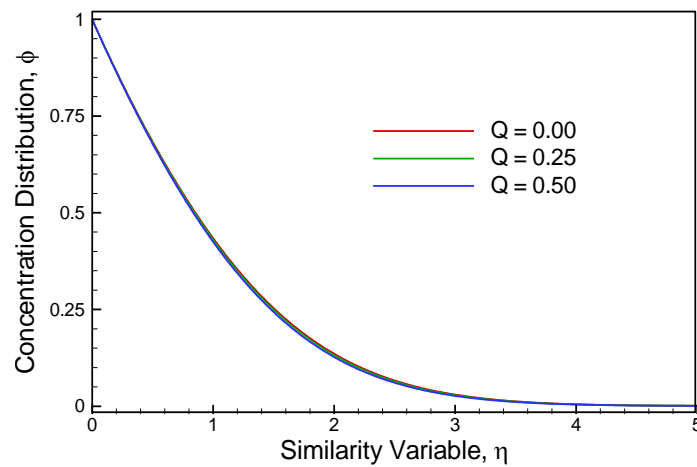


Fig. 2.7(c): Representative concentration distribution for different values of heat generation parameter Q

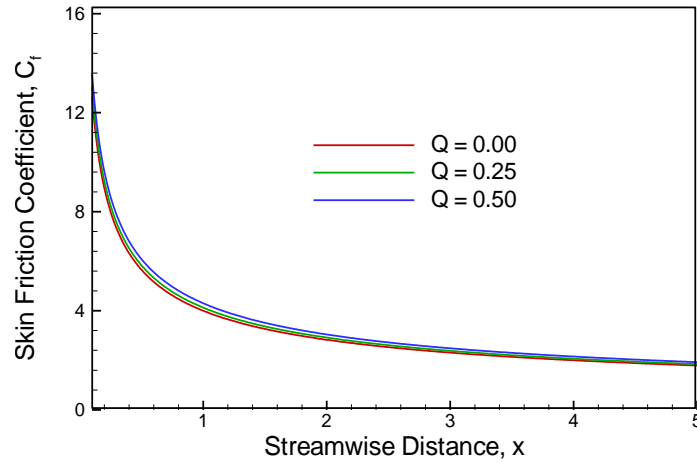


Fig. 2.7(d): Effect of heat generation parameter Q on local skin friction coefficient C_f against the streamwise distance x

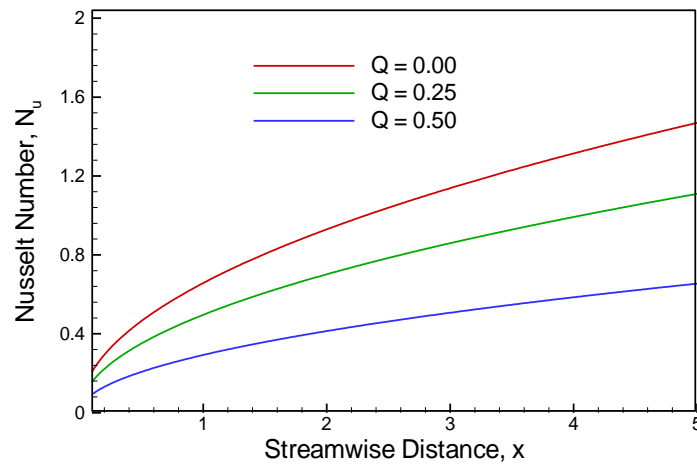


Fig. 2.7(e): Effect of heat generation parameter Q on local Nusselt number N_u against the streamwise distance x

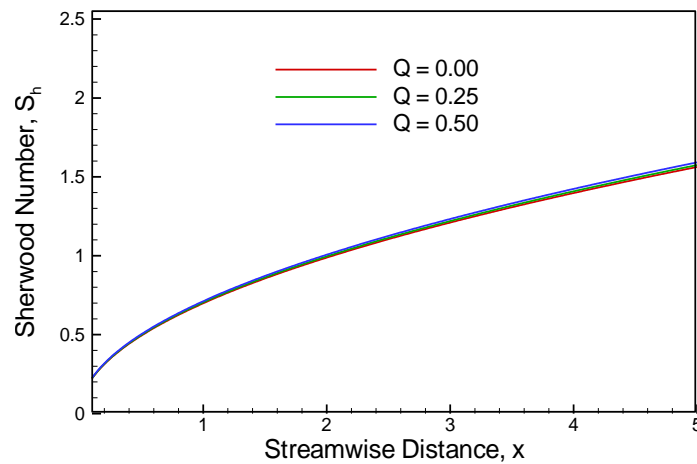


Fig. 2.7(f): Effect of heat generation parameter Q on local Sherwood number S_h against the streamwise distance x

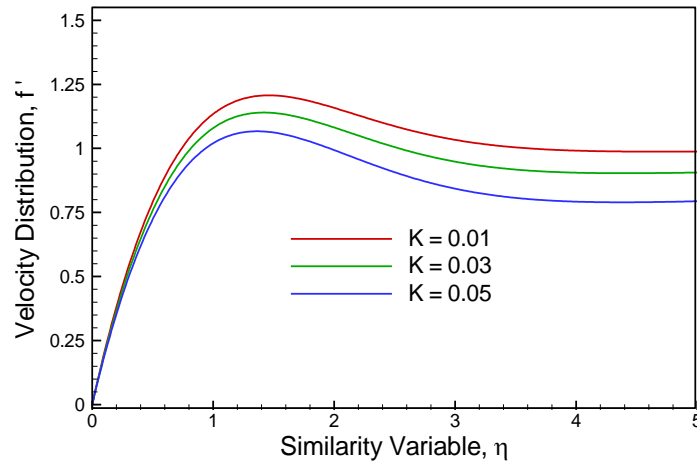


Fig. 2.8(a): Representative velocity distribution for different values of permeability parameter K

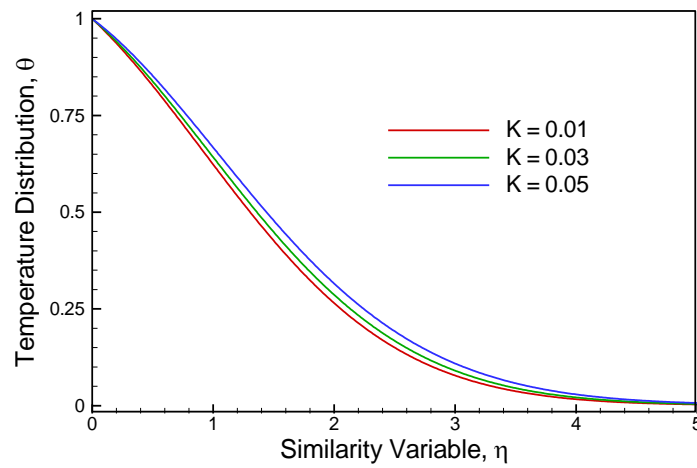


Fig. 2.8(b): Representative temperature distribution for different values of permeability parameter K

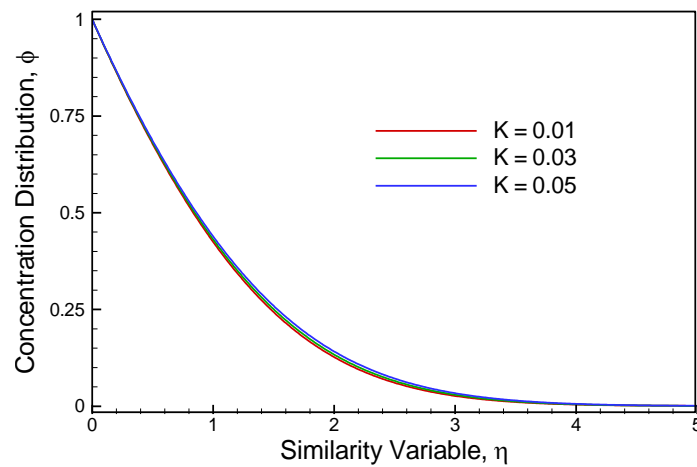


Fig. 2.8(c): Representative concentration distribution for different values of permeability parameter K

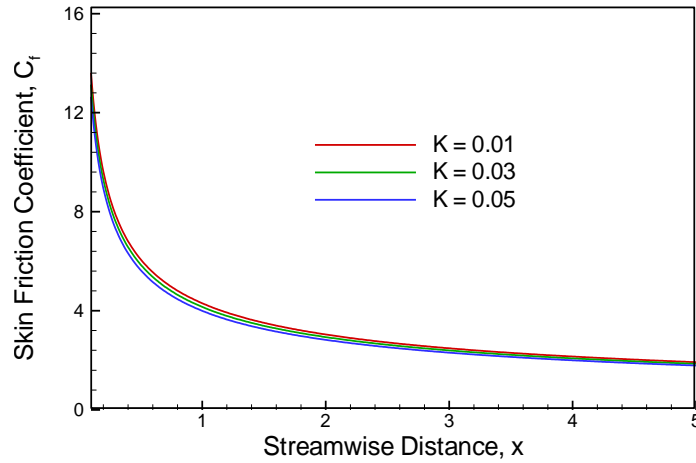


Fig. 2.8(d): Effect of permeability parameter K on local skin friction coefficient C_f against the streamwise distance x

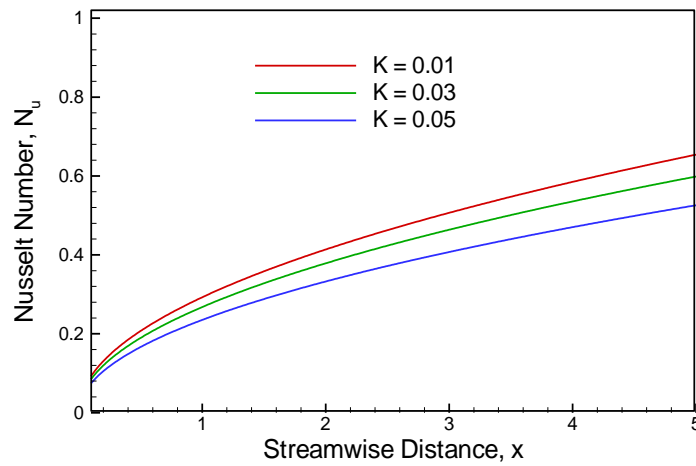


Fig. 2.8(e): Effect of permeability parameter K on local Nusselt number N_u against the streamwise distance x

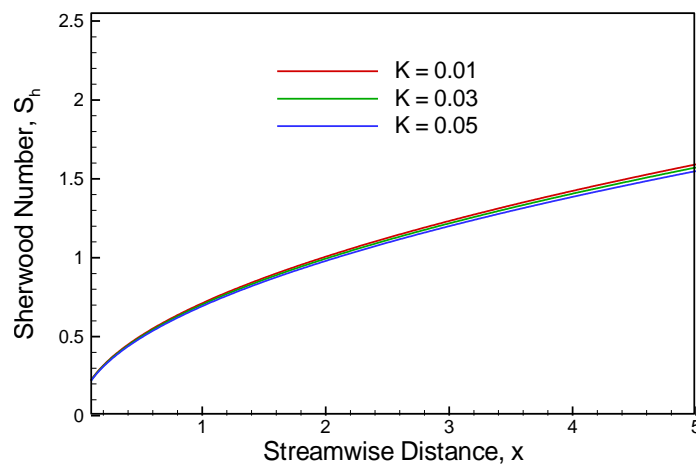


Fig. 2.8(f): Effect of permeability parameter K on local Sherwood number S_h against the streamwise distance x

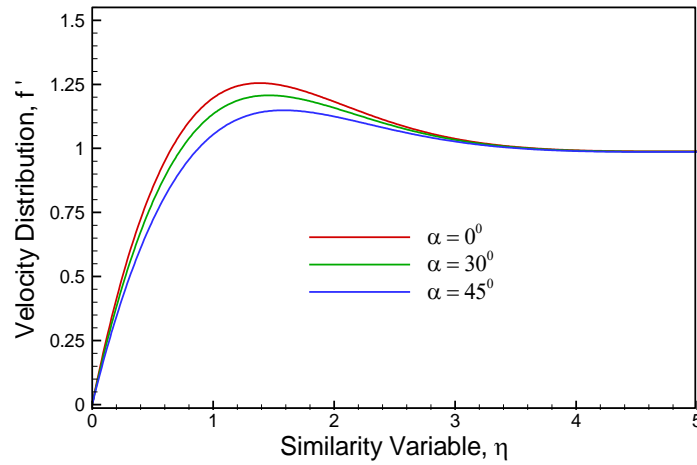


Fig. 2.9(a): Representative velocity distribution for different values of angle of inclination α

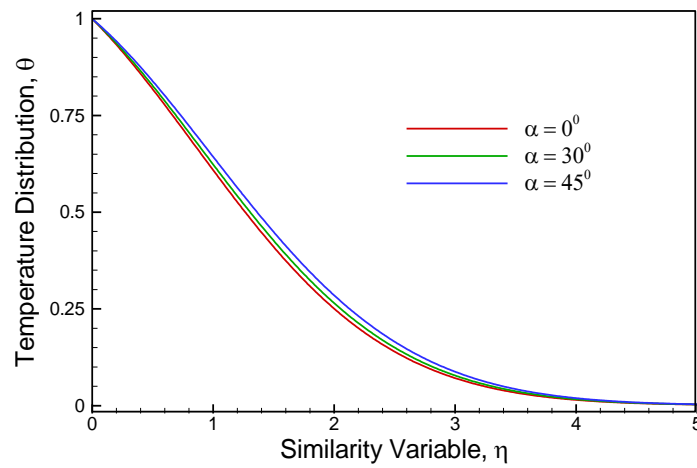


Fig. 2.9(b): Representative temperature distribution for different values of angle of inclination α

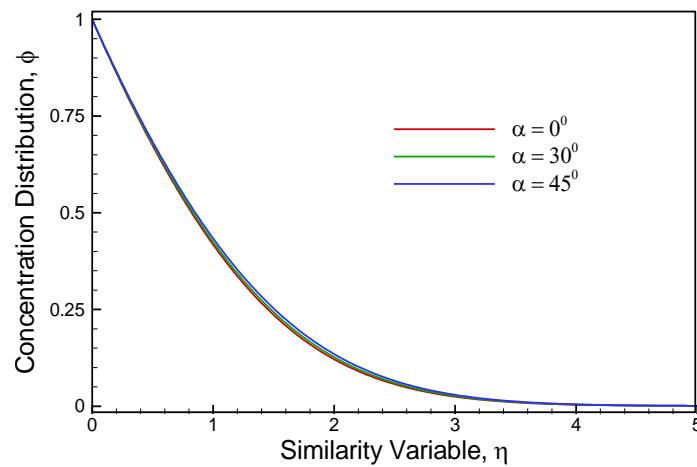


Fig. 2.9(c): Representative concentration distribution for different values of angle of inclination α

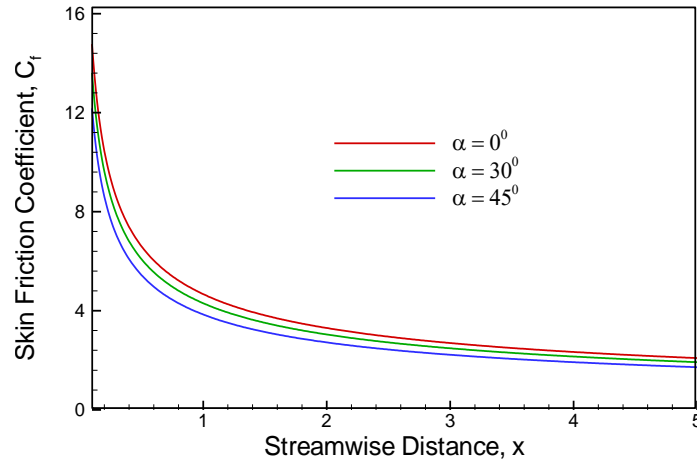


Fig. 2.9(d): Effect of angle of inclination α on local skin friction coefficient C_f against the streamwise distance x

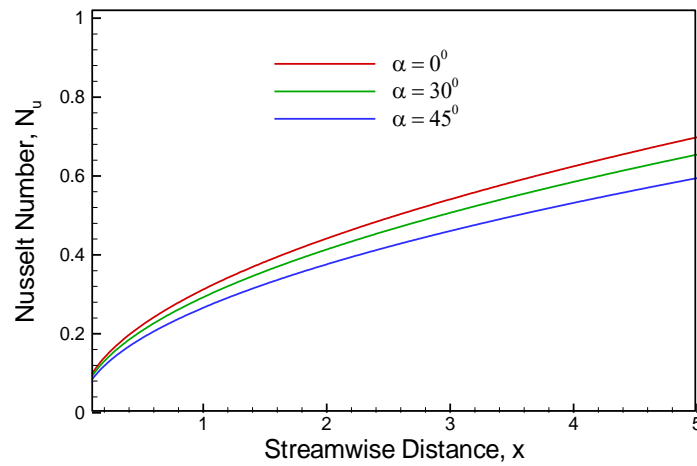


Fig. 2.9(e): Effect of angle of inclination α on local Nusselt number N_u against the streamwise distance x

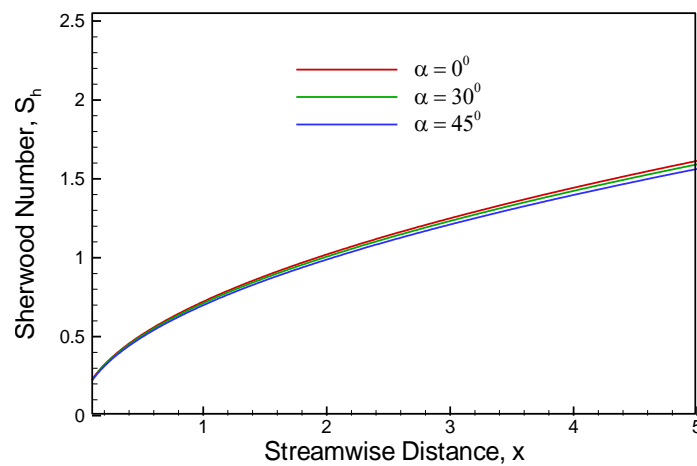


Fig. 2.9(f): Effect of angle of inclination α on local Sherwood number S_h against the streamwise distance x

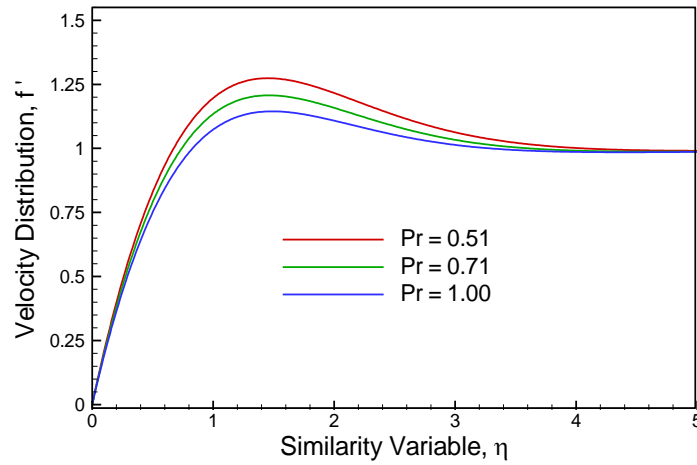


Fig. 2.10(a): Representative velocity distribution for different values of Prandtl number Pr

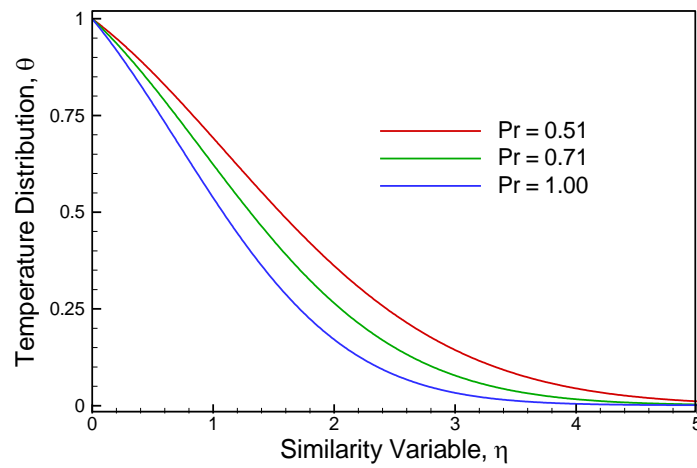


Fig. 2.10(b): Representative temperature distribution for different values of Prandtl number Pr

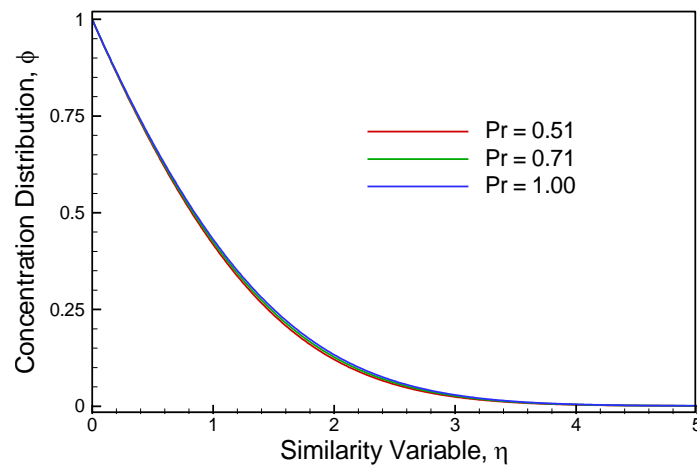


Fig. 2.10(c): Representative concentration distribution for different values of Prandtl number Pr

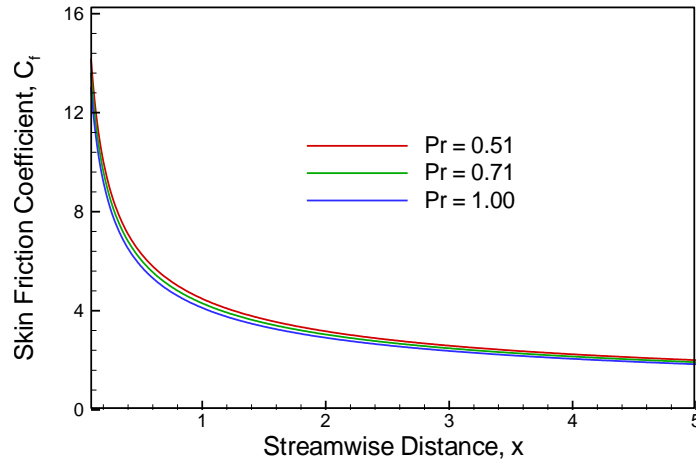


Fig. 2.10(d): Effect of Prandtl number Pr on local skin friction coefficient C_f against the streamwise distance x

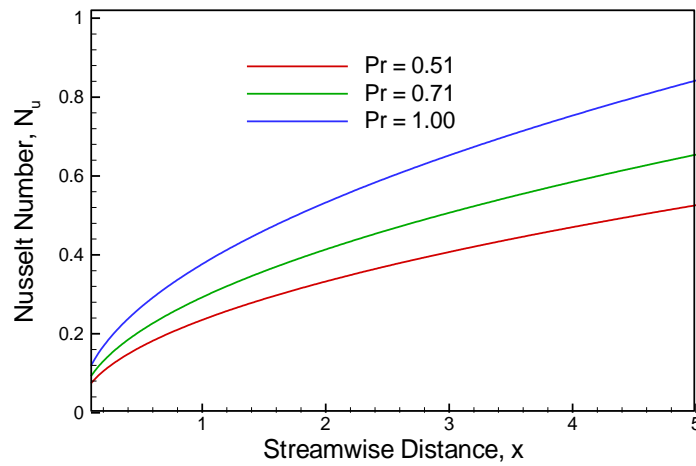


Fig. 2.10(e): Effect of Prandtl number Pr on local Nusselt number N_u against the streamwise distance x

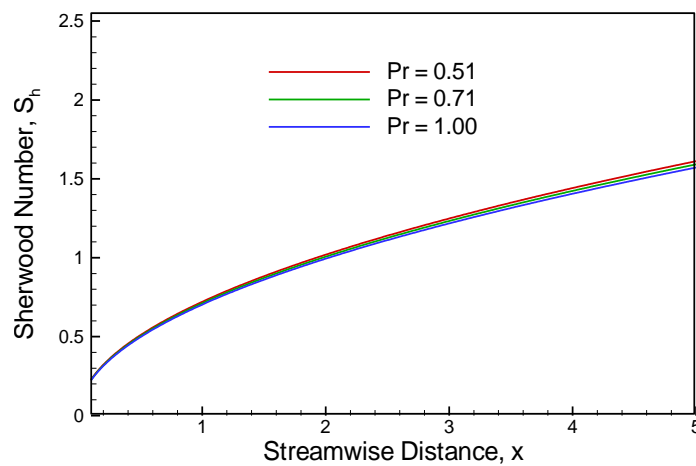


Fig. 2.10(f): Effect of Prandtl number Pr on local Sherwood number S_h against the streamwise distance x

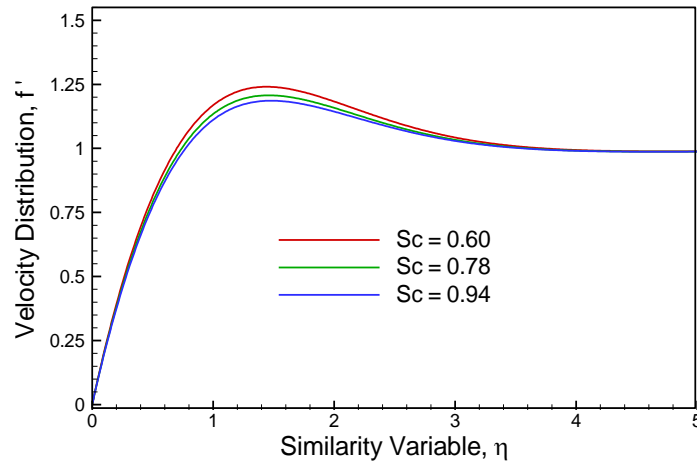


Fig. 2.11(a): Representative velocity distribution for different values of Schmidt number Sc

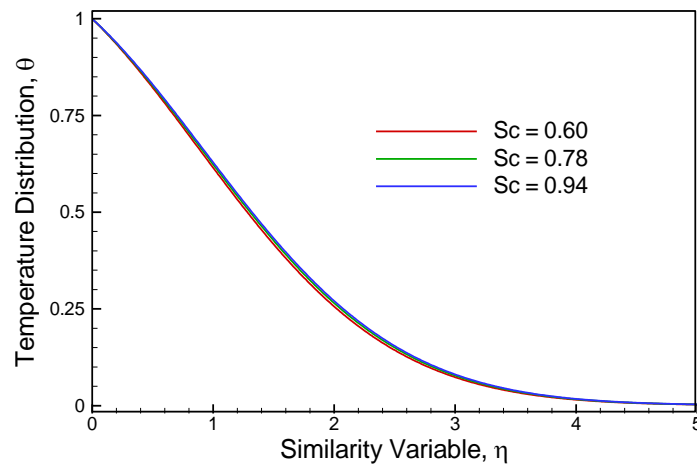


Fig. 2.11(b): Representative temperature distribution for different values of Schmidt number Sc

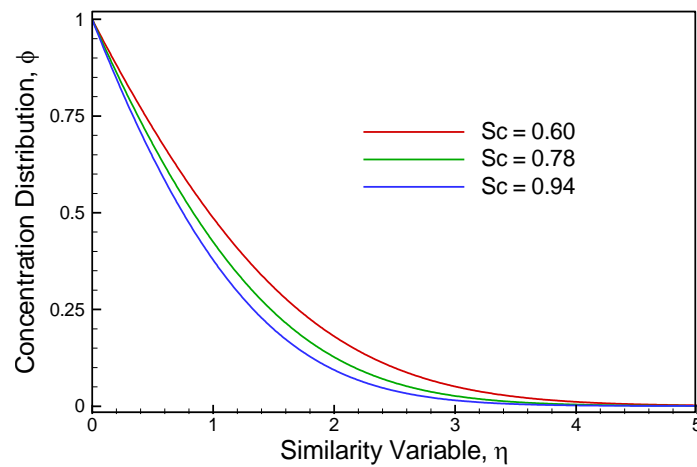


Fig. 2.11(c): Representative concentration distribution for different values of Schmidt number Sc

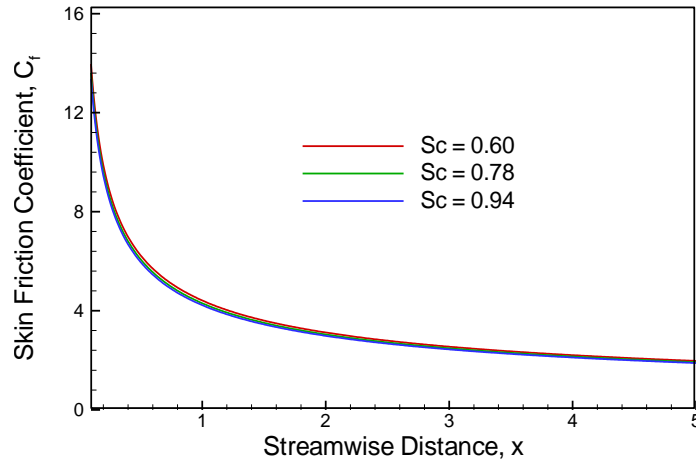


Fig. 2.11(d): Effect of Schmidt number Sc on local skin friction coefficient C_f against the streamwise distance x

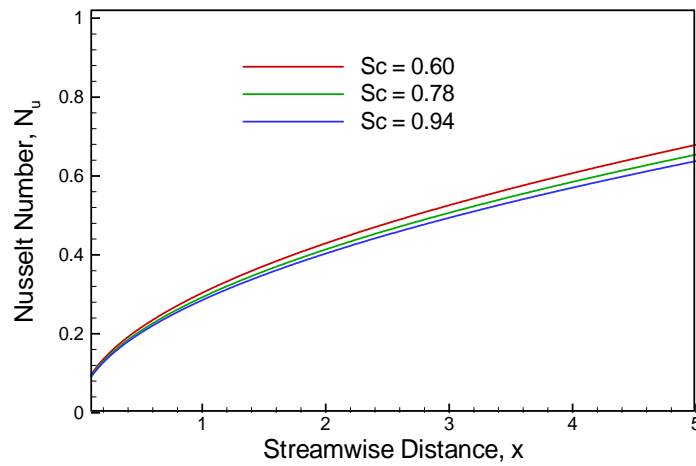


Fig. 2.11(e): Effect of Schmidt number Sc on local Nusselt number N_u against the streamwise distance x

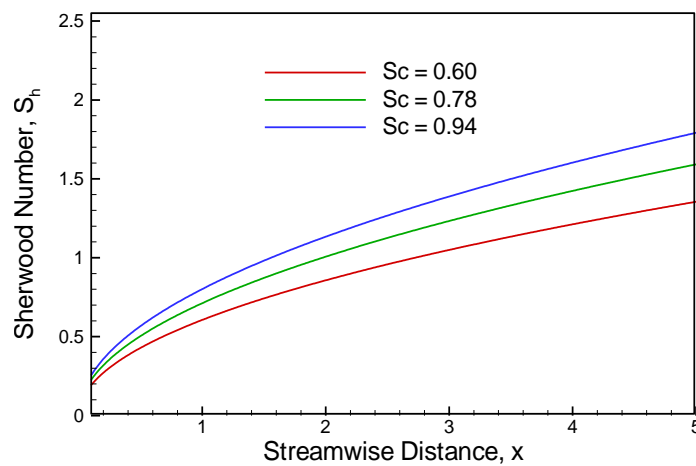


Fig. 2.11(f): Effect of Schmidt number Sc on local Sherwood number S_h against the streamwise distance x

2.6 Conclusions

From this investigation i.e. investigation of double diffusive magnetohydrodynamic mixed convective flow along an inclined flat plate in a porous medium, the following conclusions can be drawn for the effect of the fluid suction parameter, local thermal Grashof number, local mass Grashof number, magnetic parameter, heat generation parameter, permeability parameter, Prandtl number and Schmidt number on the flow field as:

- 1) Fluid suction has the effect to decrease the velocity, temperature and concentration of the flow field whereas increase the local skin friction coefficient, the local Nusselt number and the local Sherwood number.
- 2) As the local thermal Grashof number increases, the velocity tends to increase whereas the temperature and concentration decrease, and consequently the local skin friction coefficient, the local Nusselt number and the local Sherwood number decrease.
- 3) Due to increase of the local mass Grashof number, the velocity of the flow field increases but the temperature and concentration of the flow field decrease. Also the local skin friction coefficient, the local Nusselt number and local Sherwood number increase with the increase of local mass Grashof number.
- 4) In the presence of magnetic field on the fluid flow, the velocity is found to decrease while the temperature is found to increase but the concentration of the flow field changes insignificantly. Moreover, the local skin friction coefficient and the local Nusselt number decrease whereas the local Sherwood number changes insignificantly.
- 5) The increase in the values of the heat generation parameter leads to increase both the velocity and temperature on the flow field, and consequently increase the local skin friction coefficient but decrease the local Nusselt number. However, the concentration and the local Sherwood number change insignificantly.

- 6) Increases in the permeability of the porous medium, the fluid velocity decreases whereas the temperature increases, and insignificantly effect on the concentration. On the other hand, all of the local skin friction coefficient, the local Nusselt number and the local Sherwood number decrease.
- 7) The velocity of the flow field decreases but the temperature as well as concentration increase due to enhancement of the angle of inclination. However, all of the local skin friction coefficient, the local Nusselt number and the local Sherwood number decrease with increase in the angle of inclination.
- 8) Both the velocity and the temperature of the flow field decrease significantly whereas the concentration of the flow field increases insignificantly with the increase of Prandtl number. Moreover the local skin friction coefficient and local Nusselt number decrease but the local Sherwood number increases due to increase of Prandtl number.
- 9) An increase in the Schmidt number, decrease both the velocity and concentration of the flow field while the temperature of the flow field increases insignificantly. Consequently, the local skin friction coefficient and the local Nusselt number decrease but the local Sherwood number increases with the increase of Schmidt number.

Chapter 3

Investigation of Double Diffusive Magnetohydrodynamic Mixed Convective Flow with Thermodiffusion along an Inclined Flat Plate in a Porous Medium

3.1 Introduction

In previous chapter, double diffusive magnetohydrodynamic mixed convective flow along an inclined flat plate in a porous medium has been investigated and analyzed. This chapter will be concerned with the analysis of the effect of thermodiffusion on the flow field i.e. double diffusive magnetohydrodynamic mixed convective flow with thermodiffusion along an inclined flat plate in a porous medium and how it affects in the flow field.

In a theoretical investigation of thermodiffusion in multicomponent mixtures by Alireza Abbasi [1], diffusion is one of the major mechanisms of transport phenomena. Molecular diffusion is the movement of molecules from a higher to lower chemical potential. Thermodiffusion is the additional way in which molecules are transported in a multicomponent mixture driven by temperature gradient. The thermodiffusion phenomenon was first analyzed by Ludwig, 1856 and Soret, 1879. The Soret coefficient is the ratio of the thermodiffusion coefficient to the molecular diffusion coefficient. Thermodiffusion along with molecular diffusion occurs in many engineering systems and in nature. Thermodiffusion has a great effect on the concentration distribution in a multicomponent mixture. The variations of composition and temperature may either lessen or enhance the separation in mixtures. The thermodiffusion phenomenon also plays a major role in the hydrodynamic instability analysis in mixtures, investigations of mineral migration, the mass transport modeling in living matters, and composition variation studies in hydrocarbon reservoirs.

Furthermore, the study of thermohaline instability with thermodiffusion in a fluid saturated porous medium is of importance in geophysics, ground water hydrology, soil science, oil extraction (Parvathy and Patil, 1989). The reason is that the earth's crust is a porous medium saturated by a mixture of different types of fluids such as

oil, water, gases and molten from of ores dissolved in fluids. Thermal gradients present between the interior and exterior of the earth's crust may help convection to set in. The thermal gradient in crude oil can have a strange effect on the distribution of petroleum components in an oil deposit. The thermal gradient causes the Soret effect which makes the larger molecule components to have a tendency to rise, while smaller molecule components go down to the bottom of the well. However, gravity causes the heavy components in a fluid to fall and the lighter ones to rise. This means that the distribution of components in a given well is neither consistent nor predictable.

3.2 Mathematical Analysis

Thermodiffusion is the migration of small size particles in the direction of a decreasing temperature gradient and the small size particles experience a force in the direction opposite to that of temperature gradient. The molecules coming from the hot side of the particles have a greater velocity than those coming from the cold side of the particles. The faster moving molecules collide with the slower moving molecules of the particles more forcefully. This difference in momentum of the particles leads to the particles developing a velocity in the direction of decreasing temperature. The velocity acquired by the particles is called the thermophoretic velocity and the force experienced by the suspended particles due to the temperature gradient is known as thermophoretic force.

All the physical properties which are introduced and derived in previous chapter are considered with thermodiffusion effects. Therefore, the concentration equation (Eqn. 2.4) can be written as in the following form:

$$u \frac{\partial C}{\partial x} + v \frac{\partial C}{\partial y} = D \frac{\partial^2 C}{\partial y^2} - \frac{\partial}{\partial y} \{V_T (C - C_\infty)\} \quad (3.1)$$

where V_T is the thermophoretic velocity.

In Eqn. (3.1) the thermophoretic velocity V_T can be expressed in the following form as:

$$V_T = - \frac{\kappa v}{T_{ref}} \frac{\partial T}{\partial y}$$

where T_{ref} is some reference temperature and κ is the thermophoretic coefficient which defined by Talbot et al. [13] as:

$$\kappa = \frac{2C_s \left(\frac{k_g}{k_p} + C_t k_n \right) [1 + k_n (C_1 + C_2 e^{-\frac{C_3}{k_n}})]}{(1 + 3C_m k_n) (1 + 2 \frac{k_g}{k_p} + 2C_t k_n)}$$

where C_1, C_2, C_3, C_m, C_s and C_t are constants, k_g and k_p are the thermal conductivities of the fluid and diffused particle, respectively and k_n is the Knudsen number.

Using dimensionless variables of Eqn. (2.6.1) and Eqn. (2.6.2), the transformed concentration equation which is nondimensional form of Eqn. (3.1) can be written as:

$$\phi'' + Sc \left(\frac{1}{2} f - \tau \theta' \right) \phi' - Sc \tau \theta'' \phi = 0 \quad (3.2)$$

where τ is the thermohoretic parameter which is defined by Alam et al. [4] as:

$$\tau = - \frac{\kappa (T_w - T_\infty)}{T_{ref}}$$

Typical values of τ are 0.01, 0.05 and 0.10 corresponding to approximate values of $-\kappa (T_w - T_\infty)$ equal to 3, 15 and 30K for a reference temperature of $T_{ref} = 300\text{K}$.

3.3 Numerical Solutions

The system of transformed nonlinear ordinary differential Eqns. (2.9), (2.10) and (3.2), together with the boundary conditions Eqns. (2.12.1) and (2.12.2) have been solved numerically using Nachtsheim-Swigert shooting iteration technique along with sixth order Runge-Kutta initial value solver. The numerical methods are described in details, referring to Nachtsheim and Swigert [11] and Alam et al. [2].

3.4 Comparison

For the accuracy of the numerical results, the present study is compared with the previous study Reddy et al. [12] including the effect $\tau = 0.0$ which was shown in Fig. 2.2. It is observed that the present results are in good agreement with that of Reddy et al. [12]. This favorable comparison leads confidence in the numerical results to be reported in the next sections.

3.5 Results and Discussion

The effect of various physical parameters on the MHD mixed convective flow with thermodiffusion along an inclined flat plate in a porous medium are examined and discussed in this section with the subsections. The parameters that the solution are affected are the amplitude of fluid suction parameter f_w , local thermal Grashof number Gr_t , local mass Grashof number Gr_m , magnetic parameter M , heat generation parameter Q , permeability parameter K , angle of inclination α , Prandtl number Pr , Schmidt number Sc and thermophoretic parameter τ . The numerical solutions for velocity, temperature, and concentration distributions as well as the local skin friction, the local Nusselt number, and the local Sherwood number have been carried out using different values of the various physical parameters which appear in the nonlinear ordinary differential equations. The following set of considered values for the key physical parameters in the numerical solutions were adopted, unless otherwise stated; $Gr_t = 0.87$, $Gr_m = 0.87$, $M = 0.001$, $Q = 0.50$, $K = 0.01$, $\alpha = 30^\circ$, $Pr = 0.71$, $f_w = 0.50$, $Sc = 0.60$, $\tau = 0.10$ and $U_\infty / \nu = 1.0$. The value of Prandtl number Pr is taken to be 0.71 which is corresponds physically to air.

3.5.1 Effect of suction parameter (f_w) on flow field:

The dimensionless velocity, temperature and concentration distributions as well as the local skin friction coefficient, the local Nusselt number, and the local Sherwood number for different values of the fluid suction parameter f_w ($f_w = 0.00, 0.50$ and 1.00) are presented in Figs. 3.1(a) - 3.1(f) respectively keeping other parameters of the flow field constant. The increasing of the suction parameter f_w decrease the velocity (Fig. 3.1(a)), thermal (Fig. 3.1(b)) and concentration (Fig. 3.1(c)) boundary layer thickness while it increases the local skin friction coefficient C_f (Fig. 3.1(d)), the local Nusselt number N_u (Fig. 3.1(e)) and the local Sherwood number S_h (Fig. 3.1(f)). This is due to the fact that as the fluid suction through the plate increases, the plate is cooled down and the viscosity of the flowing fluid increases. Therefore, the velocity, temperature and concentration of the flow field decrease as the fluid suction increases. However, the local skin friction coefficient, the local Nusselt number, and the local Sherwood number increase against the streamwise distance x .

3.5.2 Effect of local thermal Grashof number (Gr_t) on flow field:

The influence of the thermal Grashof number Gr_t ($Gr_t = 0.57, 0.87$ and 1.17) on the dimensionless velocity, temperature and concentration distributions as well as the local skin friction coefficient, the local Nusselt number, and the local Sherwood number are displayed in Figs. 3.2(a) - 3.2(f) keeping other parameters of the flow field constant. The local thermal Grashof number Gr_t ascertains the ratio of thermal buoyancy force to the viscous hydrodynamic force. It can be seen from Fig. 3.2(a) that the fluid velocity increases due to the enhancement of the thermal buoyancy force. The increase of the local thermal Grashof number, the peak values of the velocity increases rapidly near the plate and then decreases smoothly to approach the free stream velocity. From the dimensionless temperature distribution in Fig. 3.2(b), it is found that an increase in the local thermal Grashof number results a decrease in the temperature of the flow field. This is because of the positive values of local thermal Grashof number correspond to cooling of the porous plate. The increase of local thermal Grashof number, decrease the concentration boundary layer thickness which is observed in Fig. 3.2(c). As the local thermal Grashof number increases, the species difference increases and therefore, the concentration of the flow field decreases in the concentration boundary layer. The nature of the local skin friction coefficient, the local Nusselt number, and the local Sherwood number against the streamwise distance x are shown in Figs. 3.2(d) – 3.2(f). It is seen that all of local skin friction coefficient, local Nusselt number and local Sherwood number increase due to increase in the local thermal Grashof number i.e. increase in velocity of the flow field whereas decrease in temperature and concentration of the flow field.

3.5.3 Effect of local mass Grashof number (Gr_m) on flow field:

For several values of the dimensionless parameters, values of dimensionless velocity distribution, temperature distribution, concentration distribution, local skin friction coefficient, local Nusselt number, and local Sherwood number have been computed and are presented in Figs. 3.3(a) – 3.3(f). Figs. 3.3(a) – 3.3(f) show the effect of the local mass Grashof number Gr_m ($Gr_m = 0.57, 0.87$ and 1.17) on the velocity, temperature and concentration distributions as well as the local skin friction coefficient, the local Nusselt number, and the local Sherwood number respectively

while all other parameters of the flow field are kept fixed. The local mass Grashof number Gr_m ascertains the ratio of species buoyancy force to the viscous hydrodynamic force. The velocity boundary layer thickness is found to increase in the presence of growing local mass Grashof number because the presence of growing local mass Grashof number leads to increase the species buoyancy force. As the local mass Grashof number increases, the peak values of the velocity increases rapidly in the vicinity of the plate and then decreases smoothly to approach the free stream velocity. It is noticed that the temperature and concentration distributions in Figs. 3.3(b) – 3.3(c) both decrease with the increase of local mass Grashof number. This is because as the local mass Grashof number increases, the temperature and species difference increase and therefore, the temperature as well as concentration of the flow field decrease. With an increase in the local mass Grashof number, the local skin friction coefficient, the local Nusselt number and the local Sherwood number are affected; all of local skin friction coefficient in Fig. 3.3(d), local Nusselt number in Fig. 3.3(e) and local Sherwood number in Fig. 3.3(f) increase against the streamwise distance x as the local mass Grashof number rises.

3.5.4 Effect of magnetic field parameter (M) on flow field:

Figures 3.4(a) – 3.4(f) illustrate the effect of different values of magnetic field parameter M ($M = 0.001, 0.005, \text{ and } 0.010$) on the velocity, temperature and concentration as well as local skin friction, local Nusselt number and local Sherwood number while other parameters of the flow field are kept constant. The presence of magnetic field, normal to the flow of electrically conducting fluid generates a force called the Lorentz force, which acts against the flow. Thus the velocity decreases with increasing of the magnetic field parameter as observed in Fig. 3.4(a). In Fig. 3.4(b), it has been noticed that the temperature distribution increases due to increase in the magnetic field strength. This is because of the applied magnetic field which tends to heat the fluid due to electromagnetic work, reduces the heat transfer from the wall. In Fig. 3.4(c) for dimensionless concentration distribution, it is reported that the concentration distribution changes insignificantly due to increase of magnetic parameter. In presence of magnetic field parameter, the behavior of the local skin friction coefficient, the local Nusselt number, and the local Sherwood number against the streamwise distance x are displayed in Figs. 3.4(d) – 3.4(f).

In Fig. 3.4(d), the local skin friction coefficient is found to decrease due to increase in the magnetic field parameter. The fact is that the applied magnetic field tends to impede the flow motion and thus to reduce the surface friction force. The local Nusselt number in Fig. 3.4(e) decreases with respect to increase in the magnetic field parameter. As in presence of increasing magnetic field, the temperature gradient at the wall decreases which in turn leads to a reduction in the rate of heat transfer from the surface. Similarly such situation continues in Fig. 3.4(f) for the local Sherwood number.

3.5.5 Effect of heat generation parameter (Q) on flow field:

The behavior of the velocity, temperature and concentration as well as local skin friction, local Nusselt number and local Sherwood number for different values of heat generation parameter Q ($Q = 0.00, 0.25, \text{ and } 0.50$) are shown in Figs. 3.5(a) – 3.5(f) respectively while all other parameters remain unchanged. As observed in Fig. 3.5(a), when heat is generated the buoyancy force increases, which induces the flow rate to increase, giving rise to the increase in the velocity of the flow field. Moreover the velocity boundary layer thickness within the boundary layer increases with the increase in heat generation parameter. The dimensionless temperature distribution in Fig. 3.5(b) is found to increase due to increase of the heat generation parameter Q because the presence of a heat source on the flow field, the thermal state of the fluid increases causing the thermal boundary layer to increase. In the case that the strength of the heat source is relatively large, the maximum fluid temperature does not occur at the surface of the plate, but rather in the fluid region close to it. On the other hand the concentration distribution is observed as the insignificant effect with the increase in heat generation parameter in Fig. 3.5(c). The impact of heat generation parameter on the local skin friction coefficient, the local Nusselt number, and the local Sherwood number in the boundary layer against the streamwise distance x are shown in Figs. 3.5(d) – 3.5(f). As observed in Figs. 3.5(d) – 3.5(f), it is reported that the local skin friction coefficient increases whereas the local Nusselt number decreases due to increase in the heat generation parameter, and however the local Sherwood number changes insignificantly.

3.5.6 Effect of permeability parameter (K) on flow field:

Figures 3.6(a) – 3.6(f) present the typical dimensionless velocity, temperature and concentration distributions as well as local skin friction coefficient, local Nusselt number and local Sherwood number for various values of the permeability parameter K ($K = 0.01, 0.02$ and 0.03) keeping other parameters of the flow field constant. The increase of the permeability of the porous medium has the tendency to decrease the velocity of the fluid in the boundary layer which is observed in Fig. 3.6(a). In addition, the velocity boundary layer thickness decreases due to rising in the permeability of the porous medium parameter. On the other hand the temperature distribution in Fig. 3.6(b), the temperature of the flow field and the thermal boundary layer thickness increase with respect to increase in the permeability of the porous medium parameter. However, the concentration of the flow field changes insignificantly as permeability of the porous medium parameter increases which observed in Fig. 3.6(c). Figs. 3.6(d) – 3.6(f) illustrate the nature of permeability of the porous medium on the local skin friction coefficient, the local Nusselt number, and the local Sherwood number against the streamwise distance x . All of the local skin friction coefficient in Fig. 3.6(d), the local Nusselt number in Fig. 3.6(e) and the local Sherwood number in Fig. 3.6(f) decrease with the increase of permeability of the porous medium parameter.

3.5.7 Effect of angle of inclination (α) on flow field:

Effect of different angle of inclination α ($\alpha = 0^\circ, 30^\circ$, and 45°) on flow field such as velocity, temperature and concentration as well as local skin friction, local Nusselt number and local Sherwood number are shown in Figs. 3.7(a) – 3.7(f)) while all other parameters of the flow field are kept constant. It can be seen in Fig. 3.7(a) that the velocity of the flow field inside the hydrodynamic boundary layer decreases with increasing the angle of inclination. This is because as the angle of inclination increases, the effect of the buoyancy force decreases due to thermal and mass diffusion by a factor of $\cos\alpha$. Consequently, the driving force to the fluid decreases as a result the velocity of the fluid decreases. In Fig. 3.7(b), increase in the angle of inclination leads the temperature of the flow field and thermal boundary layer thickness to increase with an accompanying decrease in the wall temperature

gradient. The fact is that the reduction in the buoyancy force as the plate is inclined from the vertical to a large angular position. The concentration gradient at the wall is seen to decrease as the buoyancy force decreases, with an associated the concentration in Fig 3.7(c) of the flow field, the concentration boundary layer thickness increases for increasing the angle of inclination. In order to examine the behavior of angle of inclination on the flow field, the local skin friction coefficient, the local Nusselt number, and the local Sherwood number against the streamwise distance x are presented in Figs. 3.7(d) – 3.7(f). As inspection of this Figs. 3.7(d) – 3.7(f), it can be seen that the local skin friction coefficient, the local Nusselt number, and the local Sherwood number decrease in presence of rising angle of inclination. This behavior is clear from the fact that as the plate is tilted from the vertical toward the horizontal; the buoyancy force effect diminishes by a factor of $\cos\alpha$ as the angle of inclination increases.

3.5.8 Effect of Prandtl number (Pr) on flow field:

Figures 3.8(a) – 3.8(f) describe the behavior of velocity, temperature and concentration as well as local skin friction, local Nusselt number and local Sherwood number on the flow field for different values of Prandtl number Pr ($Pr = 0.51, 0.71,$ and 1.00) keeping other parameters of the flow field constant. The Prandtl number is the ratio of momentum diffusivity (kinematic viscosity) to thermal diffusivity. As the Prandtl number increases, the momentum diffusivity of the flow field increases and as a results the velocity as well as the hydrodynamic boundary layer thickness decrease which are observed in Fig. 3.8(a). Inspection of the temperature and concentration distributions in Figs. 3.8(b) – 3.8(c) reveal that increase in the values of Prandtl number lead to decrease the temperature of the flow field as well as the thermal boundary layer thickness while the concentration of the flow field increases insignificantly. From Figs. 3.8(d) and 3.8(f), it can be seen that the local skin friction coefficient as well as the local Sherwood number decreases with the increasing Prandtl number against the streamwise distance x . It is evident from Fig. 2.10(e) that the local Nusselt number is found to increase due to increase in the Prandtl number. This is due to the fact that as the Prandtl number increases, the thermal boundary layer thickness decreases and the wall temperature gradient increases.

3.5.9 Effect of Schmidt number (Sc) on flow field:

Keeping all other parameters of the flow field constant except Schmidt number, Figs. 3.9(a) – 3.9(f) display the impact of Schmidt number Sc ($Sc = 0.22, 0.60$ and 0.78) on the velocity, temperature and concentration distributions as well as the local skin friction coefficient, the local Nusselt number, and the local Sherwood number against the streamwise distance. The values of Schmidt number Sc are taken to be 0.22, 0.60 and 0.78 which are corresponding physically to hydrogen, water vapor and ammonia. The Schmidt number embodies the ratio of the momentum to the mass diffusivity. The Schmidt number therefore quantifies the relative effectiveness of momentum and mass transport by diffusion in the hydrodynamic and concentration boundary layer. In Fig. 3.9(a), it is observed that when the Schmidt number increases, the velocity of the flow field decreases because in presence of heavier diffusing species. On the other hand the temperature distribution which is presented in Fig. 3.9(b) changes insignificantly compared to the velocity of the flow field. The concentration of the flow field in Fig. 3.9(c) decreases as the Schmidt number increases i.e. in presences of heavier species. This causes the concentration buoyancy effects to decrease yielding a reduction in the fluid velocity. The reductions in the velocity and concentration distributions are accompanied by simultaneous reductions in the momentum and concentration boundary layer thickness and this is the analogous to the effect of increasing the Prandtl number on the thickness of a thermal boundary layer. In order to reported the impact of Schmidt number on the flow field, the local skin friction coefficient, the local Nusselt number, and the local Sherwood number against the streamwise distance x are presented in Figs. 3.9(d) – 3.9(f). As indicated in Fig. 3.9(d), an increase in the Schmidt number produces a decrease in the local skin friction coefficient. Also it is observed from Fig. 3.9(e) that the local Nusselt number decreases with the increase of Schmidt number. However, on the basis of Fig. 3.9(f), it is found to increase the local Sherwood due to rising in the Schmidt number.

3.5.10 Effect of thermophoretic parameter (τ) on flow field:

Effect of thermophoretic parameter τ ($\tau = 0.10, 1.50$ and 3.00) on the velocity, temperature and concentration distributions as well as local skin friction coefficient,

local Nusselt number and local Sherwood number are shown in Figs. 3.10(a) – 3.10(f) while other parameters are kept constant. It can be seen from these Figs. 3.10(a) – 3.10(c) that, the velocity in Fig. 3.10(a) and the concentration in Fig. 3.10(c) of the flow field decrease with increase of the thermophoretic parameter whereas the temperature in Fig. 3.10(b) of the flow field increases with respect to increase of the thermophoretic parameter. The effect of increasing the thermophoretic parameter is limited to increasing the wall slope of the concentration distribution but decreasing the concentration of the flow field. This is true for small values of Schmidt number for which the Brownian diffusion effect is large compared to the convection effect. The nature of the thermophoretic parameter on the local skin friction coefficient, the local Nusselt number, and the local Sherwood number against the streamwise distance x are shown in Figs. 3.10(d) – 3.10(f). It is seen that the local skin friction coefficient in Fig. 3.10(d) and the local Nusselt number in Fig. 3.10(e) decrease with the increase of the thermophoretic parameter. On the other hand the local Sherwood number which is presented in Fig. 3.10(f) increases due to increase in the thermophoretic parameter i.e. increase in concentration gradient of the flow field.

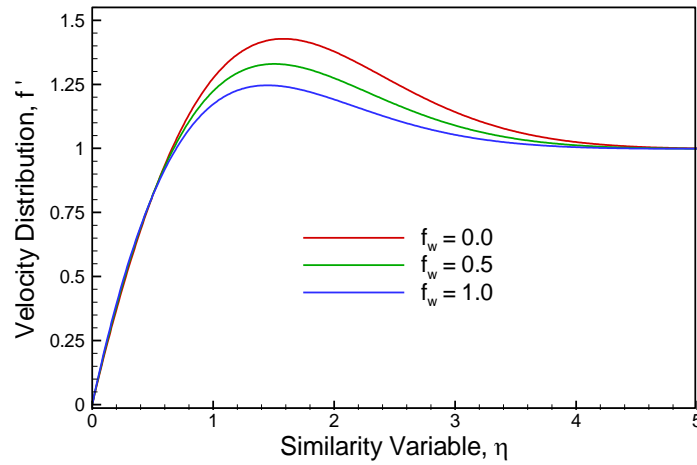


Fig. 3.1(a): Representative velocity distribution for different values of fluid suction parameter f_w while $\tau = 0.10$

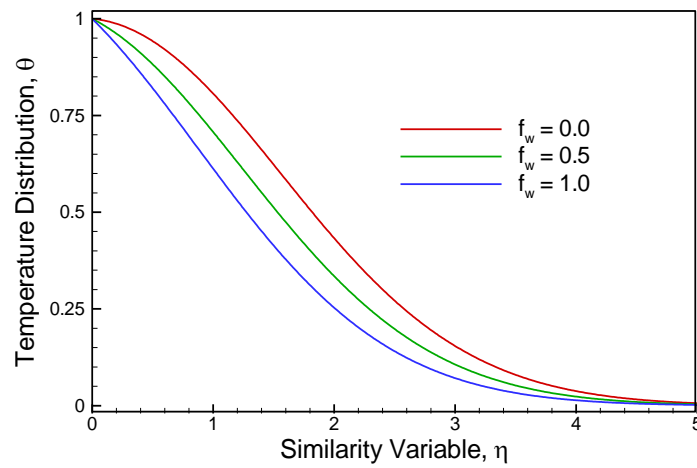


Fig. 3.1(b): Representative temperature distribution for different values of fluid suction parameter f_w while $\tau = 0.10$

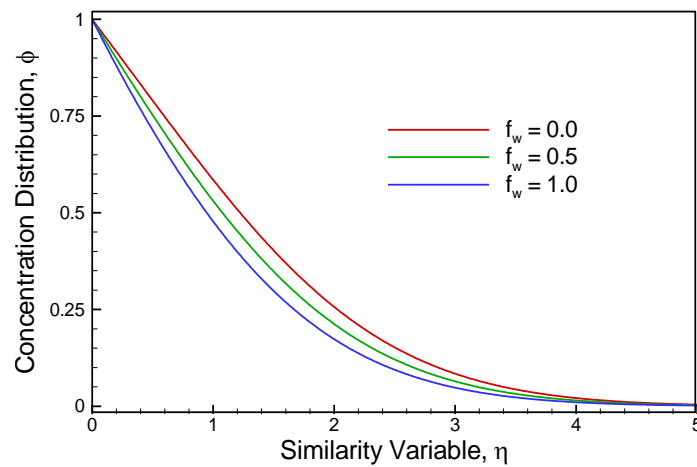


Fig. 3.1(c): Representative concentration distribution for different values of fluid suction parameter f_w while $\tau = 0.10$

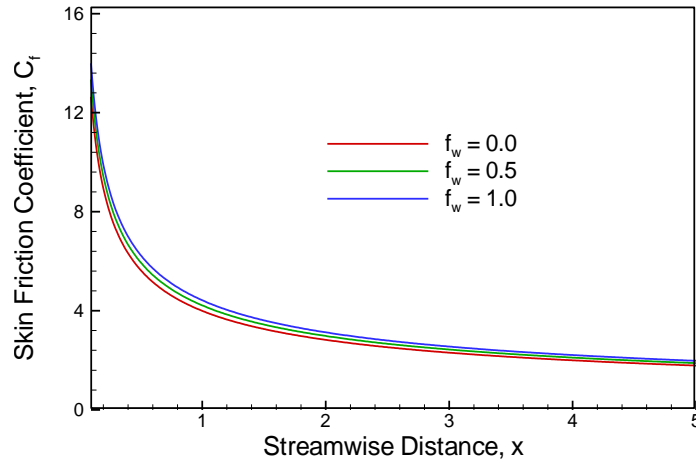


Fig. 3.1(d): Effect of fluid suction parameter f_w on local skin friction coefficient C_f against the streamwise distance x while $\tau = 0.10$

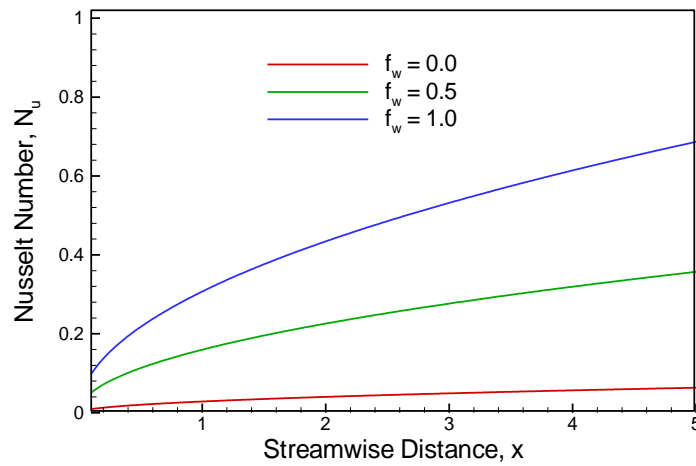


Fig. 3.1(e): Effect of fluid suction parameter f_w on local Nusselt number N_u against the streamwise distance x while $\tau = 0.10$

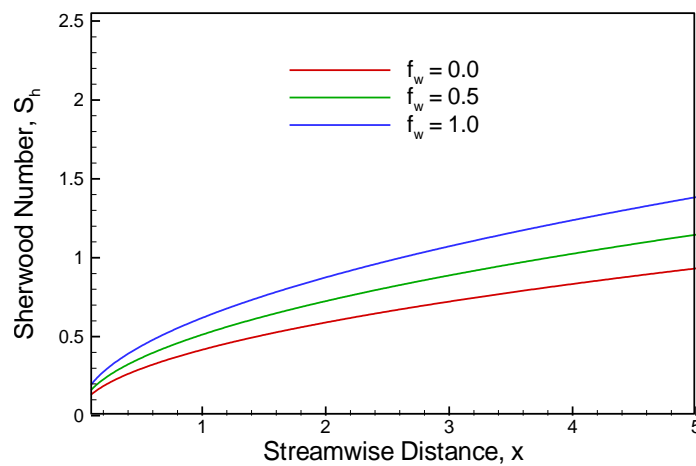


Fig. 3.1(f): Effect of fluid suction parameter f_w on local Sherwood number S_h against the streamwise distance x while $\tau = 0.10$

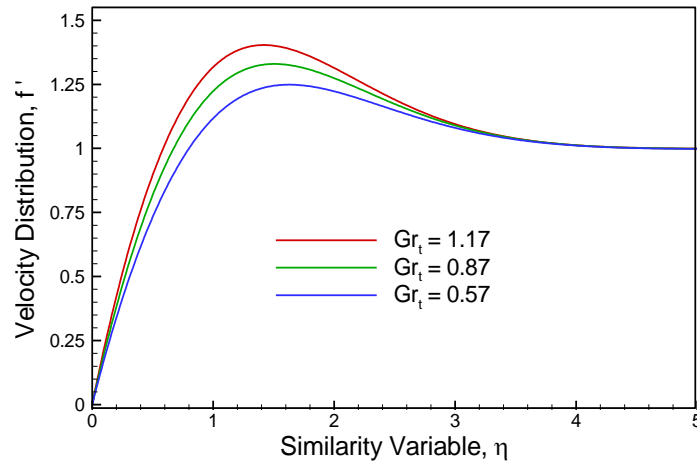


Fig. 3.2(a): Representative velocity distribution for different values of local thermal Grashof number Gr_t while $\tau = 0.10$

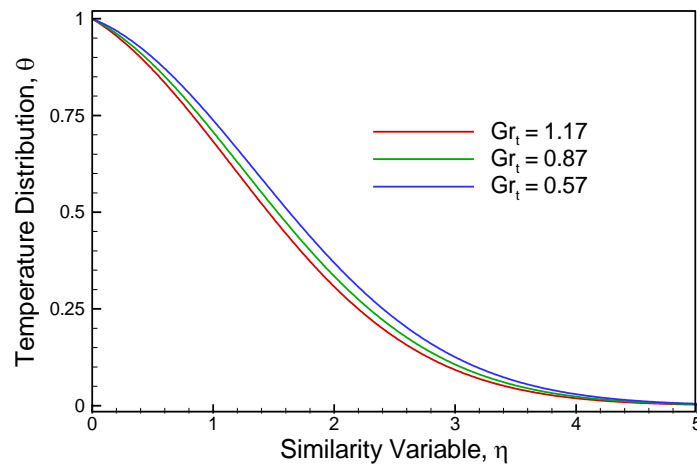


Fig. 3.2(b): Representative temperature distribution for different values of local thermal Grashof number Gr_t while $\tau = 0.10$

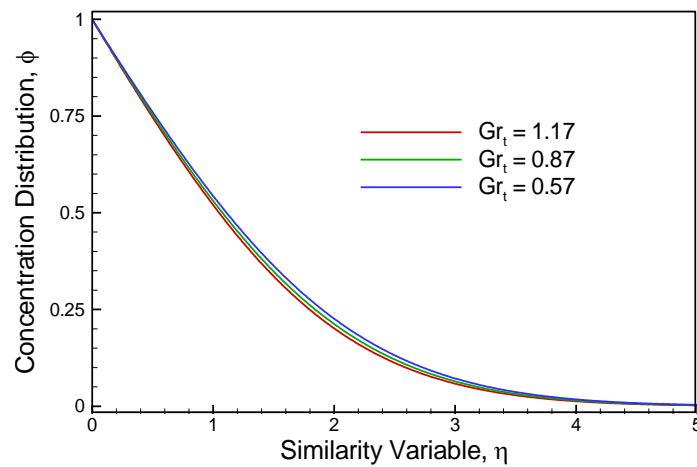


Fig. 3.2(c): Representative concentration distribution for different values of local thermal Grashof number Gr_t while $\tau = 0.10$

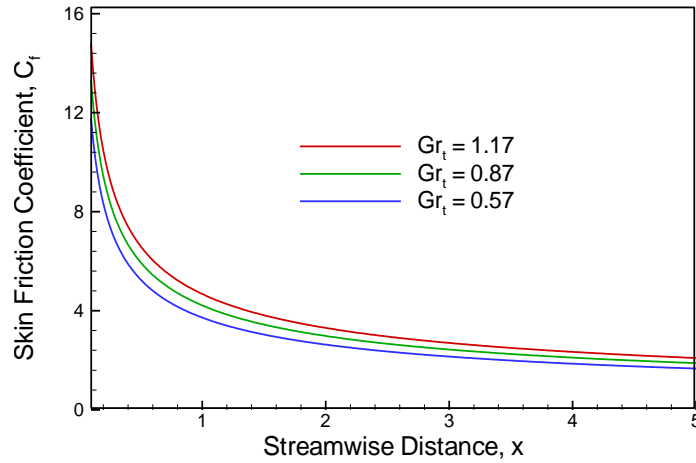


Fig. 3.2(d): Effect of local thermal Grashof number Gr_t on local skin friction coefficient C_f against the streamwise distance x while $\tau = 0.10$

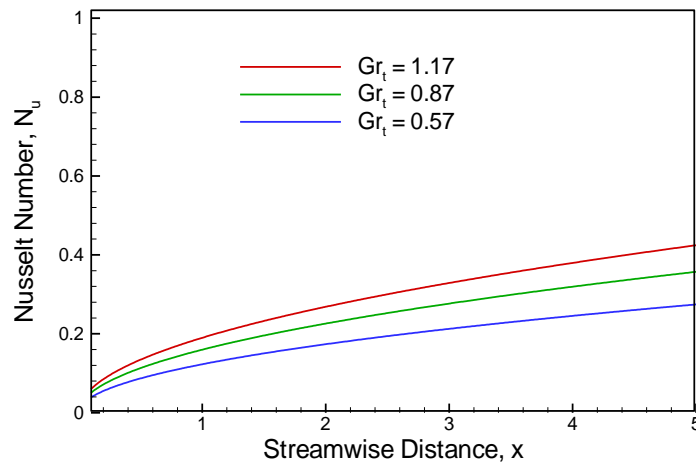


Fig. 3.2(e): Effect of local thermal Grashof number Gr_t on local Nusselt number N_u against the streamwise distance x while $\tau = 0.10$

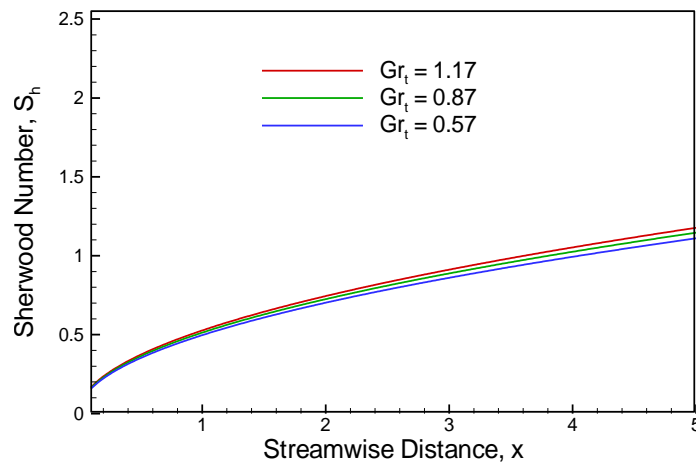


Fig. 3.2(f): Effect of local thermal Grashof number Gr_t on local Sherwood number S_h against the streamwise distance x while $\tau = 0.10$

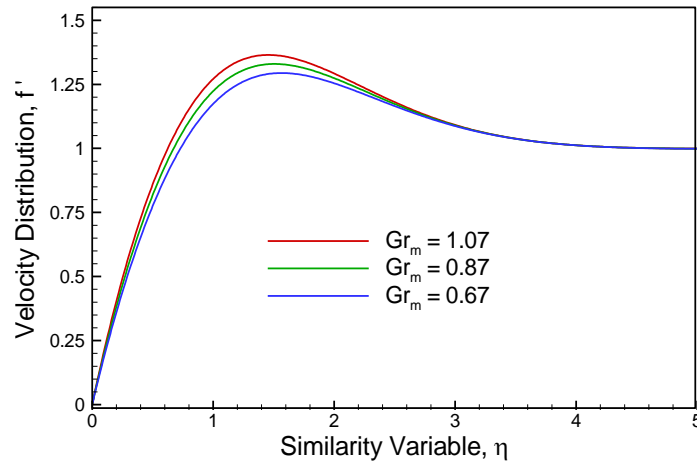


Fig. 3.3(a): Representative velocity distribution for different values of local mass Grashof number Gr_m while $\tau = 0.10$

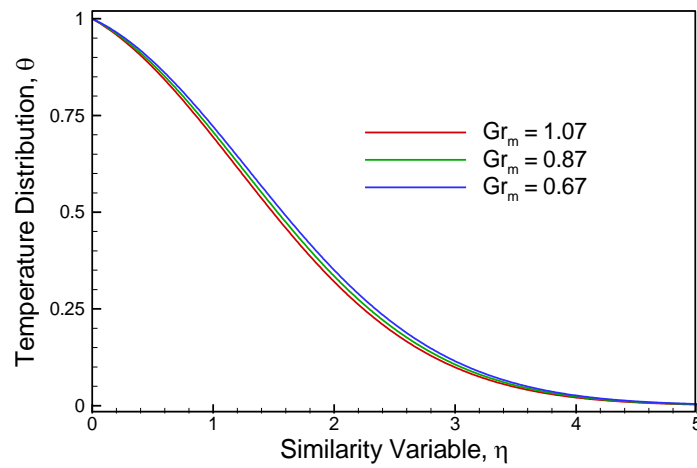


Fig. 3.3(b): Representative temperature distribution for different values of local mass Grashof number Gr_m while $\tau = 0.10$

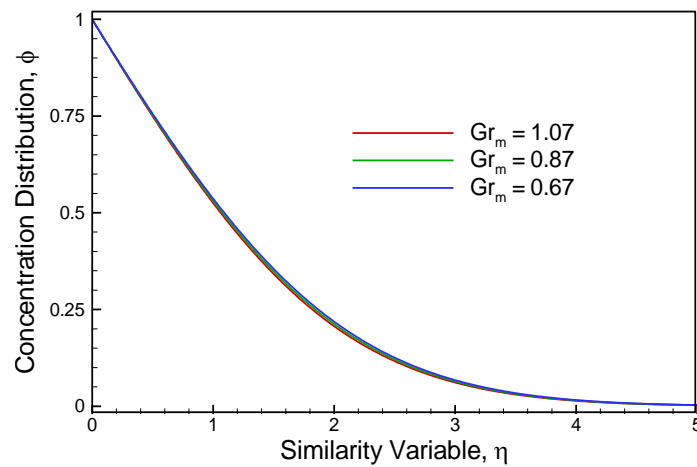


Fig. 3.3(c): Representative concentration distribution for different values of local mass Grashof number Gr_m while $\tau = 0.10$

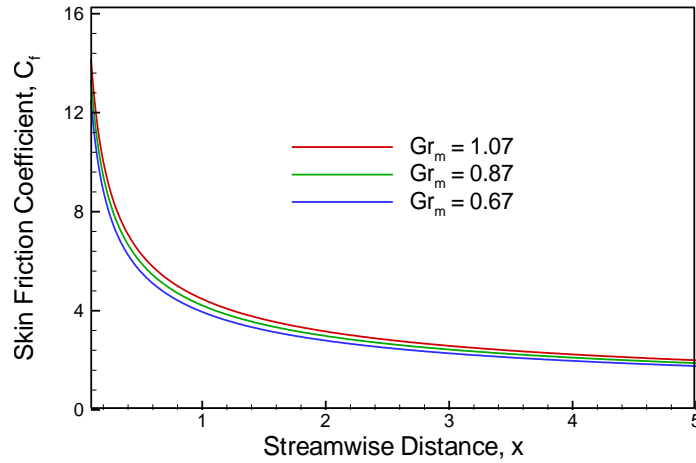


Fig. 3.3(d): Effect of local mass Grashof number Gr_m on local skin friction coefficient C_f against the streamwise distance x while $\tau = 0.10$

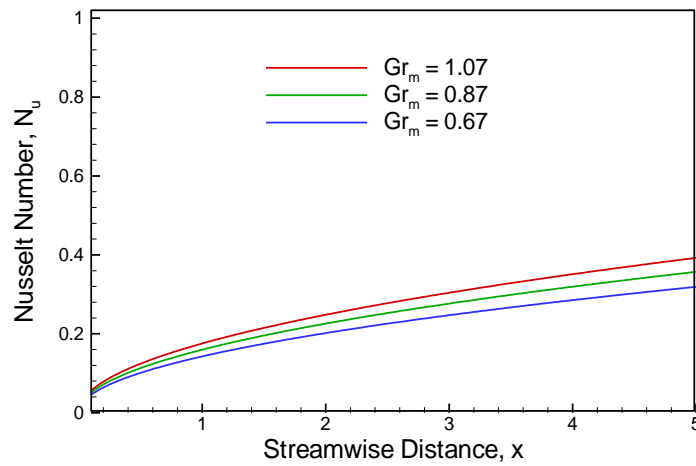


Fig. 3.3(e): Effect of local mass Grashof number Gr_m on local Nusselt number N_u against the streamwise distance x while $\tau = 0.10$

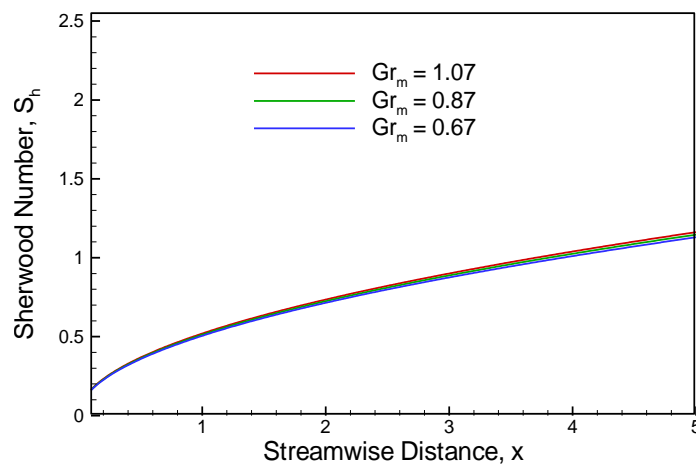


Fig. 3.3(f): Effect of local mass Grashof number Gr_m on local Sherwood number S_h against the streamwise distance x while $\tau = 0.10$

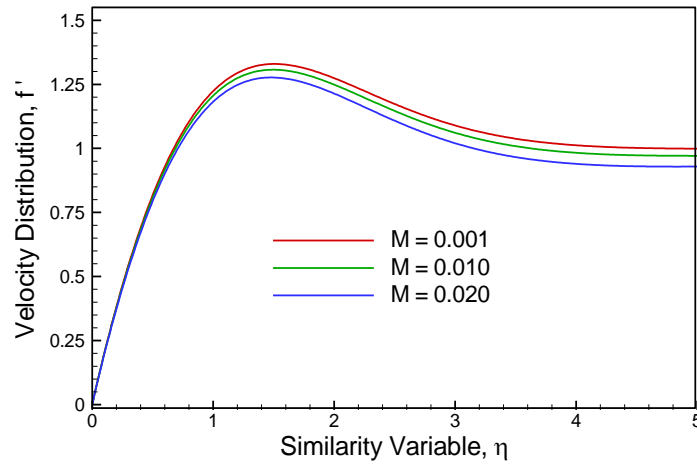


Fig. 3.4(a): Representative velocity distribution for different values of magnetic field parameter M while $\tau = 0.10$

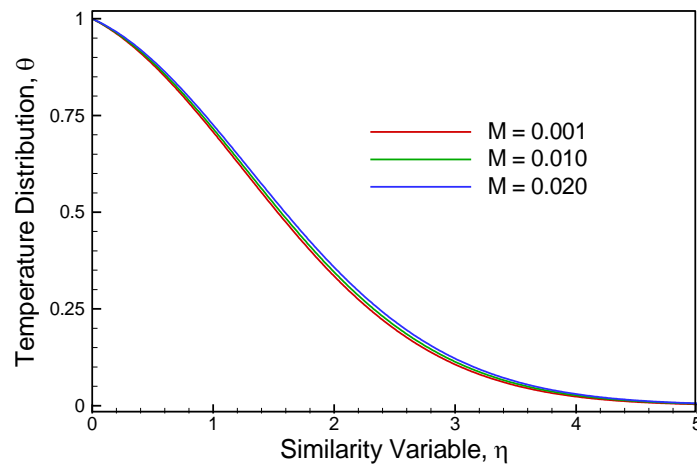


Fig. 3.4(b): Representative temperature distribution for different values of magnetic field parameter M while $\tau = 0.10$

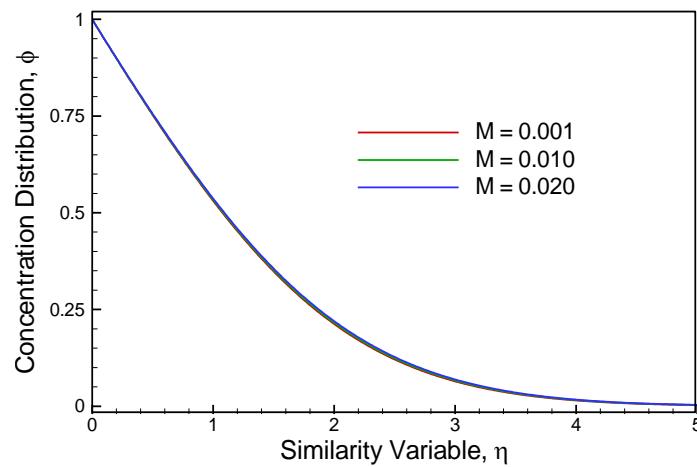


Fig. 3.4(c): Representative concentration distribution for different values of magnetic field parameter M while $\tau = 0.10$

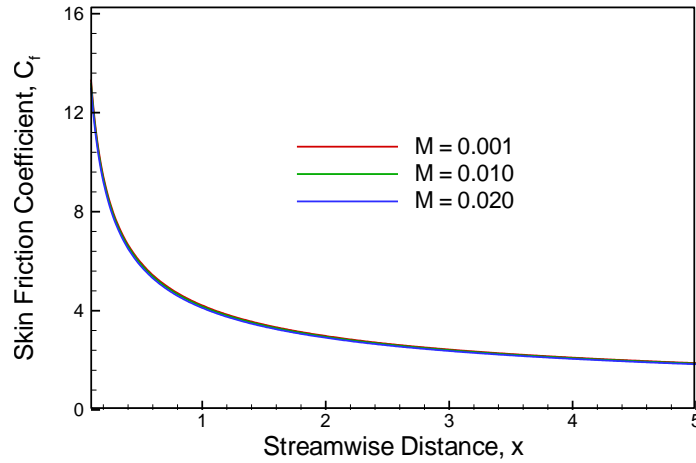


Fig. 3.4(d): Effect of magnetic field parameter M on local skin friction coefficient C_f against the streamwise distance x while $\tau = 0.10$

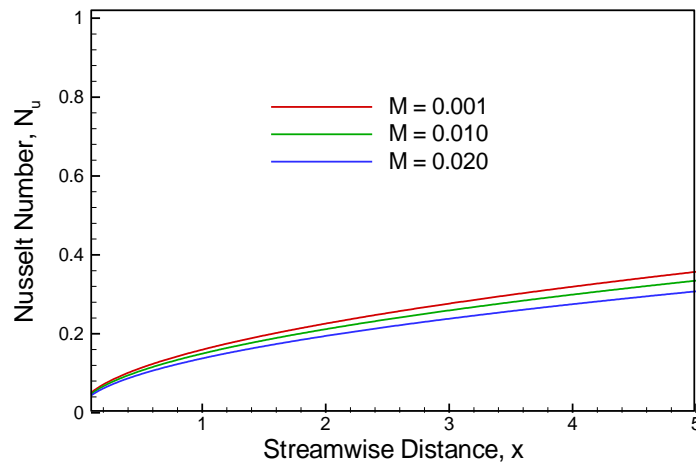


Fig. 3.4(e): Effect of magnetic field parameter M on local Nusselt number N_u against the streamwise distance x while $\tau = 0.10$

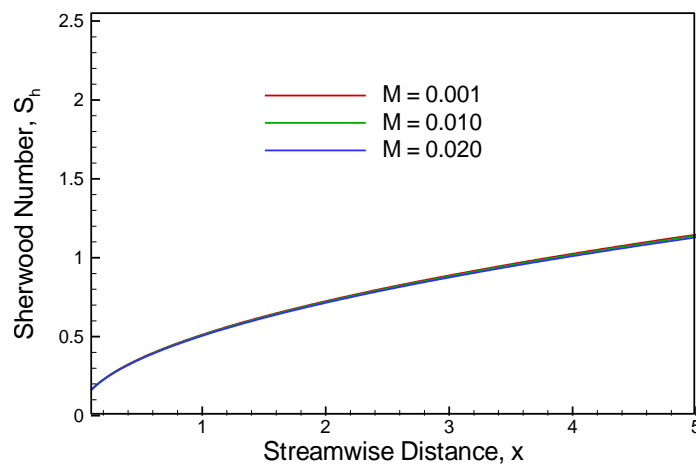


Fig. 3.4(f): Effect of magnetic field parameter M on local Sherwood number S_h against the streamwise distance x while $\tau = 0.10$

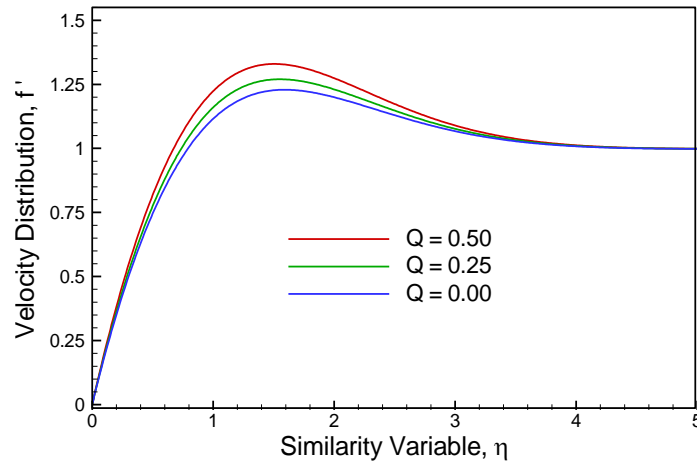


Fig. 3.5(a): Representative velocity distribution for different values of heat generation parameter Q while $\tau = 0.10$

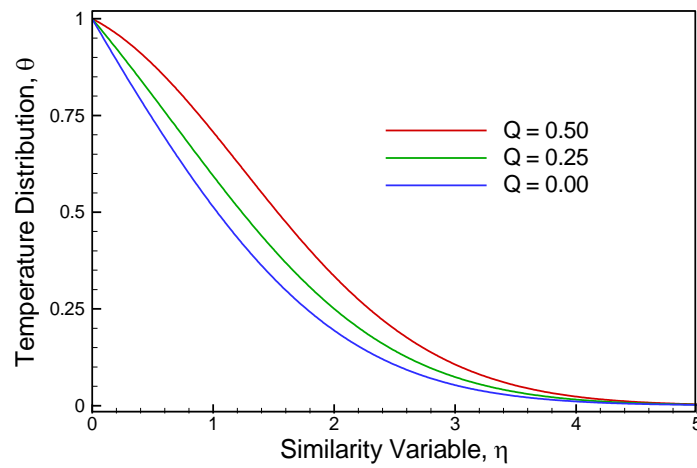


Fig. 3.5(b): Representative temperature distribution for different values of heat generation parameter Q while $\tau = 0.10$

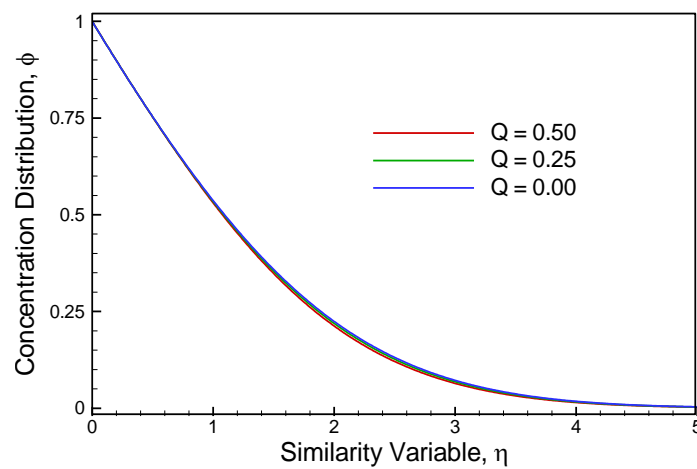


Fig. 3.5(c): Representative concentration distribution for different values of heat generation parameter Q while $\tau = 0.10$

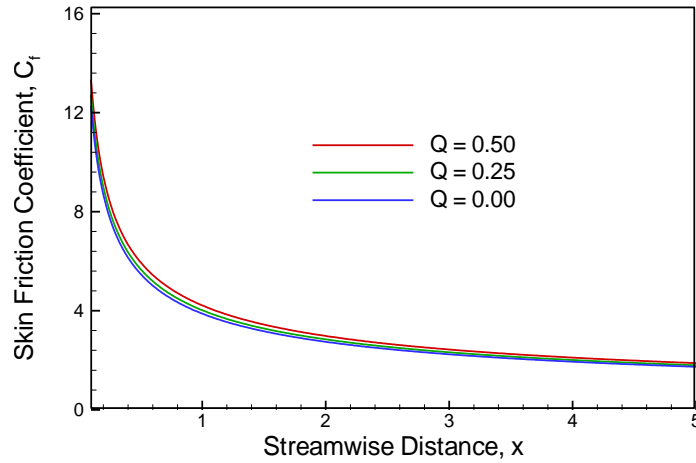


Fig. 3.5(d): Effect of heat generation parameter Q on local skin friction coefficient C_f against the streamwise distance x while $\tau = 0.10$

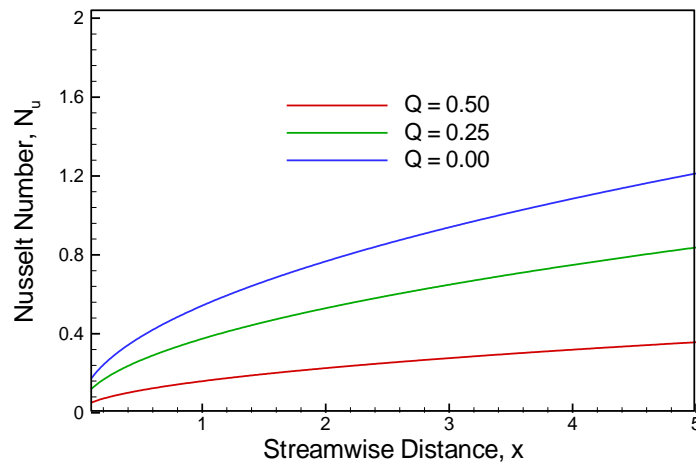


Fig. 3.5(e): Effect of heat generation parameter Q on local Nusselt number N_u against the streamwise distance x while $\tau = 0.10$

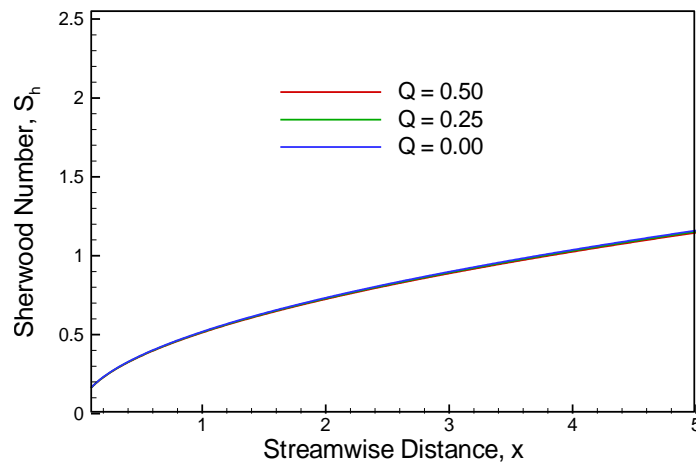


Fig. 3.5(f): Effect of heat generation parameter Q on local Sherwood number S_h against the streamwise distance x while $\tau = 0.10$

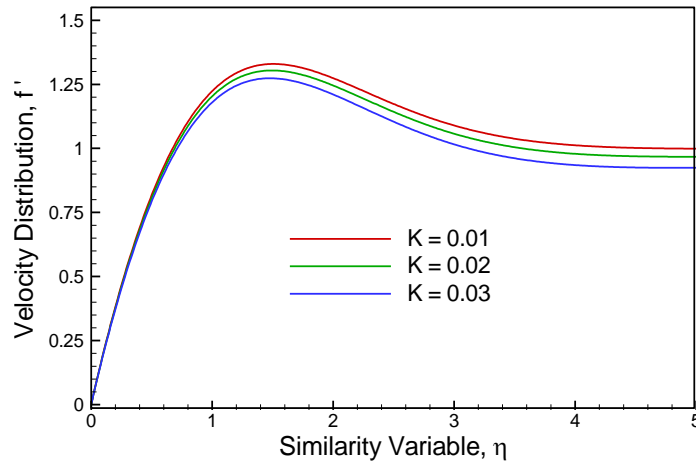


Fig. 3.6(a): Representative velocity distribution for different values of permeability parameter K while $\tau = 0.10$

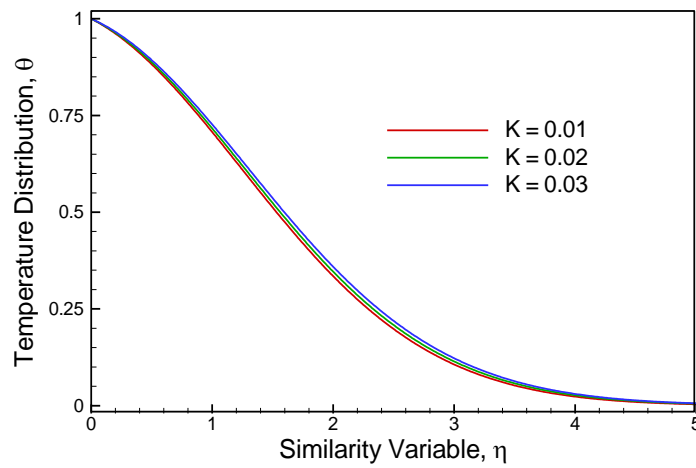


Fig. 3.6(b): Representative temperature distribution for different values of permeability parameter K while $\tau = 0.10$

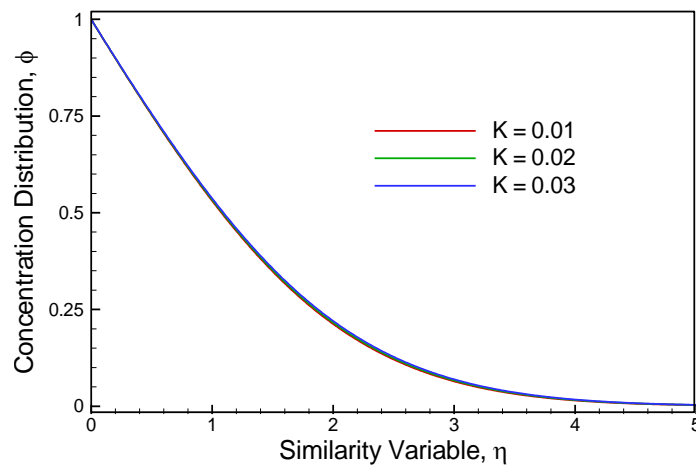


Fig. 3.6(c): Representative concentration distribution for different values of permeability parameter K while $\tau = 0.10$

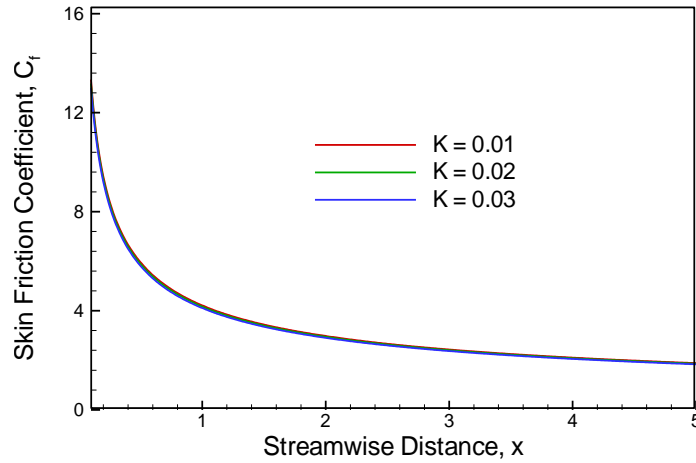


Fig. 3.6(d): Effect of permeability parameter K on local skin friction coefficient C_f against the streamwise distance x while $\tau = 0.10$

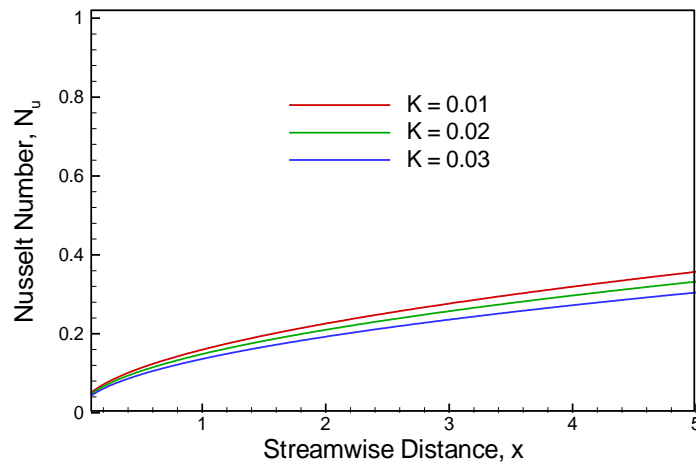


Fig. 3.6(e): Effect of permeability parameter K on local Nusselt number N_u against the streamwise distance x while $\tau = 0.10$

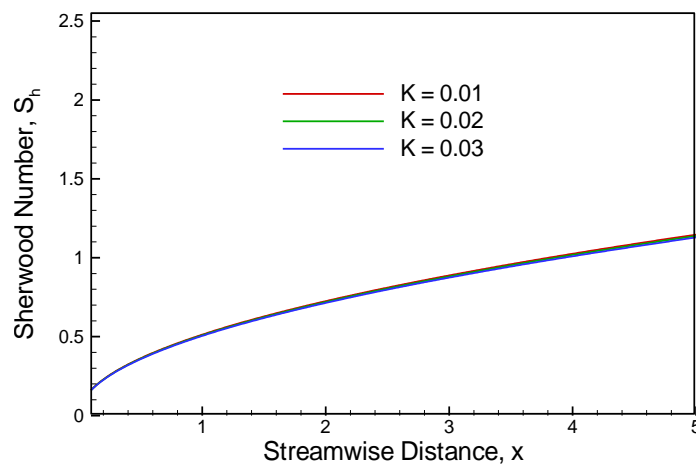


Fig. 3.6(f): Effect of permeability parameter K on local Sherwood number S_h against the streamwise distance x while $\tau = 0.10$

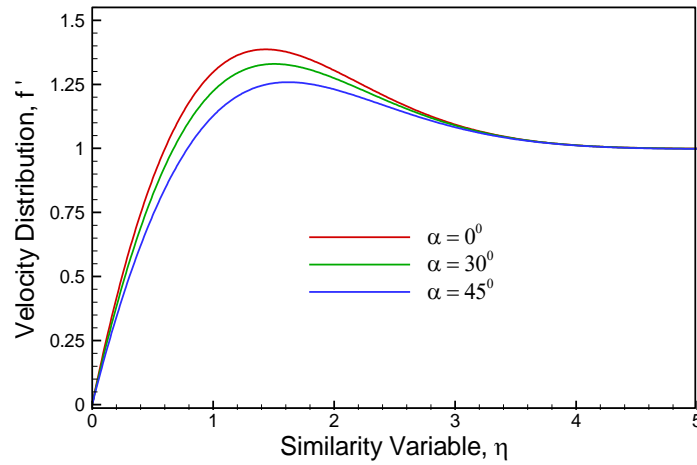


Fig. 3.7(a): Representative velocity distribution for different values of angle of inclination α while $\tau = 0.10$

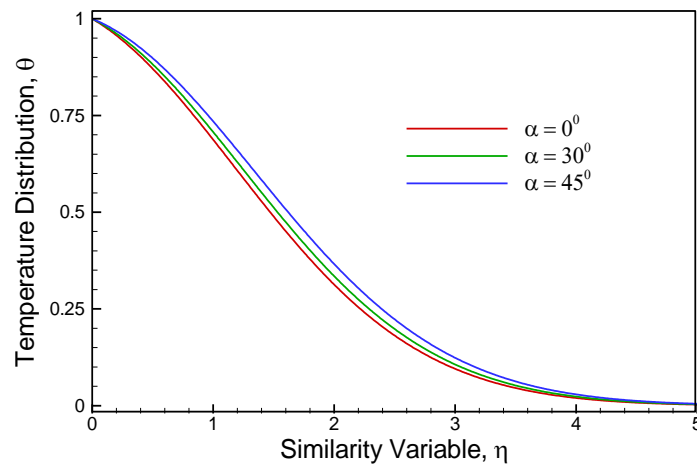


Fig. 3.7(b): Representative temperature distribution for different values of angle of inclination α while $\tau = 0.10$

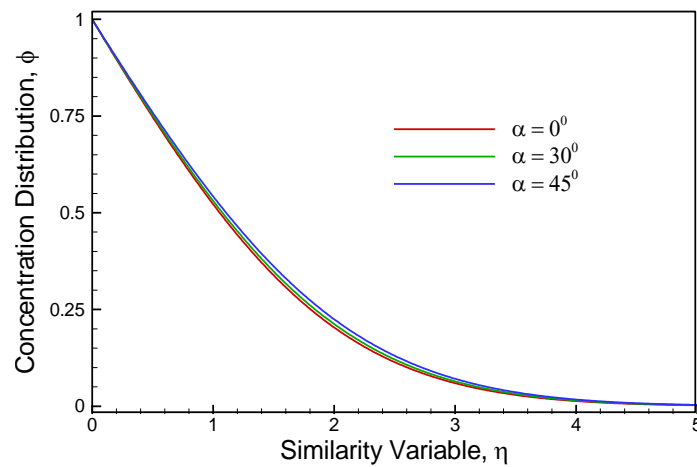


Fig. 3.7(c): Representative concentration distribution for different values of angle of inclination α while $\tau = 0.10$

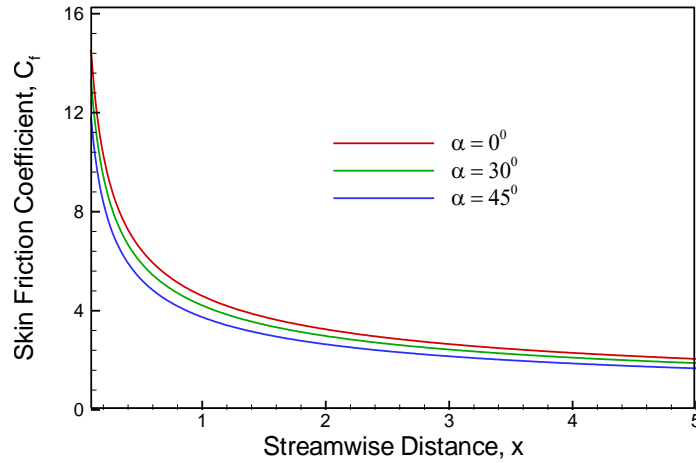


Fig. 3.7(d): Effect of angle of inclination α on local skin friction coefficient C_f against the streamwise distance x while $\tau = 0.10$

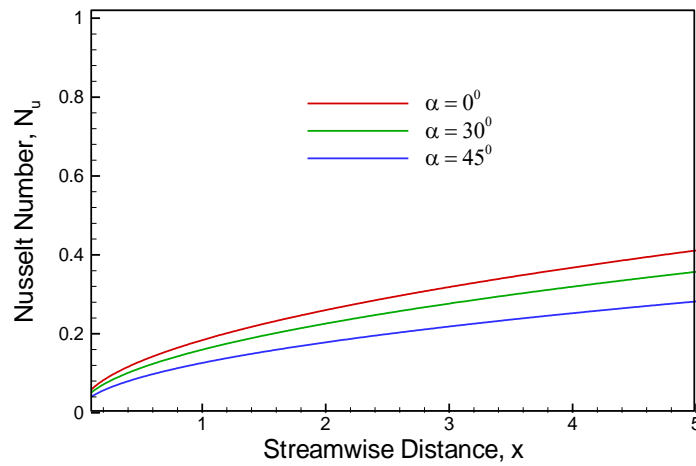


Fig. 3.7(e): Effect of angle of inclination α on local Nusselt number N_u against the streamwise distance x while $\tau = 0.10$

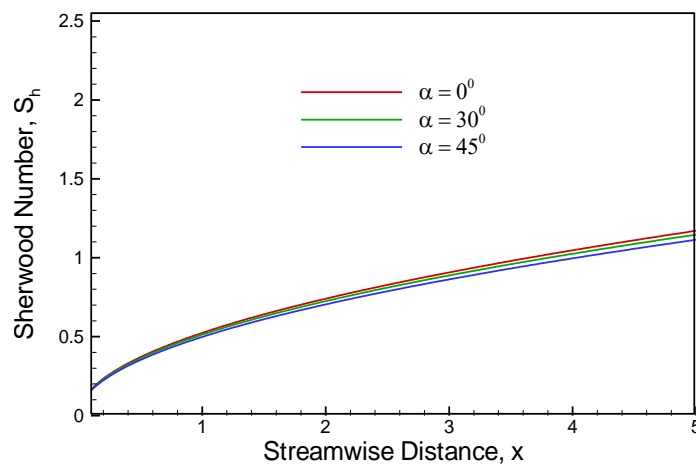


Fig. 3.7(f): Effect of angle of inclination α on local Sherwood number S_h against the streamwise distance x while $\tau = 0.10$

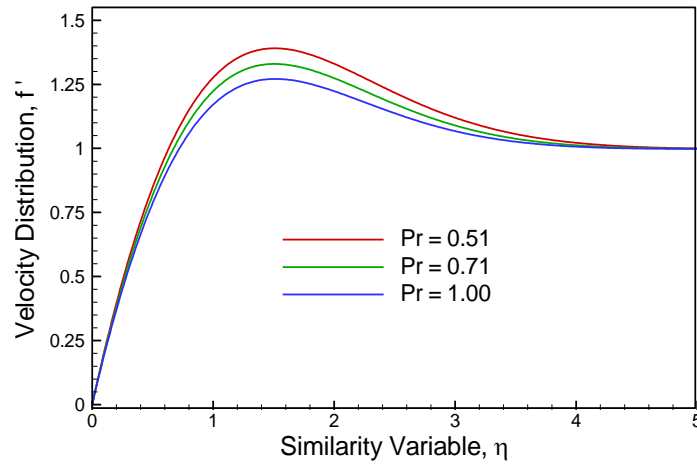


Fig. 3.8(a): Representative velocity distribution for different values of Prandtl number Pr while $\tau = 0.10$

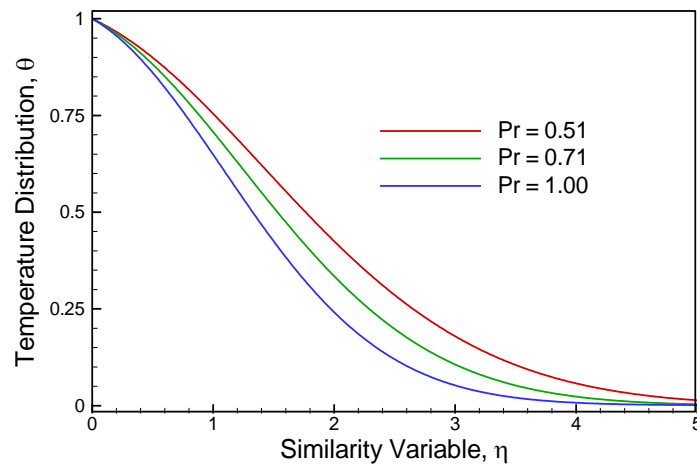


Fig. 3.8(b): Representative temperature distribution for different values of Prandtl number Pr while $\tau = 0.10$

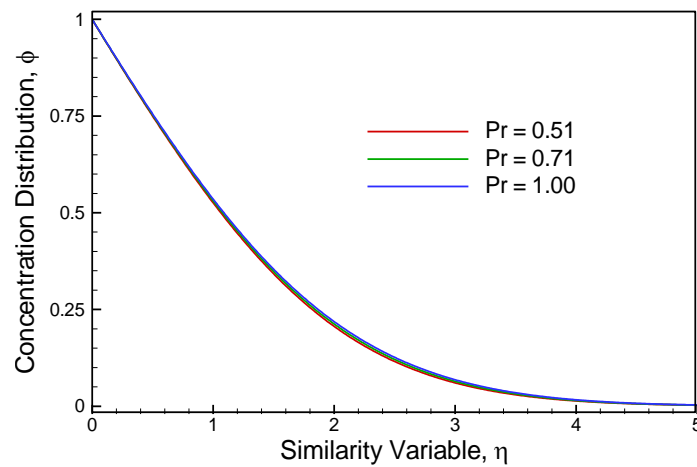


Fig. 3.8(c): Representative concentration distribution for different values of Prandtl number Pr while $\tau = 0.10$

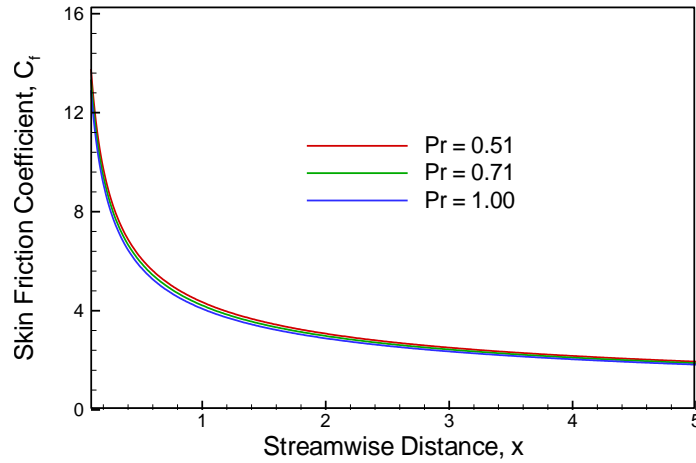


Fig. 3.8(d): Effect of Prandtl number Pr on local skin friction coefficient C_f against the streamwise distance x while $\tau = 0.10$

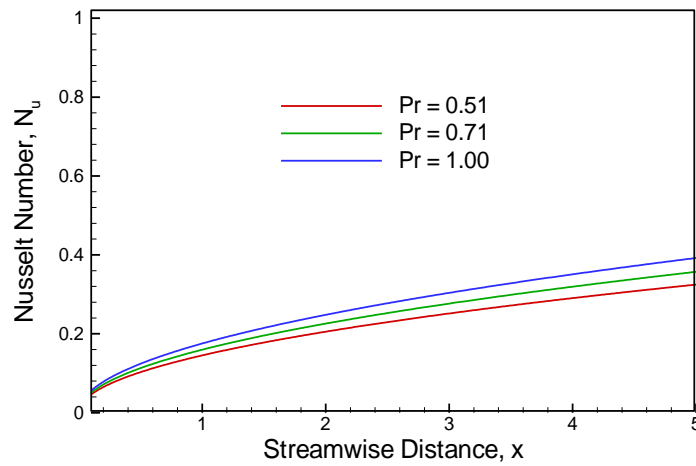


Fig. 3.8(e): Effect of Prandtl number Pr on local Nusselt number N_u against the streamwise distance x while $\tau = 0.10$

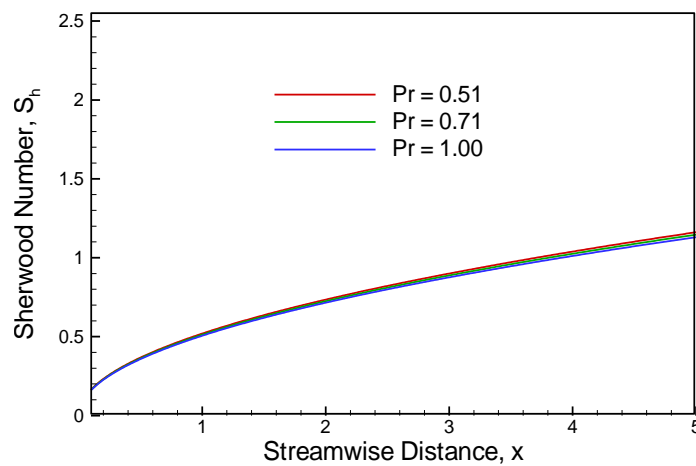


Fig. 3.8(f): Effect of Prandtl number Pr on local Sherwood number S_h against the streamwise distance x while $\tau = 0.10$

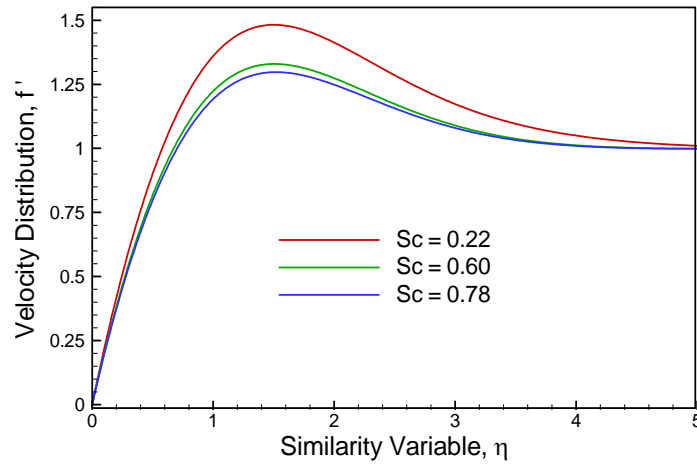


Fig. 3.9(a): Representative velocity distribution for different values of Schmidt number Sc while $\tau = 0.10$

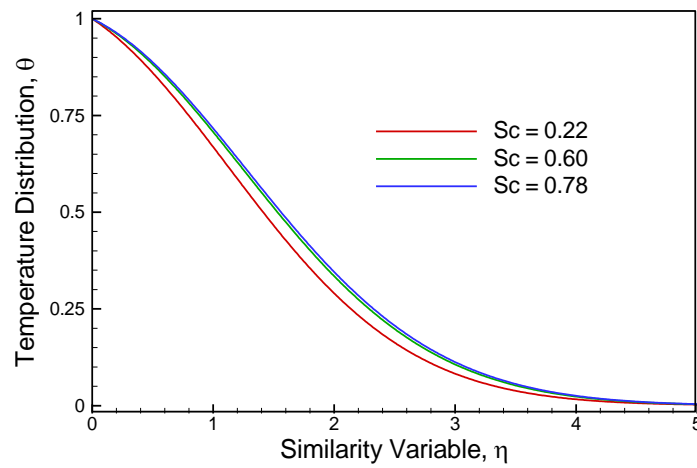


Fig. 3.9(b): Representative temperature distribution for different values of Schmidt number Sc while $\tau = 0.10$

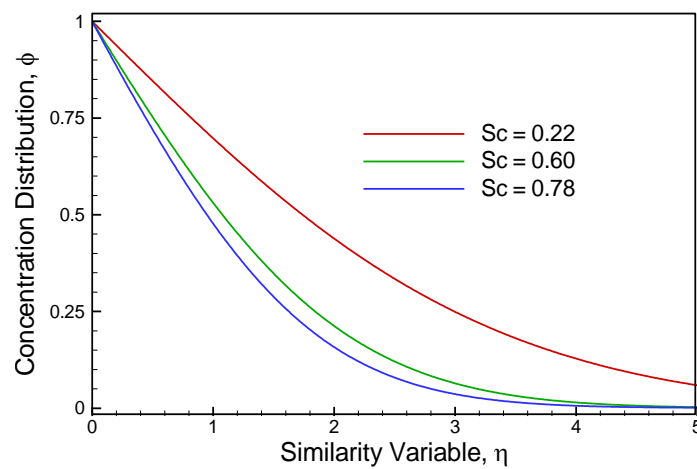


Fig. 3.9(c): Representative concentration distribution for different values of Schmidt number Sc while $\tau = 0.10$

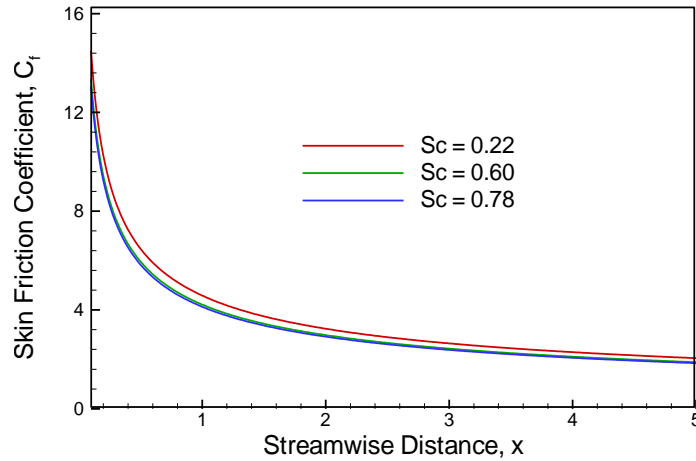


Fig. 3.9(d): Effect of Schmidt number Sc on local skin friction coefficient C_f against the streamwise distance x while $\tau = 0.10$

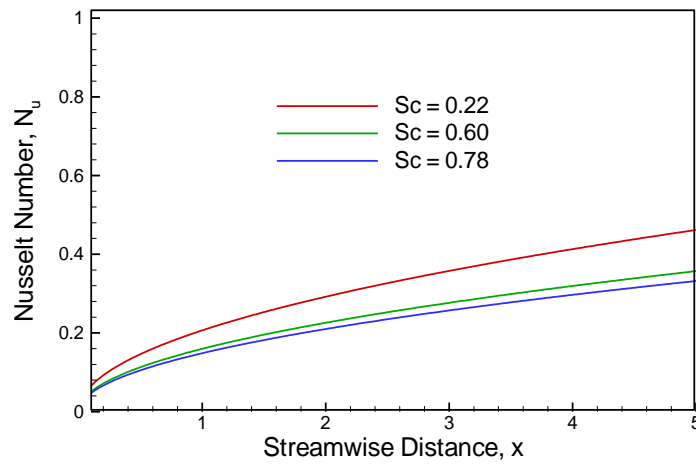


Fig. 3.9(e): Effect of Schmidt number Sc on local Nusselt number N_u against the streamwise distance x while $\tau = 0.10$

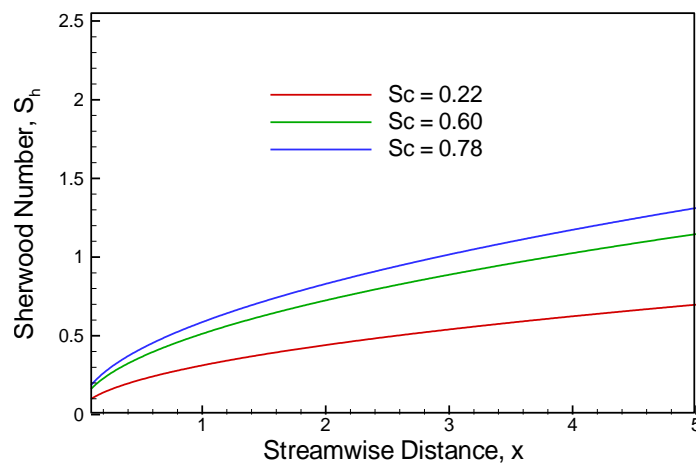


Fig. 3.9(f): Effect of Schmidt number Sc on local Sherwood number S_h against the streamwise distance x while $\tau = 0.10$

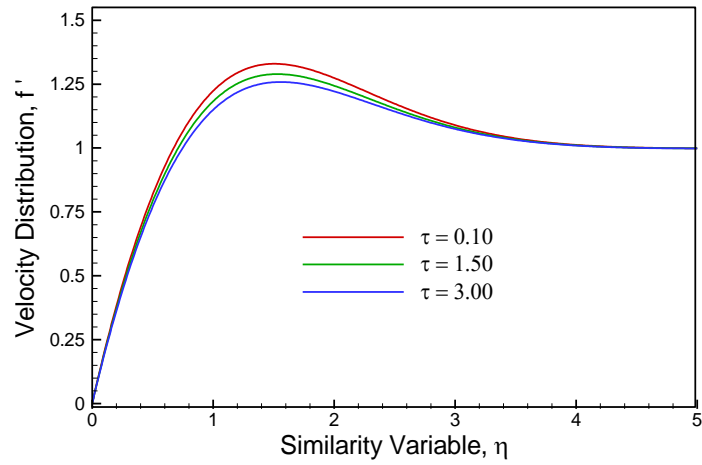


Fig. 3.10(a): Representative velocity distribution for different values of thermophoretic parameter τ

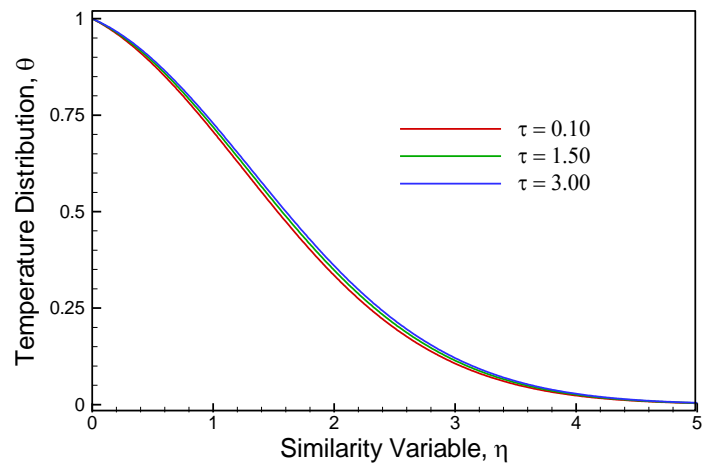


Fig. 3.10(b): Representative temperature distribution for different values of thermophoretic parameter τ

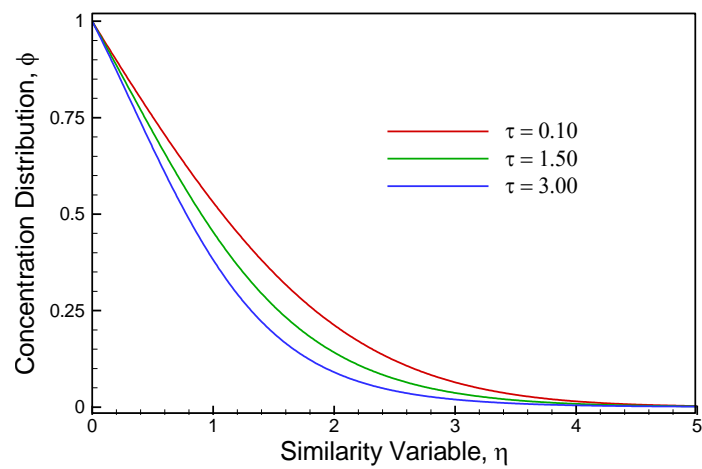


Fig. 3.10(c): Representative concentration distribution for different values of thermophoretic parameter τ

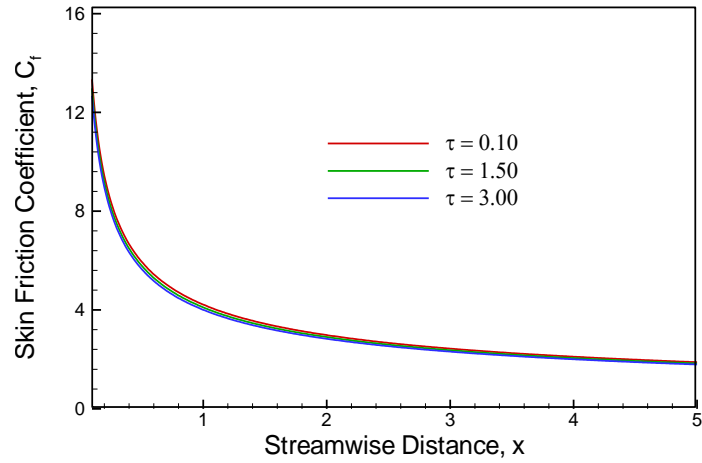


Fig. 3.10(d): Effect of thermophoretic parameter τ on local skin friction coefficient C_f against the streamwise distance x

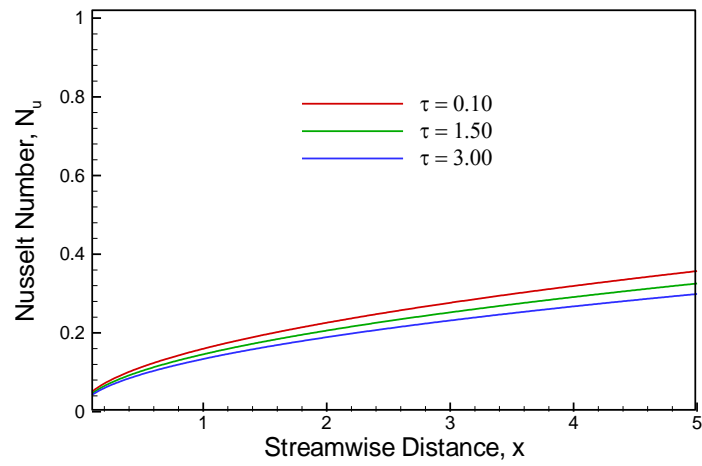


Fig. 3.10(e): Effect of thermophoretic parameter τ on local Nusselt number N_u against the streamwise distance x

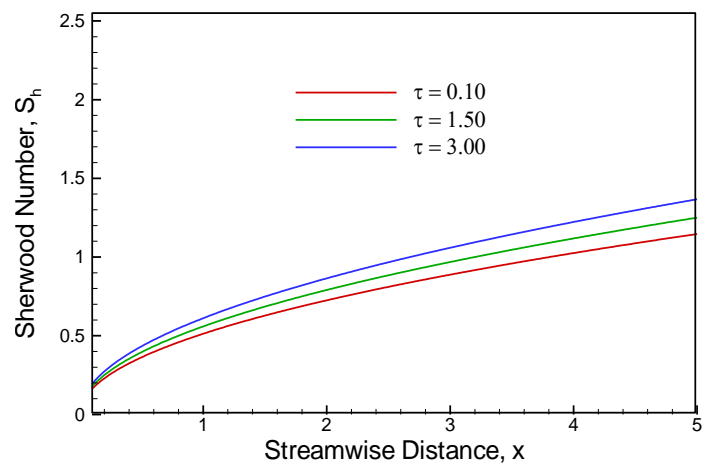


Fig. 3.10(f): Effect of thermophoretic parameter τ on local Sherwood number S_h against the streamwise distance x

3.6 Conclusions

From this investigation i.e. investigation of double diffusive magnetohydrodynamic mixed convective flow with thermodiffusion along an inclined flat plate in a porous medium, the following conclusions can be drawn for the effect of the fluid suction parameter f_w , local thermal Grashof number Gr_t , local mass Grashof number Gr_m , magnetic parameter M , heat generation parameter Q , permeability parameter K , Prandtl number Pr , Schmidt number Sc and thermophoretic parameter τ on the flow field as:

- 1) An increase in f_w , M , K , α , Pr , Sc and τ decrease the velocity of the flow field while an increase in Gr_t , Gr_m and Q increase the velocity of the flow field.
- 2) As the f_w , Gr_t , Gr_m and Pr increase, the temperature of the flow field tend to decrease whereas an increase in M , Q , K , α , Sc and τ , increase the temperature of the flow field.
- 3) Due to increase in f_w , Gr_t , Gr_m , Sc and τ , the concentration of the flow field decreases but an increase in α , the concentration of the flow field increases. On the other hand, the concentration changes insignificantly with the increase of M , Q , K and Pr .
- 4) In the presence of rising in M , K , α , Pr , Sc and τ , decrease the local skin friction coefficient of the flow field while an increase in f_w , Gr_t , Gr_m and Q , increase the local skin friction coefficient of the flow field.
- 5) Increasing the M , Q , K , α , Sc and τ , has the effect to decrease the local Nusselt number of the flow field while an increase in f_w , Gr_t , Gr_m and Pr , increase the local Nusselt number of the flow field.
- 6) According to enhancement in K , α and Pr , decrease the local Sherwood number of the flow field while an increase in f_w , Gr_t , Gr_m , Sc and τ , increase the local Sherwood number of the flow field. But, the local Sherwood number changes insignificantly with the increase of M and Q .

Chapter 5

Concluding Remarks

Investigations are carried out to find the behavior of the flow field on double diffusive magnetohydrodynamic mixed convective flow along an inclined flat plate in a porous medium i) neglecting, and ii) including the effect of thermodiffusion on the basis of boundary layer approximations. The boundary layer approximations are transformed into nonlinear boundary layer equations using suitable similarity transformations and then solved numerically using the Runge-Kutta sixth-order integration scheme together with Nachtsheim-Swigert shooting iteration technique. The validity of the numerical methodology is checked by comparing the results obtained for some specific cases with those available in the literature Reddy et al. [12], and comparatively good agreement is reached.

In these investigations the key contributions are as follows;

- Physical and mathematical model for double diffusive magnetohydrodynamic mixed convective flow along an inclined flat plate in a porous medium have been developed.
- Mathematical model has been solved numerically using Nachtsheim-Swigert iteration technique and the numerical results are reported graphically.
- From these investigations, it is observed that the fluid suction has the effect to decrease the velocity, temperature and concentration of the flow field whereas increase the wall shear stress in terms of local skin friction coefficient, the rate of heat transfer in terms of local Nusselt number and the rate of mass transfer in terms of local Sherwood number.
- Due to increase of the thermophoretic parameter, the velocity and concentration of the flow field decrease whereas the temperature of the flow field increases. However, the wall shear stress in terms of local skin friction coefficient and the rate of heat transfer in terms of local Nusselt number decrease but the rate of mass transfer in terms of local Sherwood number increases with the increase of thermophoretic parameter.

The double diffusive magnetohydrodynamic flow for an electrically conducting fluid has important applications in many engineering fields such as the magnetic behavior of plasmas in fusion reactors, liquid-metal cooling of nuclear reactors, electromagnetic casting, petroleum industries, boundary layer control in aerodynamics, MHD generators, Ship propulsion, Jet printers and so on. Therefore, it can be concluded that, the results which are obtained in these investigations, have wide range of applications for solving the relevant problems.

Last but not the least, based on the present work, further research may be carried out to investigate the unsteady cases including the variable wall temperature and concentration, and so on.

References

- [1] Abbasi, A., "Theoretical Investigation of Thermodiffusion (Soret Effect) in Multicomponent Mixtures", *University of Toronto*, Canada, 2010.
- [2] Alam M. S., Rahman M. M. and Samad M. A., "Numerical Study of the Combined Free-Forced Convection and Mass Transfer Flow Past a Vertical Porous Plate in a Porous Medium With Heat Generation and Thermal Diffusion", *Nonlinear Analysis: Modeling and Control*, Volume 11, No. 4, pp. 331-343(2006).
- [3] Alam M. S. and Rahman M. M., "Effects of Thermophoresis and Chemical Reaction on Unsteady Hydromagnetic Free Convection and Mass Transfer Flow Past an Impulsively Started Infinite Inclined Porous Plate in the Presence of Heat Generation/Absorption", *Thammasat International Journal Science Tech.*, Volume 12, No. 3, pp. 44-53(July-September 2007).
- [4] Alam M. S., Rahman M. M. and Sattar M. A., "Effects of chemical reactions and thermophoresis on magnetohydrodynamics mixed convective heat and mass transfer flow along an inclined plate in the presence of heat generation and (or) absorption with viscous dissipation and joule heating", *Can. J. Phys.*, Volume 86, pp. 1057-1066(2008).
- [5] Aydin O. and Kaya A., "MHD mixed convective heat transfer flow about an inclined plate", *Heat Mass Transfer*, Volume 46, pp. 129-136(2009).
- [6] Bergman, T. L., Lavine, A. S., and Frank, P., "Fundamentals of heat and mass transfer", *John Wiley & Sons*, United States of America, 2011.
- [7] Cebeci T. and Bradshaw P., "Physical and computational aspects of convective heat transfer", *Springer*, New York, 1984.
- [8] Chen C. -H., Yunlin and Taiwan, "Heat and mass transfer in MHD flow by natural convection from a permeable, inclined surface with variable wall temperature and concentration", *Acta Mechanica* 172, pp. 219-235(2004).
- [9] Douglas, J. F., Gasiorek, J. M., Swaffield, J. A., and Jack, L. B., "Fluid Mechanics", *Pearson education limited*, England, 2005.
- [10] Kothandaraman, C. P., "Fundamentals of heat and mass transfer", *New age international (P) limited*, New Delhi, 2006.
- [11] Nachtsheim P. R. and Swigert P., "Satisfaction of asymptotic boundary conditions in numerical solution of systems of nonlinear equations of boundary-layer type", *NASA TND 3004*(1965).
- [12] Reddy M. G. and Reddy N. B., "Mass transfer and Heat Generation Effects on MHD Free Convection Flow past an Inclined Vertical Surface in a Porous

References

Medium”, *Journal of Applied Fluid Mechanics*, Volume 4, No. 3, Issue 1, pp. 7-11(2011).

- [13] Talbot L., Cheng R. K., Schefer R. W. and Willis D. R., „Thermophoresis of particles in a heated boundary layer”; *Journal of fluid Mechanics*, Volume 101, Part 4, pp. 737-758(1979).
- [14] http://en.wikipedia.org/wiki/Combined_forced_and_natural_convection, Date: August 19, 2013, Time: 9:36:03 PM†
- [15] http://en.wikipedia.org/wiki/Forced_convection, Date: August 19, 2013, Time: 9:37:13 PM
- [16] http://en.wikipedia.org/wiki/Grashof_number, Date: August 19, 2013, Time: 9:37:14 PM
- [17] http://en.wikipedia.org/wiki/Knudsen_number, Date: August 19, 2013, Time: 9:37:14 PM
- [18] http://en.wikipedia.org/wiki/Natural_convection, Date: August 19, 2013, Time: 9:36:13 PM
- [19] http://en.wikipedia.org/wiki/Nusselt_number, Date: August 19, 2013, Time: 9:37:23 PM
- [20] http://en.wikipedia.org/wiki/Prandtl_number, Date: August 19, 2013, Time: 9:37:26 PM
- [21] http://en.wikipedia.org/wiki/Reynolds_number, Date: August 19, 2013, Time: 9:37:27 PM
- [22] http://en.wikipedia.org/wiki/Schmidt_number, Date: August 19, 2013, Time: 9:37:32 PM
- [23] http://en.wikipedia.org/wiki/Sherwood_number, Date: August 19, 2013, Time: 9:37:33 PM †
- [24] <http://www.jgmaas.com/scores/facts.html>, Date: August 19, 2013, Time: 9:39:33 PM